ESSENTIAL ROLES AND MECHANISMS OF SEIPIN IN MOUSE REPRODUCTION

by

AHMED EZAT EL ZOWALATY

(Under the Direction of XIAOQIN YE)

ABSTRACT

Reproduction is essential for the continuation of every species. During PhD, I studied reproductive biology and reproductive toxicology. The study of reproductive biology is essential to understand the mechanism of action of the male and female reproductive system at the molecular level to help physicians treat infertility. This dissertation also provides basic information essential to understand how some reproductive toxins work at the cellular and molecular levels to protect human/animals and the environment from the deleterious effects. The dissertation explained the molecular mechanism of seipin in male and female infertility using *Bscl2*-deficient mice. *Bscl2* is required for adipocyte differentiation but its role in reproduction was not known. *Bscl2* is highly and specifically expressed in round spermatids in the testis and deletion of *Bscl2* led to impaired male fertility, DNA damage in spermatocytes and spermatids, fragmented chromocenter in round spermatids, and defective mitochondrial function in sperm leading to male infertility. These findings open new avenues to understand human infertility and treat infertile males. In addition, *Bscl2*-deficient female mice have defect during parturition and delivery of pups. The *Bscl2*-deficient females die during delivery, or fail to deliver pups on day of delivery and they have slightly longer gestation period. Bscl2 is highly expressed in the uterus and in the myometrium. *Bscl2* is also essential for mammary gland development during lactation.

Bscl2 is also highly and specifically expressed in mammary luminal epithelium cells, and *Bscl2*-deficient females fail to nurse their pups. Loss of *Bscl2* leads to upregulation of cleaved caspase-3 and cell death in the mammary glands. There was upregulation of endoplasmic reticulum stress protein disulfide-isomerase (PDI), indicating that this mechanism potentially contributed to increased cell death and failure of lactation. In this dissertation, *Bscl2* function in reproduction has been studied in the uterus, mammary gland and in the testis.

INDEX WORDS: Bscl2, Chromocenter fragmentation, Male infertility, Seipin deficiency, Acrosome, Mammary gland, Lactation, Lipid droplet.

ESSENTIAL ROLES AND MECHANISMS OF SEIPIN IN MOUSE REPRODUCTION

by

AHMED EZAT EL ZOWALATY

BSC. PHARMACEUTICAL SCIENCES, EGYPT, 2009

A DISSERTATION Submitted to the Graduate Faculty of The University of Georgia in Partial Fulfillment of the Requirements for the Degree

DOCOTR OF PHILOSOPHY

ATHENS, GEORGIA

2017

ESSENTIAL ROLES AND MECHANISMS OF SEIPIN IN MOUSE REPRODUCTION

by

AHMED EZAT EL ZOWALATY

Major Professor:	XIAOQIN YE
Committee:	NIKOLAY FILIPOV
	MARY ALICE SMITH
	RABINDRANATH DE LA FUENTE

Electronic Version Approved:

Suzanne Barbour
Dean of the Graduate School
The University of Georgia
AUGUST 2017

ACKNOWLEDGEMENTS

This work has been carried out at the Interdisciplinary Toxicology Program, Department of Physiology and Pharmacology at the University of Georgia, between 2012 and 2017. I am sincerely grateful to all those who have helped and supported me during these five years to make this dissertation possible. I am sincerely grateful to my PhD advisor and mentor Dr. Xiaoqin Ye. She was more than a mentor who sparked my interest in this field and guided me during the Ph.D. I admire her knowledge, mentoring, enthusiasm, support, logical thinking, providing family-oriented work environment and her patience. I am grateful to the guidance, mentoring and support of my Ph.D. committee members, Dr. Nikolay Filipov, Dr. Rabindranath De La Fuente and Dr. Mary Alice Smith. Your support and guidance are invaluable!

I wish to thank my colleagues in the Ye lab and in the Department of Physiology and Pharmacology. I am grateful to Dr. Shuo Xiao for his valuable friendship and guidance. I am grateful to Dr. Claudia Baumann for her wonderful collaboration. Finally, I wish to express my deepest gratitude and cordial thanks to my family, my late father Dr. Ezat El Zowalaty, my mother Mrs. Zainab Mekawy, my brothers Mohamed and Mahmoud, and my sister Eman. Thank you for continuously encouraging me! I will forever be grateful to you!

TABLE OF CONTENTS

LIST OF ABBREVIATIONS

FSH, Follicle-stimulating hormone; **LH**, Luteinizing hormone; **DSB**; Double strand break, **γ-H2AX**, H2A Histone Family Member X; **BRCA1**, Breast Cancer 1; ATR, Ataxia Telangiectasia And Rad3-Related Protein; **MSCI**, Meiotic Sex Chromosome Inactivation; **MSUC**, Meiotic Silencing of Unsynapsed Chromosomes, **SPO11**, Initiator Of Meiotic Double Stranded Breaks; **PYGO2**, Pygopus Family PHD Finger 2; **SSTK** Testis Specific Serine Kinase 6; **CAMK4**, Calcium/Calmodulin Dependent Protein Kinase IV; **c-kit**, KIT Proto-Oncogene Receptor Tyrosine Kinase; **Daz1**, Deleted In Azoospermia 1; **Boule**, Boule Homolog, RNA Binding Protein; **Cdc25**, Cell Division Cycle 25C; **CREM**, CAMP Responsive Element Modulator, **FASL**, Fas Cell Surface Death Receptor Ligand; **BCL2**, B-Cell CLL/Lymphoma 2; **ROS**, Reactive Oxygen Species; **Bcl-w**, BCL2 Like 2; **p53**, Tumor Protein P53; **GnRH**, Gonadotropin Releasing Hormone; **d.p.c**, day post coitum; **P4**, Progesterone; **E2**, 17-β-Estradiol; **cAMP**, cyclic Adenosine Mono Phosphate; **ZP1/2/3**, Zona Pellucida Glycoprotein 1/2/3; **CD9**, CD9 Molecule; **GPI**, Glucose-6-Phosphate Isomerase; **JUNO**, IZUMO1 Receptor Protein JUNO; **IZUMO**, Izumo Sperm-Egg Fusion 1; **Cdx2**, Caudal Type Homeobox 2; **Oct4**, POU-Type Homeodomain-Containing DNA-Binding Protein, **Gata**, Globin Transcription Factor 1; **Nanog**, Homeobox Transcription Factor Nanog; **HB-EGF**, Heparin Binding EGF Like Growth Factor; **Cb1**, Cannabinoid Receptor 1; **EC**, Endothelial Cell; **NO**, Nitric Oxide; **bFGF**, Fibroblast Growth Factor 2; **IFN**, Interferon; **Le**, Luminal epithelium; **Ge**, glandular epithelium; **S**, stroma; **CE**, Catechol Estrogen; **LIF**, Leukemia Inhibitory Factor; **ER**, Estrogen Receptor; **PR**, Progesterone Receptor; **HMG-CoA reductase**, 3-Hydroxy-3-Methylglutaryl-CoA Reductase; **HDL**, High

Density Lipoprotein; **LDL**, Low Density Lipoprotein; **SR-B1**, Scavenger Receptor Class B Member 1; **OMM**, Outer Mitochondrial Membrane; **IMM**, Inner Mitochondrial Membrane; **STAR**, Steroidogenic Acute Regulatory Protein; **CYP11A1**, Cytochrome P450 Family 11 Subfamily A Member 1; 3βHSD, **HSD3B**; 3β-hydroxysteroid dehydrogenase; **AKR1C1**, Aldo-Keto Reductase Family 1, Member C1 (Dihydrodiol Dehydrogenase 1; 20-Alpha (3-Alpha)-Hydroxysteroid Dehydrogenase); **Notch1**, Translocation-Associated Notch Protein TAN-1; **GPCR**, G Protein-Coupled Receptor; **Nodal**, Nodal Growth Differentiation Factor; **TGFβ**, Transforming Growth Factor Beta 1; **BMP**; Bone Morphogenetic Protein; **Sox17**, Sex Determining Region Y-Box 17; **AFP**, Alpha Fetoprotein; **c-fos**, Fos Proto-Oncogene AP-1 Transcription Factor Subunit; **TNF**, Tumor Necrosis Factor; **NF-κβ**, Nuclear Factor Kappa B Subunit 1; **CAAT**, Nuclear Transcription Factor Y Subunit Beta; **AP-1**, Jun Proto-Oncogene, AP-1 Transcription Factor Subunit; **Cx43**, Gap Junction Protein Alpha 1; **PLC**, Phospholipase C; **IP3**, Inositol 1,4,5-Trisphosphate; **DAG**, Diacylglycerol; **LPS**, Lipopolysaccharide; **CYP21**, Cytochrome P450 Family 21 Subfamily A Member 2; **CYP19**, Cytochrome P450 Family 19 Subfamily A Member 1; **Dax1**, Nuclear Receptor Subfamily 0 Group B Member 1; **HPG**, Hypothalamus Pituitary Gonadotropin; **ATR**, Rad3-related protein; **Bscl2 seipin**, Berardinelli–Seip congenital lipodystrophy type 2; **DAPI**, 4',6-diamino-2-phenylindole; **ER**, endoplasmic reticulum; **H3K9me3**, histone H3 trimethylated at lysine 9; **HRP**, horseradish peroxidase**;** **ISEL+**, in situ end-labeling plus; **mES**, mouse embryonic stem; **PA-PLA1**, phosphatidic acid-preferring phospholipase A1; **PNA**, peanut agglutinin; **PND**, postnatal day; **PRM1/2**, protamines 1 and 2; **SERCA**, sarco/ER Ca2+-ATPase; **SSC**, saline-sodium citrate; **SYCP1/3**, synaptonemal complex proteins 1 and 3; **RhoA**, Ras Homolog Family Member A; **TRPML1/ Mcoln1**, Transient receptor potential cation channel, Mucolipin subfamily, member 1.; **NPC**, Niemann–

Pick's disease type C; **PCNA**, Proliferating Cell Nuclear Antigen; **LC3/MAP1LC3A**, Microtubule Associated Protein 1 Light Chain 3 Alpha; **α-SMA/ACTA2**; Actin, Alpha 2, Smooth Muscle.; **HSP60/HSPD1**, Heat Shock Protein Family D (Hsp60) Member 1, Heat Shock 60kDa Protein 1 (Chaperonin); VDAC/VDAC1, Voltage Dependent Anion Channel 1, Outer Mitochondrial Membrane Protein Porin 1; **ECM**, Extracellular matrix; **SER**, Smooth Endoplasmic Reticulum; **Pgr**, Progesterone Receptor, **eCG**, equine Chorionic Gonadotropin; **WT**, Wildtype; **DEHP**, Bis(2-ethylhexyl) phthalate (di-2-ethylhexyl phthalate, diethylhexyl phthalate,; dioctyl phthalate, DOP.

CHAPTER 1

INTRODUCTION AND LITERATURE REVIEW

Reproduction is essential for the continuation of every species. Mammalian reproduction requires both male and female partners. The male provides the sperm cell which delivers the male genome. This sperm cell is produced during a complicated developmental process called spermatogenesis. On the other hand, the female provides the oocyte in addition to carrying the fertilized oocyte during pregnancy in a specialized organ, the uterus which provides the critical environment required for development of the fertilized oocyte into a whole new organism. In this chapter, I review the literature to provide more details about the process of spermatogenesis, meiotic prophase I, male-specific meiotic arrest, spermiogenesis, chromatin remodeling during spermatogenesis, hormonal changes in spermatogenesis and regulation of spermatogenesis by apoptotic cell death. Then I will provide review of the literature about the key events during pregnancy in female mice including ovulation, fertilization, embryo transport, establishment of uterine receptivity, embryo implantation, decidualization, embryo development, placentation, and parturition. This chapter ends by review of the endocrine changes during puberty and cellular and molecular biomarkers for puberty.

1.1 **Mammalian Spermatogenesis**

Mammalian spermatogenesis is a complex developmental process during which spermatogonial stem cells differentiate into spermatozoa capable of motility. Sperm are produced in a specialized organ; the testis. The testis produces sperm indefinitely throughout the animal

life. The testis has different types of cells that interact and provide the environment for sperm production throughout life.

Cell Types of the Testis

The mammalian testis consists of long seminiferous tubules which have two types of cells for the ultimate goal of sperm production; somatic cells and germ cells. Somatic cells include Sertoli cells which are located in the outermost portion of the tubules. Sertoli cells have pyramidal to oval nucleus and a prominent nucleolus. It has a large branched cytoplasm. Unlike germ cells, they do not divide or proliferate after puberty. Sertoli cells provide nutrition and support for the developing germ cells. Another major physiological role of Sertoli cells is to separate the basal from the luminal compartments through their tight junctions (compartmentalization). The basal compartment contains diploid spermatogonia. They start to proliferate and produce haploid cells, Sertoli cells keep both populations of cells isolated for the sensitive nature of spermatogonial stem cells. Sertoli cells also control the release of spermatozoa into the lumen (Spermiation), secretion of proteins and growth factors, and phagocytosis of foreign material. Sertoli cells also form the blood-testis barrier. They also transmit androgenic signals to the developing germ cells. Sertoli cells respond to testosterone, FSH, Anti-Mullerian hormone and inhibin. Peritubular Myoid Cells produce peristaltic movement to move the non-motile spermatozoa released from Sertoli cells in the direction of the efferent ductules. Leydig Cells or Interstitial Cells mediate endocrine signals from the pituitary to the testis. They also produce testosterone upon LH stimulation. These cells are close to blood supply. Testosterone is a steroid so Leydig cells have large part of the smooth ER to aid in testosterone production [1, 2]. Germ cells include Spermatogonial Stem Cells which are the first key type of germ cells. There are three types of spermatogonial stem cells: A, Intermediate and B

spermatogonia. They are characterized by self-renewal as they continuously proliferate and differentiate into other germ cell types. Spermatogonia are diploid, have round nucleus, positioned in the basal compartment and covered by Sertoli cells. Primary spermatocytes are the second type of cells. Spermatogonial stem cells "also called A_s spermatogonia" undergo mitotic cell division to produce B spermatogonia which undergo the last mitotic division to produce primary preleptotene spermatocytes. Primary spermatocytes have round nucleus with evident chromatin. They enter meiosis which lasts for 14 days in the mouse. The process of meiosis includes Meiosis I in which 4n cells divide leading to formation of Secondary Spermatocytes (2n) that enter meiosis II to produce Haploid Round Spermatids (n) [3].

Meiosis, Meiotic Prophase I and Male-Specific Meiotic Arrest

DNA is duplicated during the S phase in preleptotene spermatocytes, this is followed by G2 phase called meiotic prophase I, a critical phase during which several critical events of spermatogenesis occur [4]. The meiotic prophase I is divided into several stages, Leptonema stage characterized by chromatin condensation and introduction of DNA double strand breaks (DSB) in the genome by the enzyme SPO11 [4]. Zygonema stage is characterized by initiation of synapsis between homologous chromosomes. During, pachynema stage, full synapsis of homologous chromosomes occurs, this synapsis is facilitated by synaptonemal complex proteins (SYCP) which include SYCP1 (Axial element) and SYCP3 (lateral element). The X and Y chromosomes are non-homologous thus they fail to synapse. This triggers recruitment of γ-H2AX, BRCA1 and ATR proteins to silence the Y chromosome in a process called meiotic sex chromosome inactivation MSCI [4]. During the late pachynema stage, visible cross over sites called chiasmata are evident, formation of chiasmata is important for meiotic recombination between chromosomes which results in genetic diversity [4]. Formation of these chiasmata is

dependent on introduction of DNA double strand breaks, homologue recognition and synapsis between homologous chromosomes, so these processes are the most critical events in spermatogenesis. When autosomes fail to synapse, γ-H2AX, BRCA1 and ATR are recruited from sex chromosomes to silence autosomes (Meiotic silencing of unsnapped chromosomes; MSUC) and this leads to failure of MSCI, which triggers stage IV meiotic arrest in spermatocytes and apoptotic cell death of spermatocytes [4]. DSB "which are introduced naturally during the leptotene stage by the enzyme SPO11" are introduced with the aim of creating recombination and genetic diversity which benefits future generations adapt to their environments. Defective DNA DSB processing leads to defective pairing and synapsis of homologous chromosomes, so from evolutionary perspective, spermatocytes with defective pairing and synapsis in their chromosomes must not develop into sperm which may fertilize an oocyte and have dire consequences on future generations such as genetic diseases aneuploidy and polyploidy. This makes MSCI a critical process to ensure fidelity of meiotic cell division.

Spermiogenesis

Once meiosis is complete, spermatocytes enters spermiogenesis, a process in which the nucleus elongates, chromatin condenses, and cell size decreases to finally form elongated mature haploid spermatozoa. Spermiogenesis or differentiation of spermatids involves four steps that involve Golgi apparatus, capping, acrosomal and maturation. Golgi apparatus is important for spermiogenesis as it produces vesicles and granules containing enzymes necessary for the acrosomal reaction. Capping (in steps 4-5 spermatids) is the process in which the vesicles form a cap over the nucleus. In step 8 spermatid which is the last round spermatid stage, the acrosome covers almost 1/3 of the nucleus. Acrosomal steps in which the acrosome migrates over the ventral system of the elongating spermatid nucleus and the chromatin continues to condense.

Maturation in which the nucleus continues to condense and the acrosome matures until it covers all the nucleus, excess cytoplasm is removed into residual bodies.

Chromatin Remodeling

In the sperm nucleus, chromatin remodeling is the process during which histone proteins are replaced by transition proteins, then replaced by protamine proteins [4]. This process is critical to stop active gene transcription in the sperm nucleus. Mice mutant for PYGO2 (Pygopus Family PHD Finger 2) which is involved in histone acetylation and SSTK (Testis Specific Serine Kinase 6) involved in histone phosphorylation show defects in chromatin condensation and male infertility. Haploinsufficiency for Protamine 1 or Protamine 2 also cause male infertility. Posttranslational modifications in protamines by CAMK4 (Calcium/Calmodulin Dependent Protein Kinase IV) kinase are essential for male fertility and *Camk4* null mice are infertile. This indicates that chromatin condensation and remodeling are essential for spermatogenesis [4]. Spermiation is the release of spermatozoa into the lumen of the tubules. Spermatozoa acquire motility and become capacitated and ready to fertilize the egg. The expression of several genes is necessary for spermatogenesis to complete for example, *Jsd, c-kit, Daz1, Boule, Cdc25, CREM* and protamine. The cellular and hormonal environment in the testis play crucial role for maintaining spermatogenesis. For example, the physical environment, soluble factors and cell adhesion molecules. Testis temperature plays a role correlated to the rate of spermatogenesis. Sperms cannot mature at normal body temperature because spermatogenic DNA polymerase β and recombinase activities have unique optimum temperature [2, 5]. After the completion of spermatogenesis, all stages of sperm production can be seen in the adult seminiferous tubules, which can be classified into different stages according to the cell associations in the seminiferous tubules.

Hormonal Environment Necessary for Spermatogenesis

Several hormones are necessary to provide a suitable environment in the seminiferous tubules to finally produce viable sperms. Testosterone secreted by Leydig cells promotes Sertoli cell functions and maintains spermatogenesis. Inhibin decreases FSH levels in the male. FSH has been reported to regulate type A spermatogonial mitotic division and induction of type A spermatogonia to proliferate. FSH is also required for Sertoli cell function. LH increases testosterone production by Leydig cells. The interplay between these signals is important for spermatogenesis.

Molecular Regulation of Spermatogenesis by Apoptotic Cell Death

Throughout development, structures that are no longer needed are eliminated by apoptosis, the process of programmed cell death. Apoptosis is characterized by membrane blabbing, nuclear condensation and DNA fragmentation into 185 bp fragments with no inflammation involved in the process. This is characteristic from necrotic or pathological cell death characterized by severe inflammatory process. Apoptotic cell contents are accurately engulfed to prevent leakage in the cellular environment. There are two pathways for apoptotic cell death. The extrinsic pathway or death receptor pathway is triggered by tumor necrosis factor receptor family activated by ligands such as FASL, leading to activation of caspases 8 and 10 and formation of death receptor signaling complex. The intrinsic pathway or the mitochondrial pathways is activated in response to cellular stress such as reactive oxygen species ROS, hypoxia, irradiation and it is regulated by the BCL2 family of proteins [6]. Germ cell apoptosis plays a crucial role in determining the total number of sperms produced. Sertoli cells have limited capacity to support germ cells so excess germ cells must die by apoptosis. Apoptosis in the testis occurs during mitotic division and during meiosis. During migration of primordial germ

cells, cells that show aberrant migration die by apoptosis. After Gonocytes differentiate into spermatogonia, the first wave of apoptosis occurs. This wave affects spermatogonia and spermatocytes to eliminate excess pre-meiotic spermatogonia. This wave involves different caspases such as caspases 2, 3, 8 and 9, so both intrinsic and extrinsic pathways of apoptosis are involved [6-8]. Apoptosis does not only occur to limit the number of germ cells supported by the limited number of Sertoli cells. Apoptosis occurs to eliminate germ cells with aberrant DNA. During the meiotic metaphase of spermatogenesis, some DNA strand breaks occur in spermatocytes. There are checkpoints that induce apoptosis in these spermatocytes with defective unrepaired DNA [8]. In some cases, apoptosis becomes deregulated and this causes infertility in males. Disruption of the hormonal environment of germ cell, exposure to toxins or radiation can increase germ cell apoptosis. Deregulation of apoptosis related genes such as proapoptotic or antiapoptotic genes will have profound effect on germ cells and sperm output. High levels of the ratio of proapoptotic to antiapoptotic genes can lead to infertility. Bcl-w is an antiapoptotic member of the Bcl2 family and appears to be important for spermatogonia and spermatocytes. The tumor suppressor protein p53 is involved in radiation-induced germ cell apoptosis. CREM also plays a role in germ cell apoptosis [9]. Apoptosis is a tightly regulated process. GnRH and FSH put brakes on apoptosis of germ cells mainly in spermatocytes and spermatids. Testosterone also plays a role in regulating germ cell apoptosis. Withdrawal of testosterone causes higher levels of apoptosis in spermatocytes and spermatids. Testosterone under some circumstances is a proapoptotic factor [8]. Apoptosis also occurs in spermatozoa. It has been reported that spermatozoa exhibit high levels of DNA fragmentation. This kind of DNA damage in spermatozoa has been connected to impaired fertilization, poor implantation rates, disruption of preimplantation embryonic development and miscarriages [6]. Apoptosis mediated DNA damage

in spermatozoa can result in mutations in the offspring as well. Spermatozoa with defective or unrepaired DNA are removed by apoptosis, which makes functional sense in order to disable defective spermatozoa and prevent passage of such defective DNA to subsequent generations. Apoptosis also contributes to the phagocytosis of defective and unviable spermatozoa by exposure of phosphatidyl serine on their membrane surfaces to signal their engulfment by phagocytes.

1.2 The Key Events During Pregnancy

The creation of new life in the uterus of the female begins by fertilization between an egg and a sperm. Ovulation results in release of a viable egg ready for fertilization by sperm.

Ovulation

The ovary develops around 9.5 d.p.c in the mouse. At that time primordial germ cells which will become oocytes migrate to the genital ridges. The oocytes divide mitotically and provide the oocyte pool that the female will have for the rest of her life. Oogonia enter meiosis and proceed to the first meiotic prophase then meiosis is arrested. The female mouse reaches sexual maturity at 6 weeks of age. Ovulation in the mouse occurs every four days. Follicles respond to the increase in FSH levels from the pituitary gland. Stimulated follicle cells lose contact with the oocyte, synthesize proteoglycans and plasminogen activator, accumulates fluids and moves toward the periphery of the ovary to become ready for releasing the oocyte. The fluid filled follicles are also called Graffian follicles. A surge in LH that coincides with estrus stage in the mouse can also stimulate ovulation by triggering the oocyte nucleus to lose the membrane, chromosomal assembly, release of polar body and the rest remains in metaphase II. The oocyte is then released from the follicle. The ovulated oocyte is surrounded by the Zona and the cumulus cells and the follicle develops into corpus luteum which produces the pregnancy hormone

Progesterone (P4). Ovulated oocytes are driven and attracted into the infundibulum of the oviduct by the action of cilia on the surface of the oviduct epithelial cells. Naturally 8-12 oocytes are released. After release of the oocyte, follicle cells in the ovary differentiate into luteinizing granulosa cells which secrete steroids essential for maintaining pregnancy [10]. Once the ovum has been released into the reproductive tract of the female and sperm are present at the same time in the female reproductive tract, fertilization can occur.

Fertilization

Fertilization is the ultimate process of sperm and egg fusion. Fertilization occurs in the ampulla of the oviduct [11]. The haploid nuclei of the sperm and the egg fuse to form a diploid nucleus of the zygote. The sperm has to pass through the *Zona pellucida* of the egg then fuse with the cell membrane of the egg. The sperm has to be capacitated in the reproductive tract of the female. The acidic environment of the vagina activates adenylate cyclase enzyme in the cytosol of the sperm cell which then produces cAMP, which initiates a sequence of events in the sperm including alteration of the lipid and glycoprotein composition of the plasma membrane, enhancing metabolism and sperm motility, and decreasing the membrane potential to become hyperpolarized [12]. The mammalian egg is surrounded by an outer layer of 5000 cumulus cells and an inner layer of thick extracellular matrix or the *Zona pellucida* [13]. In order to penetrate the cumulus, sperms depend on their motility and the activity of glycosylphosphatidyl inositol – anchored surface hyaluronidase enzyme. The sperm reach the *Zona pellucida* which has three glycoproteins: ZP1, ZP2 and ZP3. Once the sperm binds to the zona, it releases the contents of the acrosome. Binding of the sperm to ZP3 induces a signaling cascade involving phospholipase C activation and elevation of cytoplasmic calcium concentrations leading to exocytosis of the acrosome contents. Sperm motility, proteases and glycosidase are involved in this process. After

penetrating the zona, the sperm binds to the plasma membrane of the egg. Sperm proteins involved in this process include ferritin and cyritestin. Egg surface proteins that have been postulated to play a role in sperm egg interaction include CD9 and proteins with a GPI anchor [13]. Recently, an egg surface folate receptor protein JUNO has been discovered to be the egg receptor for the essential sperm surface protein IZUMO1. Female mice lacking Juno are infertile and JUNO-deficient eggs do not fuse with sperms [14]. To ensure that only one sperm fertilizes an egg and to avoid polyspermy, the egg's plasma membrane depolarizes soon after the first sperm binds. Binding of the sperm also causes elevation of cytosolic calcium concentrations and the cortical granules release their contents by exocytosis. These contents include enzymes that harden the zona to prevent other sperms from passing thorough. The fertilized egg is now called a zygote. Fertilization is complete when the two haploid nuclei fuse to form a diploid nucleus. The sperm contributes the centriole to the zygote.

Preimplantation Embryo Development

After fertilization which occurs around d.p.c 0.5 in mice, on d.p.c 1.5, the zygote or the fertilized egg divides to form the two-cell stage embryo, which becomes 4 cells on d.p.c 2, on d.p.c 2.5, 8-cell un-compacted embryo forms, on d.p.c 3 the morula or 8-16 cell stage forms which becomes a blastocyst [11]. The blastocyst has three types of cells, the trophectoderm or the outer epithelium, the primitive ectoderm, and the inner cell mass. The trophectoderm cells are the first cells that make contact with the uterus luminal epithelial cells. Zygotic genome activation is an important process that occurs after fertilization to switch from maternal to embryonic gene expression that controls later developmental programs in the embryo. There are two waves of zygotic genome activation, the first occurs around 2-4 cell stages, and the second is called the mid-preimplantation genome activation that occurs in the 8 cell to morula stages.

Several genes are critical for cell-fate and lineage differentiation during this stage for example, *Cdx2, Oct4, Gata* and *Nanog* [11]. The embryo then gets out from the *zona pellucida* and cells differentiate into epiblast and primitive ectoderm.

Embryo Transport

The early embryo is transported through the oviduct by the ciliary motion of the fimbria. Within the oviduct, smooth muscles of the oviduct wall also contract to induce movement of the early embryo [15]. When the embryo reaches the isthmus-ampulla junction, it resides for three days then the embryo continues movement into the uterus by the help of the waves of contraction and relaxation of the muscularis layer of the oviduct [16]. Sympathetic neuronal control through the direction of ovarian hormones regulates the transport of embryos through the oviduct to the uterus by controlling the opening and closure of the sphincter of the isthmus uterus junction [16]. During pregnancy, progesterone levels secreted from the newly formed corpus luteum increase, this causes the levels of noradrenaline to drop. Also, under the influence of progesterone hormone, the sensitivity of the β-adrenergic receptors in the circular smooth muscles of the oviduct isthmus increases leading to muscle relaxation and transport of embryos through the oviduct [16].

Embryo Implantation

The window of implantation is the time period during which the uterus is receptive to implant a competent blastocyst. The competency is achieved by activation of HB-EGF, expression of Cb1 in the trophectoderm and synthesis of anandamide (the ligand) in the uterus [11]. Implantation involves three main processes which are apposition of the blastocyst to the uterine luminal epithelial cells, penetration into the luminal epithelial cells and trophoblast

invasion into the uterine stromal cells. During implantation, the trophectoderm cells of the competent blastocyst attach to the endometrial stromal cells. In mice, the attachment of the trophectoderm cells to the luminal epithelial cells of the uterus is accompanied by apoptosis of luminal epithelial cells at the site to facilitate penetration of the trophoblast cells into the stromal cells of the uterus [11]. Implantation of the blastocyst requires that the uterus becomes receptive to implantation. The window of implantation and uterine receptivity is a short period of time during which the environment of the uterus is helpful to implant the blastocyst. In mice, the uterus is prereceptive to implantation on days 1 to 3, it becomes receptive on day 4 and unreceptive on day 5 [11]. Implantation is accompanied by high levels of vascular permeability of uterine stromal cells and angiogenesis which are hallmarks of implantation. This increased vascular permeability can be seen by the injection of blue dye that label implantation sites. Implantation requires apposition of the blastocyst to the uterine wall, adhesion and penetration. Close apposition of the blastocyst with the uterine wall is achieved by uterine edema and luminal closure [17]. Penetration is the process in which the implanting blastocyst invades the luminal epithelial cells into the stromal cells of the uterus. Stromal cells then differentiate into decidual cells. Steroid hormones such as progesterone stimulate decidualization to support embryo growth and maintain pregnancy.

Steroid Hormones in Uterine Receptivity

Endocrine hormones progesterone (P4) and estrogen (E2) play important roles in determining uterine receptivity and maintaining pregnancy. A Luteinizing hormone surge from the pituitary is required to initiate ovulation and secretion of estrogen and progesterone from the ovary [17]. Several molecular programs are required to initiate uterine receptivity, for example, steroid hormones, lipid signals and cytokines. E2 induces proliferation of luminal epithelial cells

however proliferation of stromal cells requires both E2 and P4 [17]. In mice, on days 1-2, E2 causes proliferation of luminal epithelial cells. On day 3, P4 produced from the *Corpus luteum* induces stromal cell proliferation as well. Epithelial cells stop proliferation and become differentiated on day 4 which is a hallmark of implantation.

Decidualization

The attachment of the blastocyst to the uterine luminal epithelial cells triggers decidualization of stromal cells into decidual cells to support embryo growth and maintain pregnancy. These changes are triggered by P4 and primed by E2. After embryo implantation, decidual cells proliferate, increase in size, become polyploid, edematous, and finally die by apoptosis to allow for placenta development. The decidual cells regress by D10.5. The role of the decidua is to secrete growth factors, cytokines, regulate trophoblast invasion and support blood vessel formation to nourish the implanted embryo [18].

Regulation of Decidualization by Steroid Hormones

The uterus must be primed by E2 and P4 for decidualization to occur. Decidualization depends on the high levels of E2 during the estrus stage, the levels of P4 and the surge of estrogen that occurs on the fourth day of gestation. This E2 surge leads to uterine expression of leukemia inhibitory factor *Lif*, a cytokine essential for implantation [10]. E2 and P4 act through their nuclear receptors ER and PR respectively, which are transcription factors that regulate expression of their target genes. P4 is essential for induction of decidualization in the uterus as $PR^{-/-}$ mice are resistant to physical deciduogenic agents as intrauterine injection of oil [19]. E2 is also required to induce decidualization since $Er\alpha^{-/-}$ mice fail to show decidualization after stimulation. When endometrial stromal cells do not respond to progesterone stimulation of decidualization, uterine dysfunctions such as endometriosis can occur. Dysregulation of E2

synthesis and metabolism also contribute to improper decidualization and hence endometriosis [18]. This indicates that regulated decidualization is an important process that can be involved in pathological conditions which might affect female fertility.

1.3 Parturition

Throughout pregnancy, the uterus is in state of quiescence as it is unresponsive to stimuli, this is followed by activation and modulation of signaling pathways that cause the uterus to respond to stimuli of contraction, leading to coordinated and active contractions that lead to delivery of the fetus [20]. Studies in animal models indicated that progesterone is a presentational hormone that is required for maintenance of pregnancy, it activates genes that keep the uterus relaxed and suppresses genes that activate uterine contractility. It was shown that withdrawal of progesterone was essential to cause uterine events leading to delivery of the fetus [20, 21]. This indicated that progesterone stimulates the relaxant pathways and suppresses the contractile pathways [20]. Progesterone also inhibits binding of oxytocin which is a potent contractile agent to its receptor. Inflammatory state and immune system changes accompany labor as well. Elevation of serum interleukin 1β levels, TNF-α, also accompany labor. Signaling pathways involving the transcription factor NF-κβ, CAAT enhancer binding protein isoform, activator protein-1 (AP-1), and specificity protein-1 (Sp-1) are activated by the proinflammatory signals during labor. This indicates strong association between immune system activation and parturition. Parturition requires strong myometrial contractions. The expression of several ion channels is required to result in increased intracellular calcium levels leading to muscle contractions. Also as parturition approaches, there is increase in the gap junctional protein connexin 43 (Cx43) and other gap junction channels all of which contribute to facilitating the spread of the rising calcium levels across all cells to aid in muscle contraction. GPCRs also play

important roles in this event to increase intracellular calcium levels and increase the sensitivity of contractile cells to calcium as well.

The Role of the Cervix in Parturition

The cervix plays an important role in the process of parturition and the morphological changes that occur in the cervix are hallmarks of parturition. During pregnancy, the cervix is a rigid cylindrical organ due to the high content of type I and type III collagen. At the end of pregnancy, cervical ripening due to changes in its connective tissue occurs, a process in which the cervix becomes soft and distensible [20]. At parturition, there's increased expression of matrix metalloproteinase which leads to breakdown of the collagen matrix, increase in water, glycosaminoglycan and hyaluronan contents of the cervix. In mice, this process of cervical ripening starts during mid- gestation E10-12 and culminates during the last two days of gestation which is accompanied by infiltration of neutrophils and immune cells into cervical tissue. This has been proven also through the observation that intrauterine application of lipopolysaccharide LPS leads to infiltration of immune cells in the cervical matrix [20].

1.4 Endocrine Changes During Puberty and Indicators/Markers for Puberty Across Species

Puberty is a process of maturation of the hypothalamus-pituitary-gonadal axis, which leads to stimulation of growth and development of the genitals, physical and psychological changes for the ultimate capacity to reproduce [22]. Pituitary gonadotropins LH, FSH play important roles in puberty development. These gonadotropins are released in a pulsatile manner throughout development in humans. The onset of puberty in humans occurs after activation of the hypothalamus-pituitary axis. The activation leads to increased LH secretion leading to secretion of sex hormones. In boys, bound and free testosterone and estradiol concentrations

increase in the middle of puberty. In girls, estradiol concentrations increase after breast stage 3. In boys and girls, estradiol comes from the aromatization of testosterone in adipose tissue [23]. In boys, pubic, axillary, facial hair, phallic enlargement, increase in muscle mass, and epiphyseal closure are due to increased androgen concentrations which are produced by the testes and a small amount from the adrenal glands. In girls, breast development, fat distribution, vaginal and uterine development are due to increased estrogen concentrations produced by the ovary [24]. Negative feedback mechanism occurs in which ovarian and testicular steroids inhibit LH and FSH secretion by the pituitary. In females, estrogen can have a positive feedback on LH secretion and this is augmented by progesterone which results in a pre-ovulatory surge in LH and FSH [24]. During the menstrual cycle in females, serum LH, FSH, estradiol and progesterone change cyclically. FSH levels increase leading to growth of the ovarian follicle which secretes estradiol. When estradiol levels reach a threshold, it triggers release of larger amounts of LH and FSH from the pituitary leading to ovulation. The increased progesterone and estrogen levels inhibit FSH and LH release from the pituitary via a negative feedback mechanism. When the corpus luteum degrades, levels of progesterone and estradiol drop leading to loss of the negative feedback on the pituitary and release of LH and FSH again [24]. In human markers can be used to assess puberty onset for example the sexual maturity scale. In girls, this scale includes age at breast development, pubic hair developmental stage, and age at menarche. In boys, physical markers include voice change, increase in testes size, and age at ejaculation. Other physical markers include skeletal growth, changes in body mass index, and increase in body fat mass with decrease in body fat percentage [25]. Genetic biomarkers of puberty include sequence variants at various susceptibility loci in the steroidogenic enzyme gene CYP21 which were associated with pubarche [25]. CYP19 aromatase which converts androgens to estrogens is also a genetic

marker of pubertal development. *Dax1* mutations have been associated with pubarche in males, and type II 3-β hydroxyl steroid dehydrogenase associated with pubarche in females. Mutations in the LH receptor are associated with pubarche in boys. This indicates that genetic variants, and potentially single nucleotide polymorphisms can be used as markers of puberty in boys and girls [25]. Biomarkers of bone growth and mineralization can also be useful indicators of puberty changes. For example some studies found correlation between presence of the bone resorption marker collagen type I N-telopeptides in urine and growth changes in males and females during puberty [25]. Hormonal levels are also very important markers of puberty. GnRH is the main hormone involved in puberty as it stimulates FSH and LH secretions from the pituitary gland. But it is difficult to measure GnRH levels due to its short half-life which is 4-8 minutes. The onset of puberty is marked by increased LH secretion. In males, anti-Mullerian hormone can be used to mark puberty as males with delayed puberty have elevated levels of this hormone. Inhibins are produced by gonads and they suppress FSH secretions. Some studies found that serum Inhibin B levels were markers of presence of spermatozoa. Leptin produced by adipocytes is also an important marker for puberty onset and regulates energy homeostasis and food uptake. In boys, at the onset of puberty, leptin concentrations increase then rapidly decrease to pre-pubertal levels, but it continues to increase in girls [25]. In boys, spermarche is indicated by presence of sperms in urine also called spermaturia, and can be used as marker of puberty. Maturation and activation of the HPG axis, growth of the reproductive systems and presentation of some behaviors as genital self-grooming are markers of puberty in rodents [26]. In female rats, serum LH and estradiol levels increase from PND21 to PND35. The first ovulation and vaginal opening occur simultaneously in female rats and these can be used to indicate puberty onset. In males, sperm production, increase in serum testosterone levels and preputial separation

are used to indicate puberty onset. There are differences in these parameters between different strains of rodents. Neuroendocrine changes in rodents are associated with some physical indicators of puberty, for example the day of vaginal opening and first ovulation around PND35 and preputial separation and appearance of sperms in the epididymis around PND42 [26].

1.5 Hypothesis and Specific Aims

This dissertation shows the critical role for *Bscl2* in male fertility, parturition and female mammary gland development. The main hypothesis of the dissertation is that *Bscl2* is critical for fertility in mammals, this hypothesis is tested in specific aims. The first specific aim is to investigate the molecular mechanisms of the *Bscl2* gene in male fertility. *Bscl2* gene encoding seipin protein is highly expressed in brain, testis and adipose tissue. Seipin is highly and specifically expressed in round spermatids, and mammary gland luminal epithelium. It has important roles in adipose tissue development. However, its roles in the testis and spermatogenesis are not know. It was found that *Bscl2*$^{-/-}$ males are infertile. A new study showed that *Bscl2* deficiency led to teratozoospermia and male infertility due to impaired phospholipid homeostasis [27]. However, other roles of *Bscl2* in germ cell apoptosis, chromatin integrity and DNA integrity of germ cells are largely unexplored. It was previously shown that *Bscl2* was upregulated upon exposure of mES to genotoxic agents, indicating interaction between *Bscl2* and DNA damage response pathway. In the second chapter, we hypothesize a critical role for *Bscl2* in germ cell apoptosis and aim to study the role of seipin in male fertility using *Bscl2*$^{-/-}$ male mouse mode. The second specific aim is to investigate the roles of *Bscl2* in mammary gland development. *Bscl2* is highly expressed in mammary luminal epithelium and *Bscl2* deficiency results in increased endoplasmic reticulum stress, and apoptosis of mammary luminal epithelium leading to failure of lactation. The third specific aim examines *Bscl2* function in the process of

parturition in *Bscl2*$^{-/-}$ females since *Bscl2* is highly expressed in the uterus and myometrium on D18.5 of pregnancy and *Bscl2*-deficient females have difficulty delivering pups.

CHAPTER 2

SEIPIN DEFICIENCY INCREASES CHROMOCENTER FRAGMENTATION AND DISRUPTS ACROSOME FORMATION LEADING TO MALE INFERTILITY

Ahmed E. El Zowalaty, Claudia Baumann, Rong Li, Weiqin Chen, Rabindranath De La Fuente, and Xiaoqin Ye, *Cell death & disease* 6.7 (2015): e1817. Reprinted here with permission of publisher.

2.1 Abstract

The Berardinelli-Seip congenital lipodystrophy 2 (*Bscl2*, seipin) gene is involved in adipogenesis. *Bscl2*$^{-/-}$ males were infertile but had normal mating behavior. Both *Bscl2*$^{-/-}$ cauda epididymis sperm count and sperm motility were ~20x less than control. *Bscl2*$^{-/-}$ seminiferous tubules had relatively normal presence of spermatogonia and spermatocytes, but reduced spermatids and sperm. Spatiotemporal expression analyses in *Bscl2*$^{+/+}$ testes demonstrated prominent *Bscl2* transcriptional activity in spermatocytes with a plateau reached around postnatal day 28. Seipin protein localization was most abundant in postmeiotic spermatids, suggesting translational repression of *Bscl2* mRNA in spermatocytes. ISEL^{+} detected increased spermatid apoptosis in *Bscl2*$^{-/-}$ testis and annexin V detected increased percentage of positive *Bscl2*$^{-/-}$ round spermatids compared to control. Immunofluorescence of marker proteins SYCP3, SYCP1 and H3K9me3 in germ cell spreads detected normal meiotic chromosome pairing and homologous chromosome synapsis in *Bscl2*$^{-/-}$ spermatocytes, but significantly increased percentages of round spermatids with chromocenter fragmentation, and late spermatids and sperm with chromatin vacuoles, indicating defective chromatin condensation in *Bscl2*$^{-/-}$ spermatids. *Bscl2*$^{-/-}$ late spermatids were disorganized within the seminiferous epithelium, despite normal appearance of Sertoli cells detected by vimentin immunofluorescence. Peanut agglutinin (PNA) staining revealed various abnormalities of acrosomes in *Bscl2*$^{-/-}$ late spermatids, including absence, irregular-shaped, and fragmented acrosomes, indicating defective acrosome formation in *Bscl2*$^{-/-}$ late spermatids, which may affect late spermatid orientation in the seminiferous epithelium. Mitotracker strongly stained the midpiece of control sperm but only very weakly labeled the midpiece of *Bscl2*$^{-/-}$ sperm, indicating defective mitochondrial activity that most likely contributed to reduced *Bscl2*$^{-/-}$ sperm motility. These data demonstrate novel roles of seipin in

spermatid chromatin integrity, acrosome formation, and mitochondrial activity. Increased spermatid apoptosis, increased chromocenter fragmentation, defective chromatin condensation, abnormal acrosome formation, and defective mitochondrial activity contributed to decreased sperm production and defective sperm that resulted in *Bscl2*$^{-/-}$ male infertility.

Keywords: *Bscl2*/Seipin, translational repression, chromocenter fragmentation, chromatin vacuole, spermatid apoptosis, acrosome.

2.2 Introduction

Berardinelli–Seip congenital lipodystrophy type 2 (*BSCL2*) gene encodes protein seipin J Magre, M Delepine, E Khallouf, T Gedde-Dahl, Jr., L Van Maldergem, E Sobel, J Papp, M Meier, A Megarbane, A Bachy, et al. [28]. Mutations of *BSCL2* are associated with generalized lipodystrophy characterized by a near complete absence of adipose tissue and early-onset metabolic complications, such as insulin resistance and diabetes [28-30]. Seipin is an integral endoplasmic reticulum (ER) membrane protein with two transmembrane domains, cytosolic N- and C-termini, and a central loop domain in ER lumen [31, 32]. Various adipocyte-associated functions of seipin have been proposed. It is found at ER lipid droplet junctions that are important for droplet morphology in yeast [33]. In *Drosophila*, it has been shown to promote adipose tissue fat storage via physical interactions with SERCA (sarco/endoplasmic reticulum Ca^{2+}-ATPase), which is an ER calcium pump solely responsible for transporting cytosolic calcium into the ER lumen [34]. Seipin is also reported to regulate cyclic AMP/protein kinase A (cAMP/PKA) mediated lipolysis that is essential for adipocyte maturation [35].

Besides adipose tissue, seipin is also highly expressed in the testis [27, 28, 36]. It was noticed that *Bscl2*$^{-/-}$ males were infertile during previous study of seipin-deficiency in adipose tissue loss and metabolic disorders [35]. A recent study demonstrated that *BSCL2* mutations in a

man and seipin-deficiency in mice led to teratozoospermia and male infertility due to impaired testicular phospholipid homeostasis [27].

Bscl2/seipin has been predominantly recognized for its role in adipogenesis [37, 38] and phospholipid homeostasis [27]. However, other potential roles, such as in germ cell apoptosis and maintenance of DNA integrity, have been largely unexplored. Male germ cell apoptosis is a physiological process that maintains homeostasis in the seminiferous tubules during spermatogenesis. An early wave of male germ cell apoptosis occurs during prepubertal development and is thought to keep a proper balance between germ cells and supporting Sertoli cells [39]. Germ cell apoptosis also occurs in seminiferous tubules of adult males [40] and it is estimated that ~75% of all male germ cells produced are discarded through apoptosis as a mechanism to remove aberrant and excess germ cells [7]. Interestingly, *Bscl2* was shown through transcription profiling of mouse embryonic stem (mES) cells to be transcriptionally activated upon exposure to a broad spectrum of genotoxic compounds [41]. This transcriptional activation of *Bscl2* was associated with inhibition of DNA replication and activation of the ataxia telangiectasia and Rad3-related protein (ATR) signaling pathway [42], suggesting that seipin might be involved in maintaining DNA integrity.

We aim to determine the role of seipin in male fertility using our *Bscl2*$^{-/-}$ mouse model [35]. Here we show that seipin-deficiency disrupts spermatid DNA integrity, increases spermatid apoptosis, and interferes with acrosome formation.

2.3 Results

Bscl2$^{-/-}$ male infertility due to reduced sperm production and impaired sperm motility

Two months of mating study revealed that all *Bscl2*$^{+/+}$ females (N=7) mated with *Bscl2*$^{+/+}$ males (100%) were pregnant. The average number of litters was 2.3±0.48 (N=7) and the average litter size was 8.8±3.0 (N=16 litters). However, none of the *Bscl2*$^{+/+}$ females (N=10) mated with *Bscl2*$^{-/-}$ males (N=10) became pregnant (0%), demonstrating that *Bscl2*$^{-/-}$ males were infertile (Fig. 1A). These *Bscl2*$^{-/-}$ males had normal mating activities indicated by comparable plugging rate and plugging latency with *Bscl2*$^{+/+}$ males (Fig. 1A, 1B).

At the end of the fertility test, there were 9.3% reduction of body weight and 14.3% reduction of testis weight in *Bscl2*$^{-/-}$ males (Fig. 1C, 1D). There was no significant difference in the relative testis weight (Fig. S1A). However, *Bscl2*$^{-/-}$ cauda epididymis sperm count was only ~5.4% of that from *Bscl2*$^{+/+}$ males (Fig. 1E). There was 15.8% reduction of absolute epididymis weight in *Bscl2*$^{-/-}$ males (Fig. S1B) but comparable relative epididymis weight with *Bscl2*$^{+/+}$ males (Fig. S1C). Interestingly, significantly increased absolute and relative weights of seminal vesicles and attached coagulating glands were observed in *Bscl2*$^{-/-}$ males (Fig. S1D, S1E).

Sperm motility could contribute to male infertility and was analyzed in another set of males. The average sperm count in *Bscl2*$^{-/-}$ group was ~3.3% of the control group (Fig. S1F). The average percentage of motile sperm in the same sperm preparations was ~0.4% from *Bscl2*$^{-/-}$ males and ~10.8% from control males (Fig. 1F). Sperm motility is essential for sperm transport in female reproductive tract [43]. The efficiency of sperm transport was expressed as the percentage of the uterine sperm count over the cauda epididymis sperm count of the mated male, which was ~7.5% and ~0.5% in *Bscl2*$^{+/+}$ and *Bscl2*$^{-/-}$ males, respectively (Figs. S1G, S1H, 1G). These data demonstrated reduced sperm count and defective sperm motility in *Bscl2*$^{-/-}$ males.

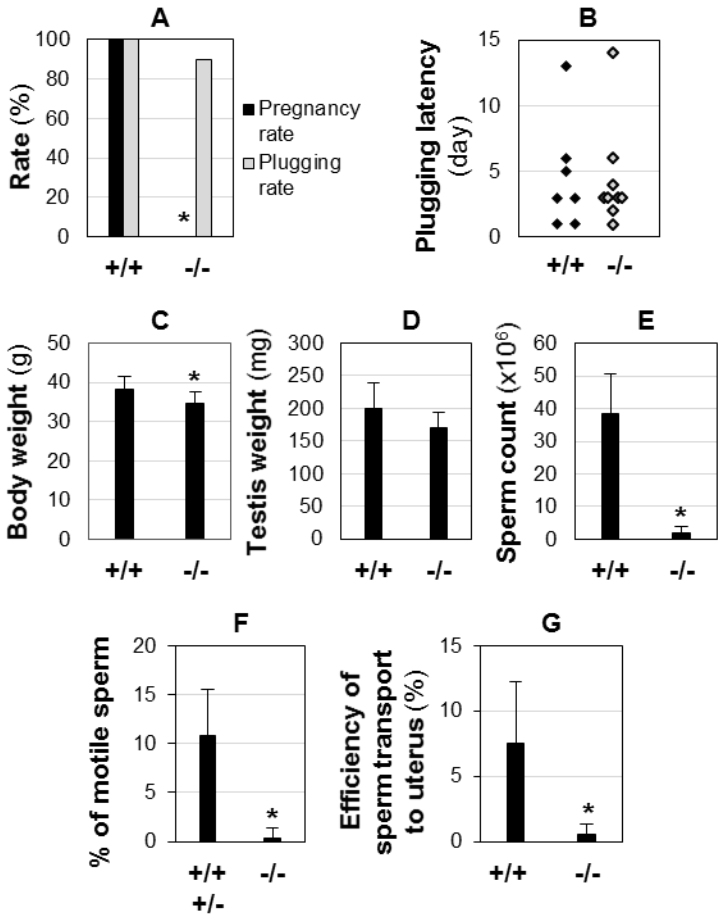

Figure 1. Male fertility test and sperm analyses. +/+, *Bscl2*$^{+/+;\ +/-}$, *Bscl2*$^{+/-;\ -/-}$, Bscl2-/-. A. Pregnancy rate and plugging rate from 2 months of fertility test. B. Plugging latency. C. Body weight. D. Testis weight. E. Sperm count from cauda epididymis. A-E: N=7 (+/+) and 10 (-/-). F. Percentage of motile sperm. N=6 (+/+ & +/-) and 9 (-/-). G. Efficiency of sperm transport to the uterus. N=5 (+/+) and 7 (-/-). Error bar, standard deviation; *, P<0.05.

Histology showing defective spermatids & spermatozoa in Bscl2$^{-/-}$ males

Testis histology showed that the seminiferous epithelial thickness of the majority seminiferous tubules in *Bscl2*$^{-/-}$ testes from PND15 to adult was comparable with their age matched *Bscl2*$^{+/+}$ control (Fig. 2A-2F). Spermatogonia and spermatocytes appeared to be comparable between *Bscl2*$^{-/-}$ and *Bscl2*$^{+/+}$ seminiferous tubules. However, the spermatids,

especially late stage spermatids in the *Bscl2*$^{-/-}$ seminiferous tubules appeared to be remarkably reduced (Fig. 2E, 2F). The elongated *Bscl2*$^{-/-}$ spermatids were often disorganized and present throughout the seminiferous epithelium (Fig. 2G-2J). The disorganized spermatids prevented accurate staging of spermatogenesis in the *Bscl2*$^{-/-}$ testes except for stages IX to XI, which lack round spermatids. There was no difference in the average number of cross-sectioned seminiferous tubules per field (20x) (Fig. S1I) or the average number of stages IX to XI seminiferous tubules (Fig. S1J) between *Bscl2*$^{+/+}$ and *Bscl2*$^{-/-}$ testes. The average number of round spermatids per seminiferous tubule was significantly reduced in *Bscl2*$^{-/-}$ testes (Fig. 2K). The cauda epididymis sperm density from *Bscl2*$^{-/-}$ males was dramatically decreased (Fig. 2L, 2M) and there were many round apoptotic cell bodies in *Bscl2*$^{-/-}$ cauda epididymis (Fig. 2M) but not *Bscl2*$^{+/+}$ cauda epididymis (Fig. 2L). Rete testis histology showed scattered germ cells that were similar as those in the cauda epididymis (Fig. 2O, 2P).

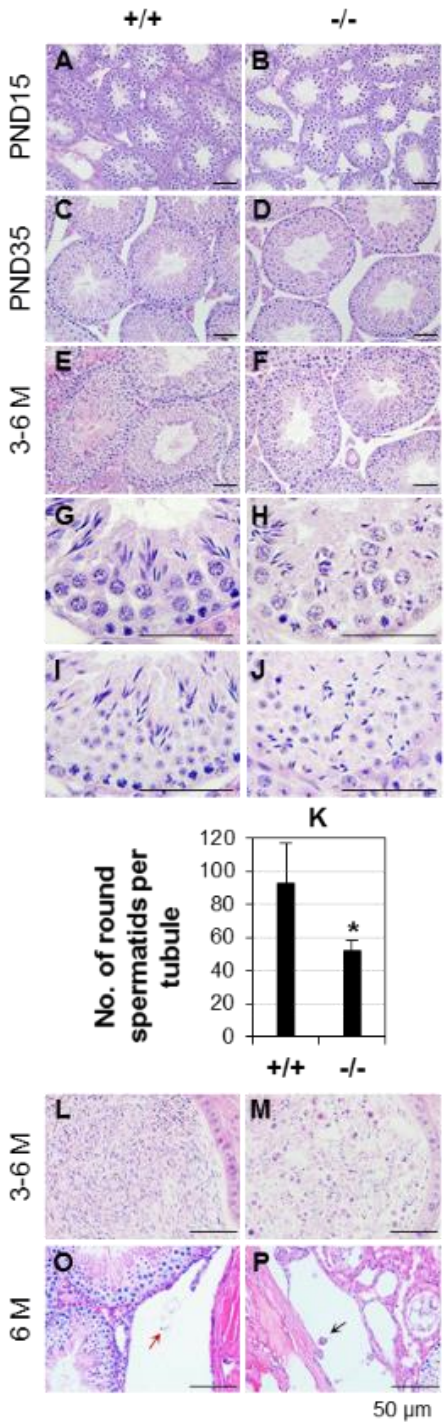

Figure 2. Histology of testis, cauda epididymis, and rete testis. +/+, *Bscl2*$^{+/+}$; -/-, *Bscl2*$^{-/-}$. Testes from 3-6 mice at each time point per genotype were analyzed. Representative images were shown. A. Postnatal day (PND) 15 *Bscl2*$^{+/+}$ testis. B. PND15 *Bscl2*$^{-/-}$ testis. C. PND35 *Bscl2*$^{+/+}$

testis. D. PND35 *Bscl2*$^{-/-}$ testis. Data in E-M were from 3-6 months (3-6 M) old males. E. *Bscl2*$^{+/+}$ testis. F. Bscl2-/- testis. G-J. Enlarged views of *Bscl2*$^{+/+}$ (G, I) and Bscl2-/- (H, J) seminiferous epithelia to show disorientated distribution of spermatids in the *Bscl2*$^{-/-}$ seminiferous epithelia. K. Number of round spermatids per seminiferous tubule. N=5-6; error bar, standard deviation; *, P<0.05. L. *Bscl2*$^{+/+}$ cauda epididymis. M. *Bscl2*$^{-/-}$ cauda epididymis. O. *Bscl2*$^{+/+}$ rete testis. P. *Bscl2*$^{-/-}$ rete testis. Scale bar, 50 μm.

Spatiotemporal expression of Bscl2/seipin in Bscl2*$^{+/+}$ *testis

Quantitative RT-PCR indicated >10 fold increase of *Bscl2* mRNA level in 3 month old *Bscl2*$^{+/+}$ testes compared to PND15 *Bscl2*$^{+/+}$ testis (Fig. S2A). *In situ* hybridization revealed that *Bscl2* mRNA was barely detectable in most areas except faint staining in some seminiferous tubules in the PND15 testis (Fig. 3A) and gradually increased in PND20 (Fig. 3B) and PND25 testes (Fig. 3C). In PND28 testis, *Bscl2* mRNA was detected in all seminiferous tubules although the levels of expression varied among different seminiferous tubules (Fig. 3D). This *Bscl2* mRNA expression pattern remained throughout 7 month old testis, the oldest time point examined (Fig. 3E). Within the seminiferous tubules, the highest expression levels were detected in the spermatocytes (Fig. 3G). Based on a study about spermatogenic cells in prepubertal mouse testis [44], *Bscl2* mRNA was most likely expressed in both pachytene spermatocytes and secondary spermatocytes. *Bscl2* mRNA did not seem to be expressed in spermatogonia and Sertoli cells (Fig. 3G). The signals in the interstitial spaces were insignificant (Fig. 3D, 3E, 3G). The negative control using a sense probe did not detect any positive signal (Fig. 3F, 3H). Interestingly, *Bscl2* mRNA was highly and specifically detected in the epithelium of coagulating gland and seminal vesicle (Fig. S2B-S2F).

Immunohistochemistry analysis showed an age-dependent increase of seipin expression in the seminiferous tubules from PND15 to 3 months old (Fig. 3I-3N). On PND25, seipin started to be detected in the round spermatids and remarkably increased in the spermatids afterwards. IgG negative control or *Bscl2*$^{-/-}$ testis did not show specific staining (Fig. 3O, 3P). Both histology (Fig. 2A-2F) and seipin expression suggested potential role of seipin in spermatid development or spermiogenesis.

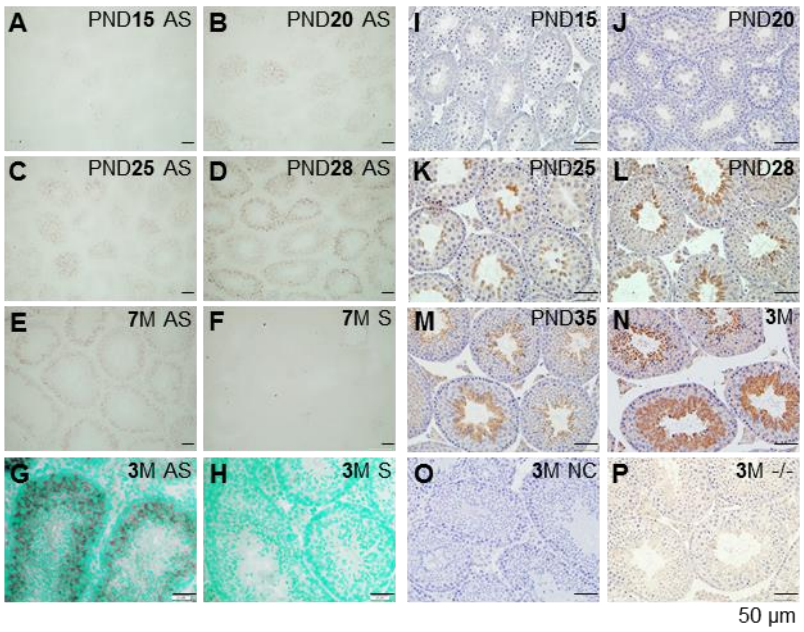

Figure 3. Spatiotemporal localization of Bscl2 mRNA by in situ hybridization (A-H) and seipin protein by immunohistochemistry (I-P) in the testis. All sections were from *Bscl2*$^{+/+}$ testes except P, which was from a *Bscl2*$^{-/-}$ testis. Testes from at least 3 mice at each time point were analyzed. Representative images were shown. A. Postnatal day (PND) 15, antisense (AS) probe. B. PND20, antisense probe. C. PND25, antisense probe. D. PND28, antisense probe. E. 7 months old (7M), antisense probe. F. 7M, sense probe, negative control. G. 3M, antisense probe. H. 3M, sense probe. G-H: counterstained with methyl green. I-P: All sections were incubated with

primary anti-seipin antibody except O, which was incubated with normal rabbit IgG. I. PND15. J. PND20. K. PND25. L. PND28. M. PND35. N. 3M. O. 3M, negative control (NC). P. 3M, *Bscl2*$^{-/-}$ (-/-), a second negative control. Scale bar, 50 μm.

Increased ISEL*$^{+}$ *staining in Bscl2*$^{-/-}$ *testis

ISEL^{+} detects DNA breaks [45, 46]. Both *Bscl2*$^{+/+}$ and *Bscl2*$^{-/-}$ males had widespread ISEL^{+} labeling (Fig. S4). However, *Bscl2*$^{-/-}$ testis sections (Fig. S4D) showed consistently more ISEL^{+} labeling than *Bscl2*$^{+/+}$ testis sections (Fig. S4A). Quantification using ImageJ indicated a 10 fold increase of ISEL^{+} labeling intensity in *Bscl2*$^{-/-}$ testis sections (Fig. 4A), for which clusters of ISEL^{+} labeled cells were a main contributor (Fig. 4B, 4D, S4). Individual ISEL^{+} labeled cells not in the clusters were also detected in both *Bscl2*$^{+/+}$ and *Bscl2*$^{-/-}$ testis sections. These cells were located in the *Bscl2*$^{+/+}$ seminiferous epithelium but rarely in the area close to the lumen where spermatids and sperm reside (Fig. 4B, 4C, 4F, 4G, 4J, S4A-S4C). However, ISEL^{+} labeled cells were detected throughout *Bscl2*$^{-/-}$ seminiferous epithelium, including the area where spermatids and sperm resided (Fig. 4D, 4E, 4H, 4I, 4K, S4F), indicating increased DNA breaks and apoptosis of the *Bscl2*$^{-/-}$ spermatids and sperm.

Annexin V staining detects cells in the intermediate stages of apoptosis. To support the association of increased DNA breaks in *Bscl2*$^{-/-}$ late germ cells detected by ISEL^{+} with apoptosis, round spermatids were examined for annexin V staining in germ cell spreads. Results indicated significantly increased percentage of annexin V positive *Bscl2*$^{-/-}$ round spermatids (Fig. 4L). Immunohistochemical analysis of cleaved caspase-3 did not show obvious difference between *Bscl2*$^{+/+}$ and *Bscl2*$^{-/-}$ testes. A few cleaved caspase-3 positive germ cells were detected in both genotypes (Fig. S3).

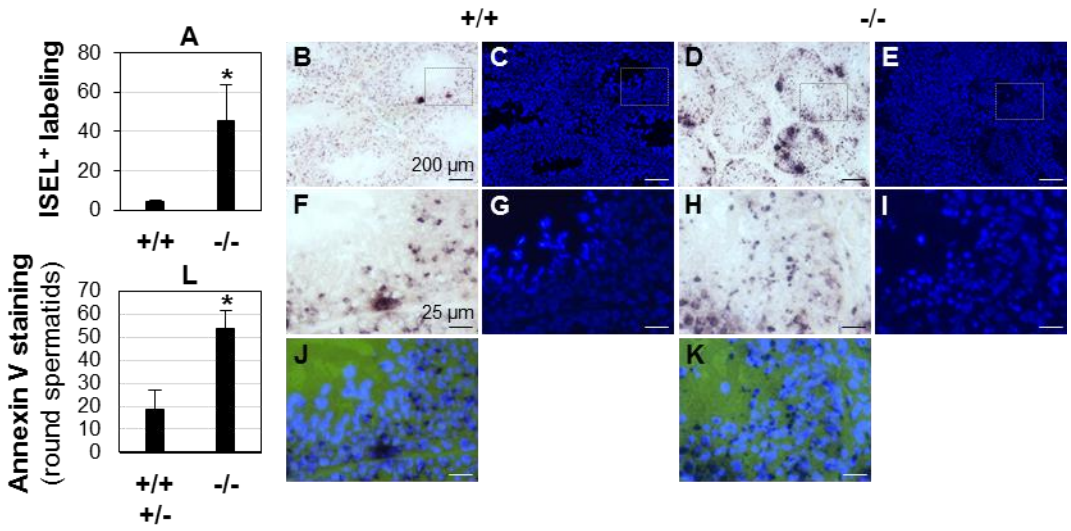

Figure 4. In situ end-labeling plus (ISEL+) and annexin V staining of male germ cells. A-K: ISEL+; 3-4 months old *Bscl2*$^{+/+}$ (+/+) and *Bscl2*$^{-/-}$ (-/-) males; N=5. A. Quantification of ISEL+ labeling using ImageJ as described in Materials and Methods. The original images used for quantification were in supplementary Figure S4. B. A representative ISEL+ testis section from a *Bscl2*$^{+/+}$ male. C. DAPI counterstaining of the section in B. D. A representative ISEL+ testis section from a *Bscl2*$^{-/-}$ male. E. DAPI counterstaining of the section in D. Scale bars in B-E, 200 µm. F, G, H, I: Enlarged images of the rectangle areas in B, C, D, E, respectively. J. Merged image of F and G. K. Merged image of H and I. Scale bars in F-K, 25 µm. Dark dots and clusters in B, D, F, H, J, K were ISEL+ labeling. L. Percentage of annexin V positive round spermatids in 5 months old control (*Bscl2*$^{+/+}$ (+/+) & *Bscl2*$^{+/-}$ (+/-), N=3) and *Bscl2*$^{-/-}$ (-/-) (N=4) males. A & L: * $P<0.05$; error bar, standard deviation.

Normal meiotic chromosome pairing and homologous chromosome synapsis in Bscl2*$^{-/-}$ *spermatocytes

To determine the causes of DNA breaks in the late *Bscl2*$^{-/-}$ germ cells, germ cell spreads from seminiferous tubules were analyzed. Since *Bscl2* mRNA was mainly detected in the

spermatocytes (Fig. 3G), spermatocytes were examined. Pairing and subsequent synapsis of homologous chromosomes are essential developmental events necessary for proper meiotic recombination and chromosome segregation during metaphase I and II [47]. The structural chromosome proteins SYCP3 and SYCP1 are key components of axial (SYCP3) and lateral (SYCP1) elements of the synaptonemal complex [48, 49] and were used as bona fide markers for prophase I of meiosis. SYCP3 was first detectable in leptotene stage spermatocytes of both *Bscl2*$^{+/+}$ and *Bscl2*$^{-/-}$ preparations and progressively labeled the axial extension of the condensing chromosomes during zygotene and pachytene stages without indication for chromosome pairing errors (data not shown). This observation was also confirmed in synapsis of homologous chromosomes as indicated by co-localization of SYCP3 and SYCP1 in all autosomes at pachytene stage of meiosis, irrespective of the genotypes (Fig. S5). In addition, the X and Y chromosomes were partially synapsed at the pseudoautosomal region in both *Bscl2*$^{+/+}$ and *Bscl2*$^{-/-}$ pachytene spreads (Fig. S5), indicating that *Bscl2*$^{-/-}$ spermatocytes did not present obvious synaptic errors during prophase I.

Chromocenter fragmentation in Bscl2*$^{-/-}$ *round spermatids

Since seipin is highly expressed in the postmeiotic spermatids (Fig. 3), we analyzed global chromatin structure during spermiogenesis. SYCP3 is a marker of meiotic cells and normally absent in the spermatids (Fig. 5A-5C) [50, 51]. However, there was an increased percentage of *Bscl2*$^{-/-}$ round spermatids with retained SYCP3 expression (Fig. 5D-5G). Surface spreading of germ cell nuclei allows fine-structural analyses of the sub-nuclear localization and distribution of chromatin domains. The chromocenter is a cluster of centromeres and pericentromeric heterochromatin [52]. As a hallmark of spermiogenesis, centromeric heterochromatin domains of the autosomes coalesce to one or two central chromocenters with

adjacent sex chromatin [53]. In surface spreads obtained from *Bscl2*$^{-/-}$ males, a significant proportion of round spermatids (31.0%, P=0.032) exhibited fragmentation of the chromocenter into 3 or more heterochromatic foci as demonstrated by labeling with a bona fide marker for centromeric heterochromatin, H3K9me3 [54], while this phenotype was detectable in only 7.1% of *Bscl2*$^{+/+}$ control (Fig 5H-5N). These findings indicated abnormalities in the regulation of chromocenter formation in *Bscl2*$^{-/-}$ males that may lead to defects in chromatin condensation and formation of proper spermatozoa and mature sperm.

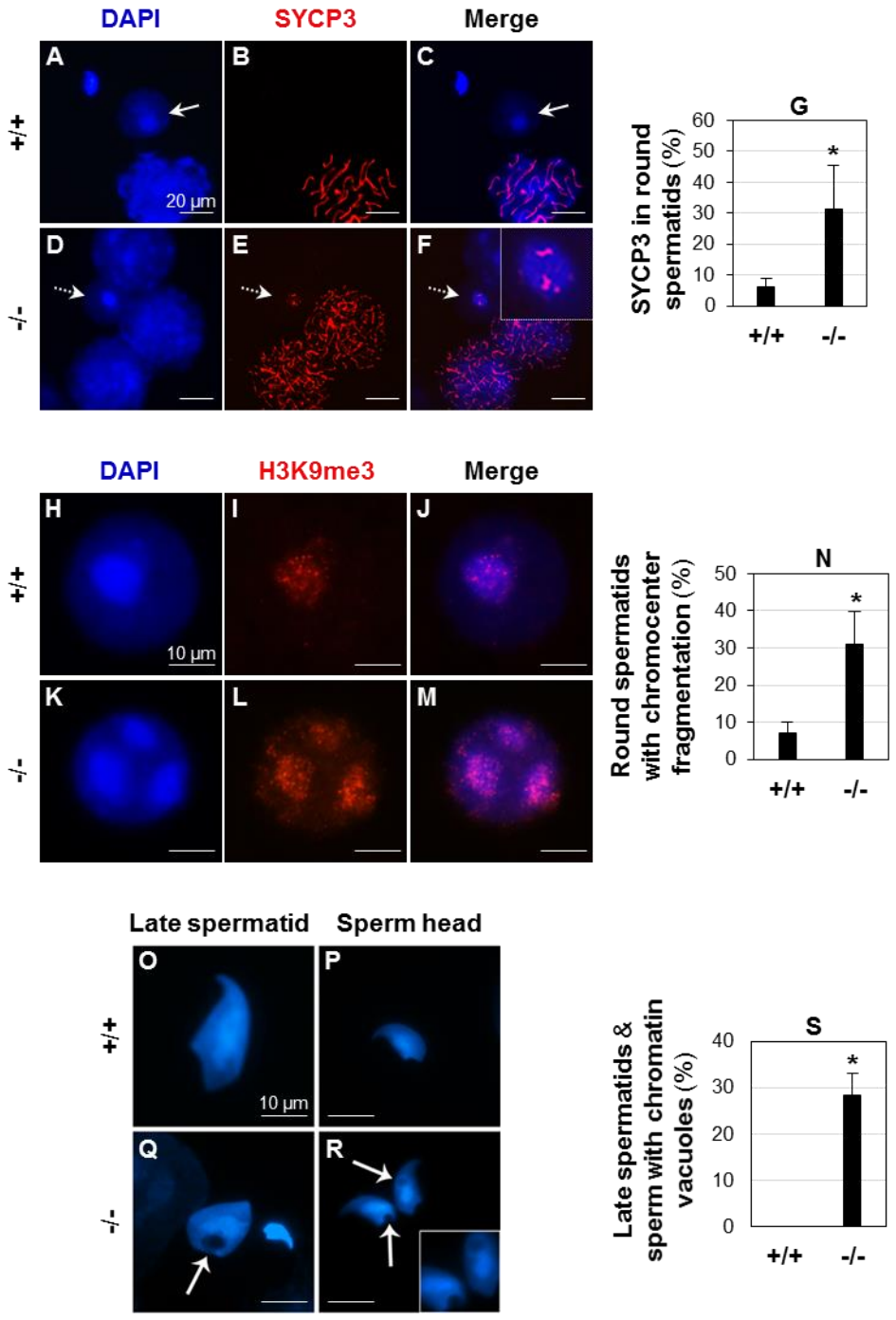

Figure 5. Analyses of round spermatids, late spermatids and sperm in 4 months old *Bscl2*$^{+/+}$ (+/+) and *Bscl2*$^{-/-}$ (-/-) germ cell spreads. A-C: A representative image from *Bscl2*$^{+/+}$ spreads; white arrows indicating a round spermatid. A. DAPI. B. SYCP3 staining chromosomes in a pachytene spermatocyte A. C. Merged image of A and B. D-F: A representative image from

Bscl2$^{-/-}$ spreads; white arrows with a broken line indicating a round spermatid. D. DAPI. E. SYCP3 staining the chromosomes in the zygotene spermatocytes and the round spermatid in D. F. Merged image of D and E. Insert, enlarged view of the round spermatid with retained SYCP3 staining. G. Percentage of round spermatids with retained SYCP3 staining. H. Blue DAPI staining of a representative *Bscl2*$^{+/+}$ round spermatid. I. Red H3K9me3 staining of the round spermatid in H. J. Merged image of H and I. K. Blue DAPI staining of a representative *Bscl2*$^{-/-}$ round spermatid. L. Red H3K9me3 staining of the round spermatid in K showing chromocenter fragmentation. M. Merged image of K and L. N. Percentage of round spermatids with chromocenter fragmentation. O-R: Representative DAPI staining of late spermatids and sperm. O. A *Bscl2*$^{+/+}$ late spermatid. P. A *Bscl2*$^{+/+}$ sperm head. Q. A *Bscl2*$^{-/-}$ late spermatid and sperm head. R. Two *Bscl2*$^{-/-}$ sperm heads. Insert, enlarged view of the chromatin vacuoles. Arrowheads in Q & R, chromatin vacuoles. Scale bar, 10 μm. S. Percentage of late spermatids and sperm with chromatin vacuoles. G, N, S: At least 100 randomly selected round spermatids from each sample were examined; N=3; error bars, standard deviation; * $P<0.05$.

High incidence of chromatin vacuoles in Bscl2$^{-/-}$ late spermatids & mature sperm

To address whether loss of seipin led to abnormal sperm chromatin condensation, morphological analyses were conducted using high-resolution microscopy of surface spread germ cells. *Bscl2*$^{-/-}$ late (elongating) spermatids and mature spermatozoa had a high incidence (28.2%, $P<0.001$) of chromatin vacuoles, which were not restricted to any particular nuclear domain, while such abnormalities were never observed in *Bscl2*$^{+/+}$ germ cell preparations (Fig. 5O-5S).

Chromocenter fragmentation in round spermatids and chromatin vacuoles in late spermatids and mature sperm indicated potential problems in chromatin condensation, a process

involving protamines 1 and 2 (PRM1/2) in mice [52, 55, 56]. Although the levels of *Prm1* mRNA and *Prm2* mRNA, which are expressed in round spermatids [57, 58], were significantly reduced in 3 months old *Bscl2*$^{-/-}$ testes compared to *Bscl2*$^{+/+}$ testes, the levels of PRM1 and PRM2 proteins, which are expressed in late spermatids and sperm, were comparable in the nuclei of individual *Bscl2*$^{+/+}$ and *Bscl2*$^{-/-}$ late spermatids and sperm (Fig. S6). Downregulation of *Prm1* and *Prm2* mRNAs in the *Bscl2*$^{-/-}$ testis most likely resulted from the reduced number of round spermatids (Figs.2K, S6A, S6B). These data demonstrated that protamines most likely did not contribute to the chromatin defects in *Bscl2*$^{-/-}$ late spermatids and sperm.

Defective acrosome formation in Bscl2*$^{-/-}$ *late spermatids

Besides chromocenter fragmentation in round spermatids and chromatin vacuoles in late spermatids and mature sperm, *Bscl2*$^{-/-}$ late spermatids were disorganized and present throughout seminiferous epithelium (Figs. 2H, 2J, S6I, S6R). Late spermatids are associated with Sertoli cells, which could be stained with vimentin. There was comparable vimentin staining between *Bscl2*$^{+/+}$ and *Bscl2*$^{-/-}$ testes (Fig. 6A, 6B), indicating no obvious structural abnormality of the Sertoli cells that support sperm cell development before the spermatids are released to the lumen.

It was previously suggested that an acrosome may be related to the alignment of the spermatid head with the ectoplasmic specialization to influence the orientation and positioning of the late spermatids within the seminiferous epithelium [59]. PNA staining revealed crescent shaped acrosomes in *Bscl2*$^{+/+}$ late spermatids (Fig. 6C-6E, 6I). However, *Bscl2*$^{-/-}$ spermatids had abnormal acrosomes (Fig. 6F-6H, 6J-6L), such as no defined acrosome (Fig. 6J), irregular-shaped acrosome (Fig. 6K), and fragmented acrosome (Fig. 6L). These data demonstrated that seipin deficiency also affected acrosome formation in late spermatids.

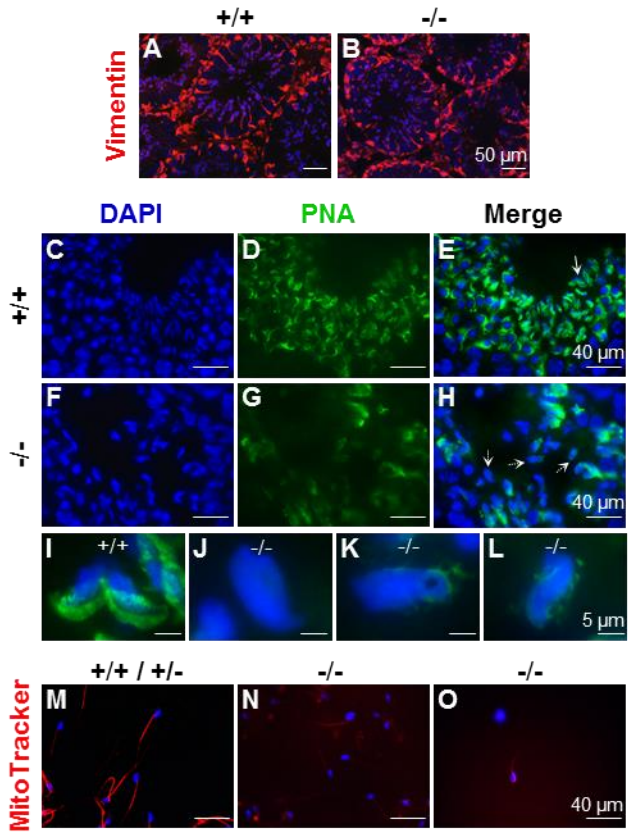

Figure 6. Detection of Sertoli cells, acrosomes, and active mitochondria. +/+, *Bscl2*$^{+/+}$; -/-, *Bscl2*$^{-/-}$. Sertoli cells were labeled by vimentin (red) immunofluorescence. Acrosomes were labeled with Alexa Fluor 488 conjugated-peanut agglutinin (PNA) (green). Testes from 3-4 month old mice (N=3-4) were used. A. *Bscl2*$^{+/+}$ testis vimentin labeling. B. *Bscl2*$^{-/-}$ testis vimentin labeling. C. DAPI staining of *Bscl2*$^{+/+}$ seminiferous epithelium. D. PNA staining of the section in C. E. Merged image of C and D. F. DAPI staining of *Bscl2*$^{-/-}$ seminiferous epithelium. G. PNA staining of the section in F. H. Merged image of F and G. I. *Bscl2*$^{+/+}$ spermatids indicated with solid white arrow in E. J-L. *Bscl2*$^{-/-}$ spermatids indicated with dashed white arrows in H. The spermatid in K had chromatin vacuole. Scale bar, 50 µm in A-B, 40 µm in C-H, and 5 µm in I-L. M-O: Red, MitoTracker staining of mitochondria at midpiece of sperm from 5 months old cauda epididymis; blue, DAPI staining sperm head. M. Representative control (*Bscl2*$^{+/+}$ & *Bscl2*$^{+/-}$)

sperm with strong staining on midpiece. N. Representative *Bscl2*$^{-/-}$ sperm with faint staining. O. A *Bscl2*$^{-/-}$ sperm with strongest red stain in the group. Note, increased exposure in N & O to show *Bscl2*$^{-/-}$ sperm midpiece.

Defective mitochondrion function in Bscl2*$^{-/-}$ *sperm

Besides low sperm count (Fig. 1E), the *Bscl2*$^{-/-}$ sperm also had low sperm motility (Fig. 1F). It has been demonstrated that there is direct and positive correlation between mitochondrial enzymatic activities and sperm motility [60]. MitoTracker, which stains active mitochondria, was used to determine mitochondrial activity of sperm freshly isolated from cauda epididymis. The majority of control sperm were motile and had strong staining at the midpiece (Fig. 6M). However, the majority *Bscl2*$^{-/-}$ sperm were immotile and the MitoTracker staining was so weak that increased exposure time was required to visualize the flagellum (Fig. 6N), even the strongest stained *Bscl2*$^{-/-}$ sperm required increased exposure time (Fig. 6O).

2.4 Discussion

This study systemically analyzed the spatiotemporal expression of *Bscl2* mRNA and seipin protein in the mouse testis. Although both mRNA and protein levels gradually increased in the postnatal testes, with detectable levels by both *in situ* hybridization and immunohistochemistry after PND20, the mRNA levels seemed to reach a plateau ~PND28, while the protein levels were still increasing ~PND35. This was due to the main protein localization of seipin in spermatids. Round spermatids start to appear after PND18 and elongating spermatids start to appear ~PND35 and continue to develop till adulthood [44, 61]. The temporal expression of seipin protein correlated with the onset of spermiogenesis and suggested its potential function in spermiogenesis. Indeed, in seipin-deficient testis, there was a reduction of round spermatids; escaping spermatids often lacked normal maturation features and

showed signs of DNA damages; only a limited number of spermatids would go into the elongation phase yet they would have aberrations, such as chromatin vacuoles and abnormal acrosome formation; and the minimal number of sperm produced had diminished mitochondrial activity and motility.

Interestingly, *Bscl2* mRNA and seipin were not co-localized in the same male germ cells, with the mRNA mainly in the spermatocytes and the protein mainly in the spermatids, indicating translational repression in the spermatocytes. Translational repression in the male germ cells has also been reported for other genes in the testis. For example, mRNAs for transition proteins and protamines are synthesized in round spermatids but translated in elongated spermatids [57, 58].

There were increased percentages of round spermatids with retained SYCP3 expression or chromocenter fragmentation in the *Bscl2*$^{-/-}$ germ cell spreads. Although it is unknown about the significance of retained SYCP3 expression in the round spermatids, chromocenter fragmentation could lead to defects in chromatin condensation and the formation of proper spermatozoa and mature sperm. Chromocenter fragmentation has been reported in mice lacking the first bromodomain of testis-specific double bromodomain protein Brdt [62] and mice deficient of TBP-like factor [63], both of which have impaired male fertility [62-64]. Interestingly, the former was not associated with spermatid apoptosis [62] but the later was associated with increased spermatid apoptosis [64].

There were increased ISEL^{+} labeled cell clusters in *Bscl2*$^{-/-}$ seminiferous epithelium as well as increased ISEL^{+} labeled individual spermatids at the center or close to the lumen of *Bscl2*$^{-/-}$ seminiferous tubules. Male germ cell apoptosis is a normal process during spermatogenesis [40]. It is most likely that chromocenter fragmentation contributed to the increased spermatid apoptosis in *Bscl2*$^{-/-}$ testis. However, the causes for increased ISEL^{+} labeled

cell clusters in the *Bscl2*$^{-/-}$ seminiferous epithelium are unknown. Such clusters were also seen in the *Bscl2*$^{+/+}$ seminiferous epithelium but at a much less frequency. Since spermatids are connected by cytoplasmic bridges and *Bscl2*$^{-/-}$ spermatids were often observed in abnormal locations near the periphery of seminiferous tubule, it is possible that the increased ISEL^{+} labeled cell clusters near the base of seminiferous epithelium was due to increased *Bscl2*$^{-/-}$ spermatid apoptosis. In addition, since germ cells at different stages are supported by the same Sertoli cells, it is unknown if the defects in the spermatids could affect earlier germ cells that share the same Sertoli cells. The increased germ cell death in the *Bscl2*$^{-/-}$ testis was obviously unassociated with caspase-3 pathway. This scenario had been reported in RARalpha$^{-/-}$ testes as well [65], which also had disorganized late spermatids and increased spermatid apoptosis.

Chromatin vacuoles were only observed in late spermatids and spermatozoa from the *Bscl2*$^{-/-}$ testis. Since the localizations of the chromatin vacuoles could be found in different areas, it is possible that these vacuoles are formed by defects in large-scale chromatin condensation during spermatid elongation and thus had much less density upon DAPI staining. It is possible that defects in chromatin condensation might be associated with chromocenter fragmentation in round spermatids. One study revealed that the small vacuoles in human sperm were abnormal nuclear concavities associated with noncondensed chromatin [66]. Chromatin vacuoles are also observed in sperm deficient of chromodomain helicase DNA binding protein 5 [52].

One defect in the *Bscl2*$^{-/-}$ testis was the disorganized late spermatids. Although the role of acrosome in spermatid orientation has not been established, it was suggested decades ago that an acrosome may play a role in aligning the spermatid head with the ectoplasmic specialization to influence the orientation and positioning of the late spermatids [59]. The *Bscl2*$^{-/-}$ spermatids had various defects in their acrosomes and were often disorganized. Seipin was shown to be localized

on the ER membrane [31, 32]. ER is closely associated with Golgi apparatus where the acrosome is derived from. It is possible that seipin is directly involved in acrosome formation in late spermatids.

A recent study on *Bscl2*$^{-/-}$ testes from a different line of global seipin knockout mice and germ cell conditional knockout mice demonstrated that the defective sperm production was due to local deficiency of seipin in the germ cells [27]. The percentages of motile sperm were much lower in our study, which was due to different sample preparations. Increased phosphatidic acid (PA) level was observed in the *Bscl2*$^{-/-}$ testis [27]. Phospholipases A PLA_1 and PLA_2 are involved in PA metabolism. Phosphatidic acid-preferring phospholipase A_1 (PA-PLA_1) is highly expressed in the testis. PA-PLA_1-deficient sperm have a bent flagellum and severely impaired sperm motility [67]. Sperm tail defects were also observed in the *Bscl2*$^{-/-}$ sperm [27], which might be related to the function of PA-PLA_1 in flagellum and sperm motility [67]. In addition, lack of active mitochondria in the *Bscl2*$^{-/-}$ sperm midpiece could be a main reason for defective sperm motility.

In addition to its critical role in adipogenesis [37, 38], *Bscl2*/seipin most likely has other uncharacterized roles. Its transcriptional upregulation in mES cells upon exposure to genotoxins involving ATR signaling pathway [41, 42] would suggest its potential role in maintaining DNA integrity upon genotoxic insults. Although testicular-derived seipin was suggested to be essential for male fertility by modulating testicular phospholipid homeostasis [27], we think that defective lipid homeostasis in *Bscl2*$^{-/-}$ male germ cells could contribute to a defective flagellum with low mitochondrial activity thus impaired sperm motility, while impaired DNA integrity and chromatin condensation could contribute to both reduced sperm count and impaired sperm motility because DNA damage can induce apoptosis and is negatively related with sperm

motility [68, 69]. Reduced sperm count, reduced sperm motility, and defective acrosome formation contribute to male infertility in the *Bscl2*$^{-/-}$ mice.

2.5 Materials and Methods

Animals. *Bscl2*-deficient mice (*Bscl2*$^{-/-}$) in C57BL/6J background were derived from a colony at Georgia Regents University, which was originally derived from a colony at Baylor College of Medicine with backcrosses to C57BL/6J background for five generations [35]. They were genotyped as previously described [35] using mouse tail genomic DNA and PCR with wild type allele-specific forward primer 5´-GGACGTGATCGGGTGAGTATGAGAA-3´ and reverse primer 5´- GAGATAGGGTCTGGCTATGAA-3´ and the neo-specific primer 5´-CTATCGCCTTCTTGACGAGT-3´. All mice were maintained on PicoLab mouse diet 20 with soybean as a main protein source. They were housed in polypropylene cages with free access to food and water on a 12 h light/dark cycle (0600–1800) at 23±1°C with 30–50% relative humidity at the College of Veterinary Medicine animal facility at the University of Georgia. The animals were sacrificed by CO2 inhalation followed with cervical dislocation. All methods used in this study were approved by the University of Georgia Institutional Animal Care and Use Committee (IACUC) Committee and conform to National Institutes of Health guidelines and public law.

Male mating behavior and fertility tests. *Bscl2*$^{+/+}$ males (N=7) and *Bscl2*$^{-/-}$ males (N=10) at 2-3 months old were each housed with one 2 months old virgin *Bscl2*$^{+/+}$ female for two months. Each female was checked for the presence of a vaginal plug every morning to determine mating activity during the previous night. Mating activity was evaluated with two parameters, plugging latency (the duration between cohabitation and the detection of the first plug) and plugging rate (the percentage of males in each group that ever successfully mated with females during the 2 months of cohabitation). Fertility was assessed using the litter size at birth and the number of

litters per female. At the end of the two-month cohabitation, the males were separated from the mating females and the females were observed for three more weeks for pregnancies that occurred during the last period of mating study. The average ages of males were ~20 weeks old for both *Bscl2*$^{+/+}$ (20.4±3.8 weeks) and *Bscl2*$^{-/-}$ (20.0±2.3 weeks) males. Two *Bscl2*$^{+/+}$ males and three *Bscl2*$^{-/-}$ males that finished mating and fertility tests before the rest males were sacrificed for sperm counting only, the rest five *Bscl2*$^{+/+}$ males (20.6±4.4 weeks old) and seven *Bscl2*$^{-/-}$ males (19.9±0.6 weeks old) were mated with one virgin female (2-3 months old) each for determining sperm count in the uterus before being sacrificed for sperm counting. Positive mating was determined by the presence of a vaginal plug in the morning and the uterine horns from the positively mated females were flushed with 1x PBS for sperm counting from the uterus. Cauda epididymis sperm count was determined one week after mating and uterine sperm count was determined in the morning after mating. The efficiency of sperm transport was expressed as the percentage of the uterine sperm count over the cauda epididymis sperm count of the mated male.

Sperm count and sperm motility. All males were housed individually for one week before sperm counting. Each cauda epididymis was dissected, finely minced in 1 ml 1x PBS in a 1.5 ml microcentrifuge tube, and shaken at 37°C/5% CO_2 for 30 minutes. Sperm count was expressed as the total sperm number from both cauda epididymides. Since sperm motility was not determined in the males from mating study, another set of males was used. Both *Bscl2*$^{+/+}$ and *Bscl2*$^{+/-}$ males were used in the control group because they did not show any obvious difference in the phenotypes. Cauda epididymides from control males (N=6, 25.1±6.4 weeks old) and *Bscl2*$^{-/-}$ males (N=9, 24.0±5.1 weeks old) were dissected and prepared for sperm counting as described above. Meanwhile, the number of motile sperm from each preparation was also determined.

Sperm motility was expressed as the percentage of motile sperm. The sperm number in the uterine flushing from each of the females mated with a subset of males in the fertility test was also counted using a hemocytometer.

Testis and rete testis histology and spermatogenesis staging. Testes from *Bscl2*$^{+/+}$ and *Bscl2*$^{-/-}$ males at postnatal day 15 (PND15), PND35, and 3-6 months old, as well as testes together with rete testis and epididymis from 6 months males were fixed in Bouin's solution (*Ricca Chemical Company, Arlington, TX, USA*) for 24 hours. They were then kept in 70% ethanol until embedded in paraffin for sectioning. Each testis was cut perpendicular to the long axis of the seminiferous tubules. Paraffin sections (5 μm) were processed and stained with hematoxylin and eosin [46]. N=3-6 for each time point and each genotype. To determine spermatogenesis stages, a representative 20x testis histology image with only cross-sectioned round seminiferous tubules from each adult mouse (3-6 months old) was analyzed. Since spermatids in the *Bscl2*$^{-/-}$ seminiferous tubules were disorientated thus prevented accurate staging, the following information was collected: the number of intact seminiferous tubules in each image, the number of seminiferous tubules without round spermatids (stage IX-XI), and the total number of round spermatids in all intact seminiferous tubules in each 20x image. Histology of rete testes was obtained by sectioning through the testis and rete testis and stained with hematoxylin and eosin as described above.

Quantitative RT-PCR. Testes from wild type C57BL/6J males at PND15 (N=5) and 3 months old (N=3) were snap frozen on dry ice. Total RNA was extracted with Trizol (Life Technologies, Grand Island, NY, USA). Complementary DNA was transcribed using Superscript III reverse transcriptase (Life Technologies) with random primers as previously described [46, 70, 71]. Quantitative PCR was performed in 384-well plates using SYBR-Green I intercalating dye on

ABI 7900 (Applied Biosystems, Carlsbad, CA, USA). The mRNA expression levels of *Bscl2* were determined using gene specific primers from different exons (Integrated DNA Technology, Coralville, IA, USA), m*Bscl2*e3F: 5'-GTGCACTTCCACTACAGGAC-3', and m*Bscl2*e6R: 5'-CTCCAGTTGTTGGCACATAC-3'. *Gapdh* (glyceraldehyde-3-phosphate dehydrogenase) was used as a loading control and *Hprt1* (hypoxanthine phosphoribosyltransferase 1), another housekeeping gene, served as a second control as previously described [72]. For quantification of protamine 1 (*Prm1*) and protamine 2 (*Prm2*), total RNA was extracted from three months old $Bscl2^{+/+}$ and $Bscl2^{-/-}$ males (N=5) with Trizol (Life Technologies) and cDNA was transcribed as described above. Quantitative PCR was performed using Ssoadvanced SYBR Green Supermix (Bio-Rad) on CFX384 Touch™ Real-Time PCR Detection System (Bio-Rad). Gene specific primers (Integrated DNA Technology) were designed as reported previously [73]: m*Prm1*e2F: 5´-AGGTGTAAAAAATACTAGATGCACAGAATAG-3´, m*Prm1*e2R: 5´-TTCAAGATGTGGCGAGATGCT-3´; m*Prm2*e2F: 5´-GAATAGTCACCTGCCCAAGCA-3´, m*Prm2*e2R: 5´-GCAGCTCAGGGCTCAGACA-3´. *Gapdh* and *Hprt1* were used as control as described above.

***In situ* hybridization.** *Bscl2* sense and antisense cRNA probes were synthesized as previously described [74] except that the template for cRNA probe synthesis was amplified from m*Bscl2* cDNA using primers m*Bscl2*e3F and m*Bscl2*e6R for PCR. The amplified *Bscl2* cDNA fragment was recovered from agarose gel and cloned into pGEM®-T Easy Vector (Promega, Madison, WI, USA). The recombinant plasmid was amplified with T7 and SP6 primers to produce templates for labelling antisense and sense probes, respectively. Testes from wild type males at PND15, PND20, PND28, PND35, 3 months old, and 7 months old were snap-frozen on dry ice and kept at -80°C. Frozen testis cross sections (10 µm) were cut and processed. Testis sections

were mounted on (3-aminopropyl) triethoxy silane-coated slides, fixed in 4% paraformaldehyde in diethylpyrocarbonate (DEPC)-treated H_2O for 1 hour at room temperature. Sections were washed twice with 1x PBS in DEPC H_2O for 5 minutes, treated with 1% Triton X-100 for 20 minutes, then washed three times in 1x PBS for 5 minutes each. Sections were prehybridized in 50% formaldehyde/5x saline-sodium citrate (SSC) buffer at room temperature for 15 minutes then hybridized with digoxigenin-labeled sense (as a negative control) or antisense riboprobes for 16-20 hours. Sections were next washed in 5x SSC, 50% formamide at 55°C for 15 minutes, 2x SSC, 50% formamide at 55°C for 30 minutes, 0.2x SSC, 50% formamide twice at 55°C for 30 minutes each, and 0.2x SSC at room temperature for 5 minutes, then washed in buffer B1 (1 M Tris-HCl pH7.5, 2.5 M NaCl in ddH_2O) for 5 minutes at room temperature. Slides were incubated with 1% blocking agent (Boehringer-Mannheim, Germany) in buffer B1 at room temperature for 1 hour. Slides were next incubated with 1:2000 Anti-Digoxigenin-AP, fab fragment (Roche Applied Science, Indianapolis, IN, USA) in 1% blocking reagent at 4°C overnight. After being washed three times in buffer B1 for 5 minutes each, slides were washed in buffer B3 (1 M Tris-HCl pH9.5, 0.5 M $MgCl_2$, 2.5 M NaCl in ddH_2O) for 5 minutes at room temperature. The hybridization was visualized with substrates nitroblue tetrazolium (NBT) and 5-bromo-4-chloro-3-indolyl phosphate (BCIP) (Roche Applied Science) in buffer B3, and endogenous alkaline phosphatase activity was inhibited with 2 mM Levamisole (Sigma-Aldrich, St. Louis, MO, USA) added to the substrate solution. Some sections were counterstained with methyl green as previously described [74, 75]. Testes from at least 3 different mice were examined for each time point.

Immunohistochemistry. Paraffin sections (5 μm) were used to detect seipin expression in the testes from PND15, PND20, PND35, and 3 months old wild type mice using our customized

rabbit polyclonal anti-seipin antibody (1:1,000, 2.21 μg/ml, Thermo Scientific) which was raised against the C-terminal 17 amino acids of mouse seipin as previously described [76]. Briefly, testis sections were rehydrated, subjected to antigen retrieval in 10 mM sodium citrate (pH 6) for 20 minutes in a microwave and then washed in 1x PBS and ddH_2O for 5 minutes each. All steps were carried out at room temperature unless specified. Endogenous horseradish peroxidase (HRP) was blocked with 3% H_2O_2 in methanol for 10 minutes, and then washed in ddH_2O and 1x PBS for 5 minutes, respectively. Non-specific staining was blocked with 10% goat serum for 1 hour. Sections were then incubated with rabbit anti-seipin overnight at 4°C. Sections were washed in 1x PBS for 5 minutes, incubated with biotinylated goat anti-rabbit IgG (1:200, 7.5 μg/ml, BA-1000, Vector laboratories, Burlingame, CA, USA) in 1% BSA for 30 minutes. After washing three times with 1x PBS for 5 minutes each, sections were incubated with HRP streptavidin (SA-5004, Vector Laboratories) for 30 minutes and then washed three times in 1x PBS for 5 minutes each. After development with 3,3' diaminobenzidine tetrahydrochloride (DAB, 0.03-0.05% in 0.05 M Tris-HCl, pH 7.6, 0.01-0.03% H_2O_2) for 5-10 minutes, sections were counterstained with hematoxylin, dehydrated, cleared and mounted. Cleaved caspase-3 was detected in testes from 4-6 months old *Bscl2*$^{+/+}$ males (N=3) and *Bscl2*$^{-/-}$ males (N=4) using rabbit anti-cleaved caspase-3 (Asp175) antibody (1:300 dilution, Cell Signaling Technology) in paraffin sections. Two types of negative control were used: sections from 3 months old *Bscl2*$^{-/-}$ males incubated with anti-seipin antibody, and sections of 3 months old *Bscl2*$^{+/+}$ males incubated with normal rabbit IgG (1: 1,000, Santa Cruz Biotechnology). All other procedures were the same as described above. Testes from at least three different mice were used.

In situ end-labeling plus (ISEL$^+$). ISEL$^+$ detects DNA breaks [45, 46]. One testis each from 3-4 months old *Bscl2*$^{+/+}$ and *Bscl2*$^{-/-}$ males (N=5) was analyzed. Five consecutive testis sections (10 μm) separated by 200 μm each from each testis were processed for ISEL$^+$ labeling as previously described [45, 46]. All fifty sections (10 mice, 5 sections each) were processed at the same run and low magnification (4x) images were taken at the same setting. Only the entire area covered with testis section from each image was quantified using ImageJ (National Institutes of Health, Bethesda, MD) to determine the stained area. ISEL$^+$ labeling was expressed as ISEL$^+$ labeled area x 100 / total area analyzed. The average of all five sections was used to represent each sample for statistical analysis. Testis sections from another set of 3-4 month old mice (N=3) were processed for ISEL$^+$ labeling and counterstained with DAPI as previously described [46].

Annexin V staining. Testes from 5 months old control (N=3) and *Bscl2*$^{-/-}$ (N=4) males were decapsulated and the seminiferous tubules were incubated in 0.25% trypsin at 37°C for 10 minutes. The trypsin solution was removed and a small piece of the seminiferous tubules was minced in annexin-V binding buffer and subsequently incubated with annexin V (Annexin V-FITC Apoptosis Kit, BioVision, Milpitas, CA, USA) at room temperature for 5 minutes in the dark. The cells were counterstained with DAPI. At least 100 round spermatids from each male were examined. The percentage of annexin V positive round spermatids was calculated.

Mitotracker staining. One cauda epididymis from each of the control mice (N=3) and two cauda epididymides from each of the *Bscl2*$^{-/-}$ mice (N=4) used for annexin V staining above were collected for staining mitochondria of sperm. Each sample was minced in 1 ml (for control) or 0.2 ml (for *Bscl2*$^{-/-}$) 1x PBS in a 1.5 ml microcentrifuge tube, and shaken at 37°C/5% CO2 for 5 minutes. Therefore, the *Bscl2*$^{-/-}$ samples were 10x concentrated in order to get sufficient sperm density due to low sperm count in the *Bscl2*$^{-/-}$ male. Mitotracker stock solution (MitoTracker®

Deep Red FM, Life Technologies, Grand Island, NY, USA) was added into the sperm suspensions to a final concentration of 10 μM and incubated in the dark at 37°C for 10 minutes. One drop of sperm suspension from each sample was added on a slide, air dried, and counterstained with DAPI.

Immunofluorescence. Frozen testis sections (10 μm) from 3-4 months old *Bscl2*$^{+/+}$ and *Bscl2*$^{-/-}$ males (N=4) were used for detecting the expression of vimentin, protamine 1, and protamine 2 following the procedure as described previously [74]. Sections were incubated with vimentin antibody (1:50 dilution, sc-373717, Santa Cruz Biotechnology, Dallas, Texas, USA), or protamine 1 antibody (1:100 dilution, 21 μg/ml, Hup1N, Briar Patch Biosciences, Livermore, CA, USA), or protamine 2 antibody (1:100 dilution, 21 μg/ml, Hup2B, Briar Patch Biosciences) overnight at 4°C. Vimentin, protamine 1, and protamine 2 signals were detected by incubating with Alexa Fluor 568 goat anti-mouse antibody (1:200 dilution, Life Technologies) for 30-60 minutes at room temperature. Testis sections were counterstained and mounted in DAPI (4',6-diamino-2-phenylindole)-containing Vectashield (Vector Laboratories, Burlingame, CA, USA). Two types of negative control were used: sections of 3 months old *Bscl2*$^{+/+}$ males incubated with mouse IgG (1:100, Santa Cruz Biotechnology) or without any primary antibody. All other procedures were the same as described above. In addition, protamine 1 and protamine 2 were also detected in the sperm spreads from *Bscl2*$^{+/+}$ and *Bscl2*$^{-/-}$ males (4 months old, N=3) using the same condition as for testis sections.

Acrosome labeling. Acrosomes were highlighted with Alexa Fluor 488 conjugated-peanut agglutinin (PNA) [77]. Briefly, fixed frozen testis sections from three young adult male mice in each group were treated with 0.3% Triton for 10 minutes at room temperature. Subsequently they

were incubated with 10 µg/ml PNA in 1% BSA in 1x PBS for one hour at room temperature, counterstained with DAPI, and mounted.

Spermatogenic surface preparations for chromatin analysis. Testes from *Bscl2*$^{+/+}$ and *Bscl2*$^{-/-}$ males (4 months old, N=3) were dissected and the tunica albuginea was removed to expose individual seminiferous tubules in 1x PBS. The seminiferous tubules were immediately processed for cytological analysis of marker proteins of meiotic chromosome synapsis as described previously [78]. Hypotonic treatment was used to aid in the dissociation of germ cells from the seminiferous tubules and to facilitate meiotic chromosome spreading and subsequent marker protein analysis by chromatin decondensation. Briefly, seminiferous tubules were incubated in a sodium citrate solution (30 mM Tris, 50 mM sucrose, 17 mM trisodium citrate, 5 mM EDTA, pH 8.2) for 25 to 35 min at room temperature. Following dissociation, drops of cell suspension were applied to wet glass slides containing 2% paraformaldehyde (PFA) (Electron Microscopy Services, Hatfield, PA, USA) and 0.15% Triton X-100 (Bio-Rad, Hercules, CA, USA) in H_2O to facilitate nuclear protein cross-linking. Slides were allowed to air-dry and then stored at −80°C until immunochemical analysis.

Immunofluorescence of spermatogenic surface spreads. Meiotic prophase I staging and the degree of chromosome synapsis in *Bscl2*$^{+/+}$ and *Bscl2*$^{-/-}$ spermatocytes were determined by co-immunochemical detection of the synaptonemal complex proteins 1 (SYCP1) and 3 (SYCP3) using polyclonal mouse anti-SYCP3 (Abcam, Cambridge, MA, USA) and polyclonal rabbit anti-SYCP1 (Abcam) antibodies at a 1:500 dilution in dilution buffer (1 mg/ml BSA (Sigma) in 1x PBS, 0.01% Triton X-100). Following overnight incubation at 4°C and repeated wash steps in dilution buffer, an Alexa Fluor 555 goat anti-mouse (Life Technologies) and an Alexa Fluor 488 goat anti-rabbit secondary antibody were applied at a dilution of 1:1000 for 1 h at room

temperature. The male germ cells were then counterstained and mounted in DAPI-containing Vectashield (Vector Laboratories). Similarly, the subnuclear localization of pericentric heterochromatin domains was detected using a rabbit anti-histone H3 tri-methylated at lysine 9 (H3K9me3) antibody (1:400, Upstate, Charlottesville, VA, USA). Immunofluorescence and chromatin configurations were visualized using a Leica DMRE fluorescence microscope (Buffalo Grove, IL, USA), and images were captured using a Leica DFC 350F CCD camera. At least 100 randomly selected round spermatids from each sample were examined for the presence of chromocenter fragmentation. At least 100 randomly selected elongating spermatids and sperm from each sample were examined for the presence of chromatin vacuoles. The percentages of round spermatids with chromocenter fragmentation as well as elongating spermatids and sperm with chromatin vacuoles were quantified.

Statistical analyses. Data are presented as mean±SD. Wilcoxon-rank sum test was used for plugging latency. Chi-square test was used for pregnancy rate and plugging rate. Two tail unequal variance student t-test was used for the rest parameters. For the parameters with percentages, student t-test was performed after arcsin transformation. The significance level was set at $P<0.05$.

Acknowledgements

The authors thank the Department of Pathology in the College of Veterinary Medicine, University of Georgia for access to the imaging system; Dr. James N. Moore in the Department of Large Animal Medicine for access to the ABI 7900 Realtime PCR machine; Dr. Qien Yang at Northwest Plateau Institute of Biology, The Chinese Academy of Sciences for insightful suggestions; the Office of the Vice President for Research, Interdisciplinary Toxicology Program, and Department of Physiology and Pharmacology at the University of Georgia, the

National Institutes of Health (NIH R15HD066301 and NIH R01HD065939 (co-funded by ORWH and NICHD) to XY and NIH 2R01HD042740 to RDLF) and the Georgia Cancer Coalition (to RDLF) for financial support.

2.6 Supplementary Figures

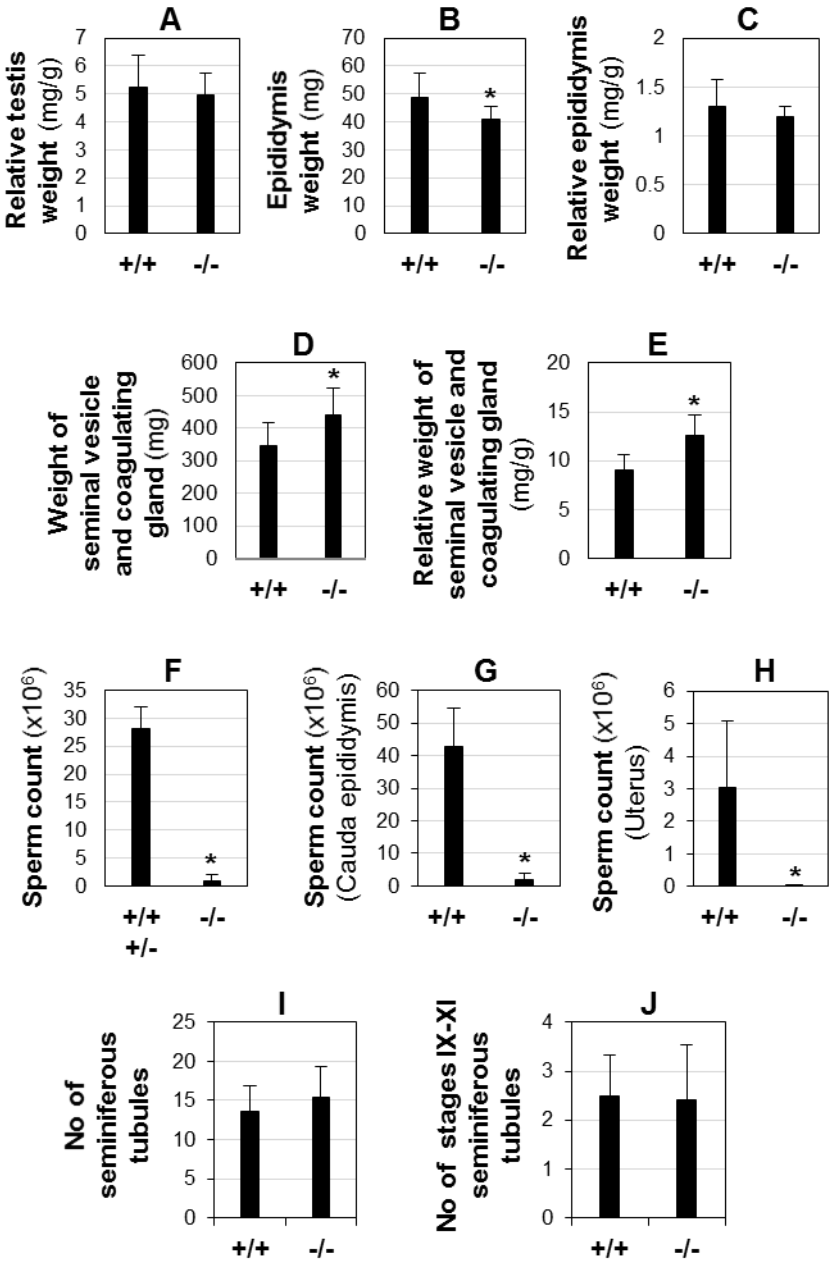

Figure S1. Male fertility test, sperm analyses, and quantification of seminiferous tubules. +/+, *Bscl2*$^{+/+}$; +/-, *Bscl2*$^{+/-}$; -/-, *Bscl2*$^{-/-}$. A-E: data from males at the end of 2 months fertility test. A. Relative testis weight. B. Epididymis weight. C. Relative epididymis weight. D. Weight of seminal vesicle and coagulating gland. E. Relative weight of seminal vesicle and coagulating gland. A-E: N=7 (+/+) and 10 (-/-). F. Sperm count for determining percentage of motile sperm.

N=6 (+/+ & +/-) and 9 (-/-). G. Sperm count in the cauda epididymis of mated males 1 week after mating. H. Sperm count in the uterus of the mated females in the morning after mating. G-H: N=5 (+/+) and 7 (-/-). I. Number of seminiferous tubules in 20x testis histology images. J. Number of stages IX-XI seminiferous tubules in 20x testis histology images. I-J: N=6 (+/+) and 5 (-/-), 3-6 months old. A-J: error bar, standard deviation; *, P<0.05.

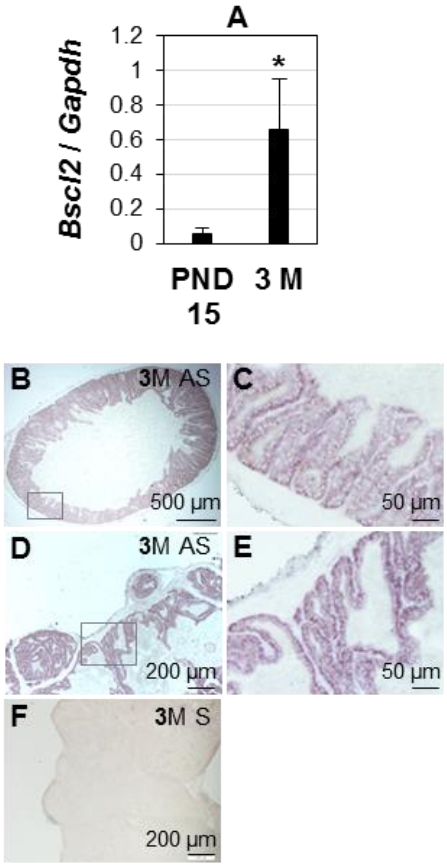

Figure S2. Expression of *Bscl2* mRNA in *Bscl2*$^{+/+}$ testis, coagulating gland, and seminal vesicle. A. Upregulation of *Bscl2* mRNA in testis from postnatal day 15 (PND15) to 3 months (3M) old by quantitative PCR. N=5 (PND15) and 3 (3M); error bar, standard deviation; *, P=0.069. B-F: in situ hybridization; tissues from 3 months old males. B. Localization of *Bscl2* mRNA in epithelium of a coagulating gland. Antisense (AS) probe; scale bar, 500 µm. C. Enlarged image

of the rectangle area in B. Scale bar, 50 µm. D. Localization of *Bscl2* mRNA in epithelium of a seminal vesicle. Antisense probe; scale bar, 200 µm. E. Enlarged image of the rectangle area in D. Scale bar, 50 µm. F. A seminal vesicle section incubated with a sense probe as the negative control.

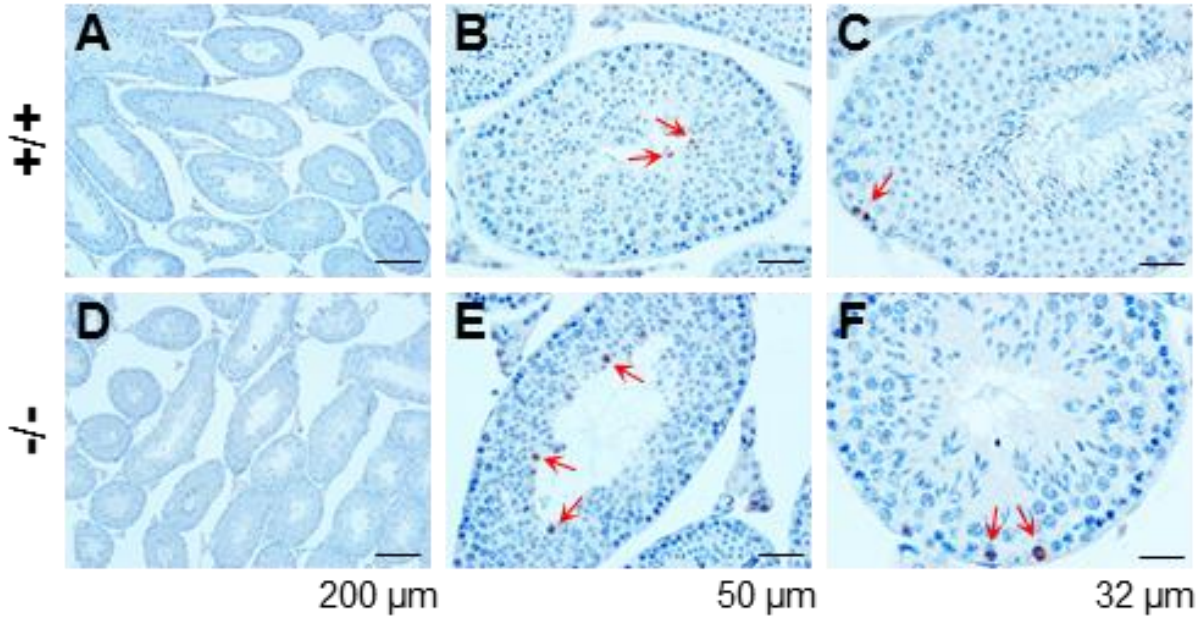

Figure S3. Detection of cleaved caspase-3 using immunohistochemistry in 4-6 months old *Bscl2*$^{+/+}$ (+/+) and *Bscl2*$^{-/-}$ (-/-) testes. A-C. *Bscl2*$^{+/+}$ testis. D-F. *Bscl2*$^{-/-}$ testis. Red arrows, cleaved caspase-3 positive germ cells; scale bars, 200 µm (A, D), or 50 µm (B, E), or 32 µm (C, F).

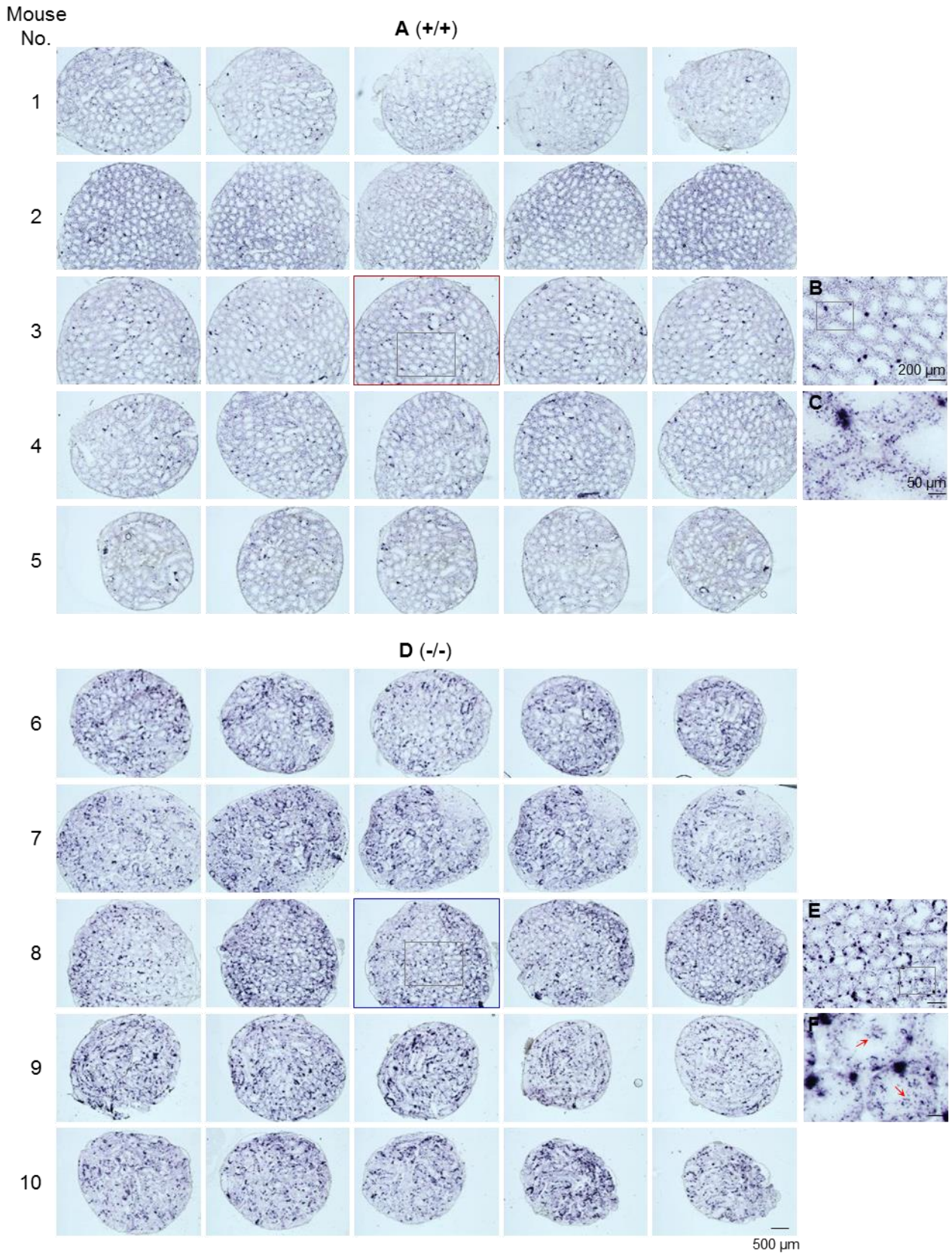
Mouse No.
A (+/+)
1
2
3
4
5
B
200 μm
C
50 μm
D (-/-)
6
7
8
9
10
E
F
500 μm

Figure S4. In situ end-labeling plus (ISEL+) of 3-4 months old *Bscl2*$^{+/+}$ (+/+) and *Bscl2*$^{-/-}$ (-/-) testes. One testis from each mouse (N=5 per group) was analyzed. Mouse number from each group was indicated on the left. Five consecutive testis sections (10 μm) separated by 200 μm each from each testis were shown. All these sections were quantified and the average of the five sections from each mouse was used for quantification shown in Figure 4A. A. *Bscl2*$^{+/+}$ testis sections. B. Enlarged image of the rectangle area in the third section of male No. 3. C. Enlarged image of the rectangle area in B. D. *Bscl2*$^{-/-}$ testis sections. E. Enlarged image of the rectangle area in the third section of male No. 8. F. Enlarged image of the rectangle area in E. Red arrows indicating ISLE+ labeled spermatids. C & F: Green arrows indicating clusters of ISLE+ labeled germ cells. Scale bars: 500 μm in A & D; 200 μm in B & E; and 50 μm in C & F.

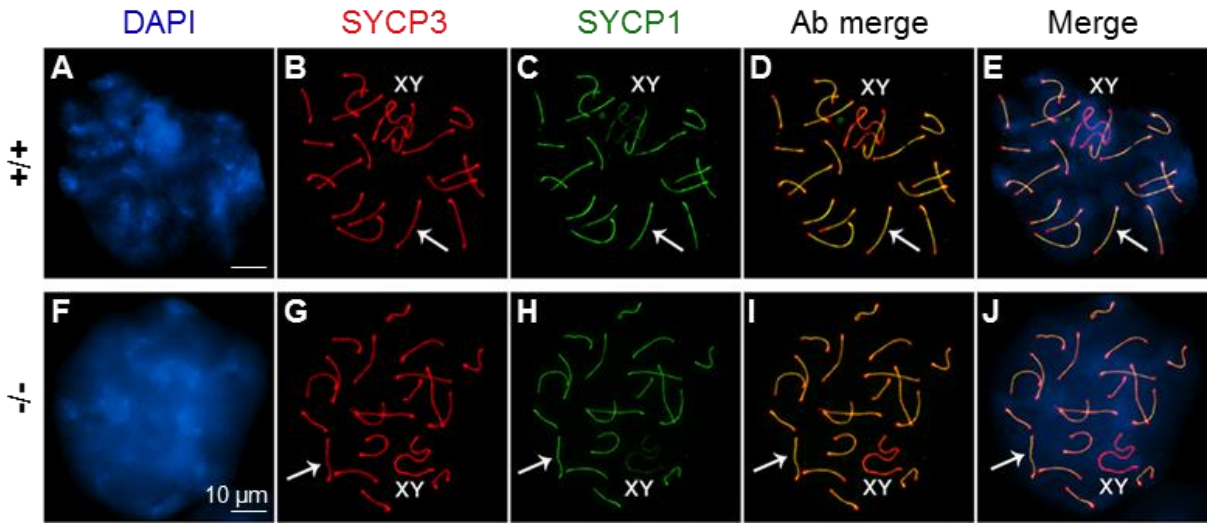

Figure S5. Homologous chromosome synapsis in spermatocytes. A. Blue DAPI staining of a *Bscl2*$^{+/+}$ (+/+) spermatocyte. B. Red SYCP3 staining of the spermatocyte in A. C. Green SYCP1 staining of the spermatocyte in A. D. Merged image of B and C. E. Merged image of A, B, and C. F. Blue DAPI staining of a *Bscl2*$^{-/-}$ (-/-) spermatocyte. G. Red SYCP3 staining of the spermatocyte in F. H. Green SYCP1 staining of the spermatocyte in F. I. Merged image of G and

H. J. Merged image of F, G, and H. Arrows, autosomes; XY, position of the sex chromosomes at the XY body. Scale bar, 10 µm.

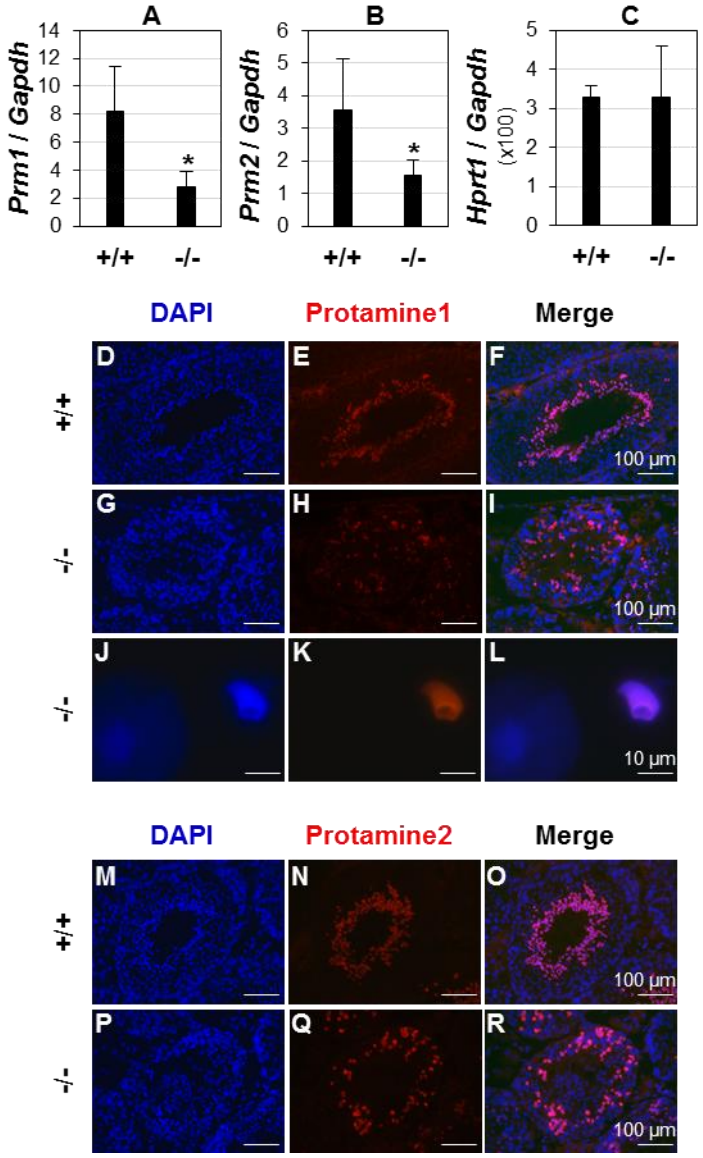

Figure S6. Expression of protamine 1 and 2 mRNAs and proteins in testis. Males at 3-4 months old were used in the studies. A-C. mRNA expression of protamine 1 (Prm1) (A), Prm2 (B), and hypoxanthine phosphoribosyltransferase 1 (Hprt1) (C) in *Bscl2*$^{+/+}$ (+/+) and *Bscl2*$^{-/-}$ (-/-) testis. N=5; error bars, standard deviation; * P<0.05. D. DAPI staining of *Bscl2*$^{+/+}$ seminiferous epithelium. E. Protamine 1 staining of the section in D. F. Merged image of D and E. G. DAPI

staining of *Bscl2*$^{-/-}$ seminiferous epithelium. H. Protamine 1 staining of the section in G. I. Merged image of G and H. J. DAPI staining of *Bscl2*$^{-/-}$ sperm spread. A round spermatid on the left side and a late spermatid with chromatin vacuoles on the right side. K. Protamine 1 staining of the late spermatid in J. L. Merged image of J and K. M. DAPI staining of *Bscl2*$^{+/+}$ seminiferous epithelium. N. Protamine 2 staining of the section in M. O. Merged image of M and N. P. DAPI staining of *Bscl2*$^{-/-}$ seminiferous epithelium. Q. Protamine 2 staining of the section in P. R. Merged image of P and Q. Scale bar, 100 μm in D-I and M-R, 10 μm in J-L.

CHAPTER 3

ASSOCIATION OF LIPODYSTROPHY WITH DEFECTIVE PARTURITION IN MICE

Ahmed E. El Zowalaty, and Xiaoqin Ye. Manuscript submitted to *Biology of Reproduction.*

3.1 Abstract

Seipin is an integral endoplasmic reticulum membrane protein encoded by Berardinelli–Seip congenital lipodystrophy type 2 (*BSCL2*/*Bscl2*) gene. Seipin deficiency results in lipodystrophy and muscle hypertrophy in both human and mouse. *Bscl2*$^{-/-}$ female mice mated with WT stud males had normal embryo implantation and pregnancy. In the first cohort monitoring four consecutive pregnancies, *Bscl2*$^{-/-}$ females had reduced delivery rates from 2nd-4th pregnancies and reduced numbers of pups delivered from 1st-4th pregnancies. In the second cohort charactering parturition from first pregnancy, *Bscl2*$^{-/-}$ females had increased gestation period and parturition problems, including uterine prolapse, difficulty in delivery, undelivered fetuses, and undelivered tissues. *Bscl2*$^{-/-}$ uterine weight was comparable to control at three weeks old but significantly increased with myometrial hypertrophy at 10 months old. *In situ* hybridization revealed relatively low expression of *Bscl2*$^{-/-}$ mRNA in myometrium from prepubertal to adult and from pregnancy to postpartum, suggesting that systemic effect (e.g., high insulin level) rather than local seipin-deficiency in myometrium might be a main contributing factor to myometrial hypertrophy. On near term gestation day 18.5 (D18.5), *Bscl2*$^{-/-}$ females had normal levels of serum progesterone and 17β-estradiol, indicating functional ovary and placenta. PCNA staining showed minimal myometrial cell proliferation in both D18.5 WT and *Bscl2*$^{-/-}$ uteri. Histology and α-SMA staining indicated disorganized D18.5 *Bscl2*$^{-/-}$ myometrium. LC3 immunofluorescence revealed strong staining in myometrium of both WT and *Bscl2*$^{-/-}$ postpartum day 1 (PPD1) uteri, indicating autophagy in postpartum uterine involution. PPD1 *Bscl2*$^{-/-}$ myometrium was disorganized. This study demonstrates the associations among lipodystrophy, myometrial function, and parturition.

3.2 Introduction

Parturition is the end of pregnancy. The timing of parturition is critical for the health of the mother and the newborn. Preterm births count for ~11.5% of all live births in US and are the main cause of perinatal mortality and morbidity worldwide [79]. Based on WHO 2011 report, up to 25% of all deliveries at term in developed countries involve induction of labor, although it is unclear about the incidence of induced labor due to difficulties in parturition. Uterine quiescence is essential for maintaining pregnancy and uterine transition from quiescence to contraction is a prerequisite for natural parturition. Research from past decades has provided critical insights into parturition, but the molecular mechanisms involved in the initiation of parturition remain largely unknown. It is known that the myometrium plays an essential role in regulating uterine quiescence and contraction, and progesterone and estrogen play important roles in regulating myometrium activities [79]. Similar as other muscle cell contractions, myometrial contractions are also mediated by elevated intracellular calcium concentration ($[Ca^{2+}]_i$), which is regulated by both Ca^{2+} release from intracellular stores in the sarcoplasmic reticulum (SR) and Ca^{2+} entry from the extracellular space [80-82]. Both SR Ca^{2+} efflux [83, 84] and extracellular Ca^{2+} influx [85, 86] in myometrial smooth muscle cells are important for myometrial contractions during pregnancy. The molecular mechanisms regulating Ca^{2+} mobility in the myometrium and uterine contractility during parturition are not fully understood thus constrain efforts to develop effective therapies to regulate parturition timing, especially for preterm labor.

Seipin is an integral endoplasmic reticulum (ER) membrane protein encoded by *BSCL2* gene and seipin deficiency results in lipodystrophy and muscle hypertrophy in both human and mouse [27, 35, 87, 88]. It has been demonstrated that seipin physically interacts with the sarco/endoplasmic reticulum Ca^{2+}-ATPase (SERCA), an ER Ca^{2+} pump solely responsible for Ca^{2+} influx into ER lumen; and mutated seipin causes decreased ER Ca^{2+} and increased $[Ca^{2+}]_i$ in

adipocytes [34]. SERCA plays a critical role in myometrial smooth muscle contraction [89]. In addition, *Bscl2*$^{-/-}$ mice have dramatically increased plasma insulin levels [35]. Insulin has many major effects on muscle cells that could lead to muscle hypertrophy [90]. Therefore, seipin could also regulate muscle functions via a systemic effect, e.g., insulin.

We have been studying the functions of seipin in reproductive systems using seipin-deficient *Bscl2*$^{-/-}$ mice and identified roles of seipin in mammary gland development, vaginal opening, and spermatogenesis [87, 88]. Since muscle hypertrophy is a common clinical feature associated with Berardinelli-Seip congenital lipodystrophy (BSCL) [91] and uterine smooth muscle contractions are critical for parturition, it was hypothesized that seipin played a role in parturition. This hypothesis was tested in seipin-deficient *Bscl2*$^{-/-}$ adult female mice.

3.3 Materials and Methods

Animals. *Bscl2*$^{-/-}$ mice in C57BL/6J background were derived from a colony at Georgia Regents University, which was originated from a colony at Baylor College of Medicine with backcrosses to C57BL/6J background for five generations [35]. Genotyping was done as previously described [87, 88]. *Bscl2*$^{+/+}$ (WT) and *Bscl2*$^{+/-}$ females were used as the genotype control for *Bscl2*$^{-/-}$ females. They were housed in polypropylene cages with free access to food and water on a 12 h light/dark cycle (0600–1800) at 23±1°C with 30–50% relative humidity at the College of Veterinary Medicine animal facility at the University of Georgia. The animals were sacrificed by CO_2 inhalation followed with cervical dislocation. All methods used in this study were approved by the University of Georgia Institutional Animal Care and Use Committee (IACUC) Committee and conform to National Institutes of Health guidelines and federal law.

Fertility. Young virgin WT and *Bscl2*$^{-/-}$ females were mated with WT stud males. Pregnancy was initially determined by the increase of body weight (>30%) and the continuous changes of the belly shapes. In the first cohort, pregnant WT (N=20) and *Bscl2*$^{-/-}$ females (N=25) were

included. After each pregnancy and lactation period, they were mated with the stud males again to produce up to 4 litters by 10 months old. Delivery rate was determined as the percentage of term pregnant females that had pups found in the cages after the reduction of body weight or euthanasia. The delivery rates of four consecutive litters were recorded. In the second cohort, young virgin adult control (WT) females and *Bscl2*$^{-/-}$ females were mated with WT stud males for determining the parameters of the 1st pregnancy. They were checked daily for the presence of a vaginal plug. The detection of a vaginal plug was defined as gestation day 0.5 (D0.5). Plugging rate was defined as the percentage of females with a vaginal plug. Plugging latency was determined by the time between cohabitation and the detection of the 1st vaginal plug. Gestation day was the time period between mating (indicated by the presence of a vaginal plug) and detection of pups in the morning. A total of 15 WT and 23 *Bscl2*$^{-/-}$ term pregnant females were included in this cohort. Gestation period was determined as the period between the detection of a vaginal plug and the detection of pups in the cage. Parturition problems, such as difficult delivery, death from delivery, and uterine prolapse were recorded.

Number of implantation sites on D13.5. WT and *Bscl2*$^{-/-}$ females (4 months old) were mated with WT stud males. On D13.5, the pregnant WT (N=16) and *Bscl2*$^{-/-}$ (N=7) females (determined by the change of body weight) were dissected. The numbers of healthy-looking and resorbed implantation sites were recorded. The healthy-looking implantation sites were also dissected and weighted. The average weight of healthy-looking implantation sites from each female was counted as one data point.

Uterine weight and uterine histology. Body weight and uterine weight from prepubertal 3 weeks old control (N=6) and *Bscl2*$^{-/-}$ (N=4) females were recorded. At the end of four consecutive four litters from fertility test, the ~10 months old WT (N=15) and *Bscl2*$^{-/-}$ (N=11)

females were checked for estrous cycle as previously described [92]. They were dissected on metestrus stage. The body weight, uterine weight, and uterine length were recorded.

Uterine histology. Histology of D18.5 and 10 months old WT and *Bscl2*$^{-/-}$ uteri was performed as previously described [74, 93].

Serum progesterone (P4) and 17β-estradiol (E2) measurement. D18.5 WT (N=7) and *Bscl2*$^{-/-}$ females (N=6) females (2-4 months old) were anesthetized ~11:00 h for blood collection via orbital sinus. Serum was collected after blood clotting at room temperature for 90 minutes and stored at -80°C. Serum P4 and E2 levels were measured at the Ligand Assay and Analysis Core of the Center for Research in Reproduction at the University of Virginia (Charlottesville, Virginia).

In situ hybridization. *Bscl2* mRNA was detected using *in situ* hybridization as previously described [72, 87, 94-98].

Immunohistochemistry and immunofluorescence. Frozen uterine sections (10 um) were used for immunohistochemistry and immunofluorescence as previously described [74, 87] using the following antibodies: alpha-SMA (1:200, A2547, Sigma), PCNA (1:1,000, D3H8P, Cell Signaling Technology), and LC3/MAP1LC3A (1:300, NB100-2220, Novus Biologicals).

Statistical analyses. Two-tailed Fisher's exact test was used to compare the rates (e.g., delivery rate). Two-tail unequal variance Student's t-test was used to compare other parameters. The significant level was set at $p<0.05$.

3.4 Results

Reduced delivery rate and litter size in Bscl2$^{-/-}$ *female mice*

Young adult WT and *Bscl2*$^{-/-}$ female mice were mated with WT stud males for up to 4 consecutive pregnancies or up to 10 months old. All the WT pregnant females except one in the 3rd pregnancy had pups in the cages upon the sharp drop of body weights after delivery.

However, some pregnant *Bscl2*$^{-/-}$ females did not have pups in the cages and/or had problems in delivering pups. The percentages of pregnant *Bscl2*$^{-/-}$ females that had pups in the cages were significantly decreased in 2nd-4th pregnancies (Fig. 1A). The litter sizes from those having pups in the cages were significantly decreased in all four pregnancies in the *Bscl2*$^{-/-}$ females (Fig. 1B). In this cohort, one WT female died after having delivered 2 litters and two WT females died after having delivered 4 litters with unknown causes that were not related to parturition; while 6 *Bscl2*$^{-/-}$ females were lost during 1st and 2nd pregnancies, 5 of them caused by parturition problems. There were no significant differences in the average ages of the pregnant females on the same order of pregnancies or the term pregnancy rates between WT and *Bscl2*$^{-/-}$ females in this cohort (data not shown). These data indicated that *Bscl2*$^{-/-}$ females had no problem getting pregnancy to term but had problem with parturition.

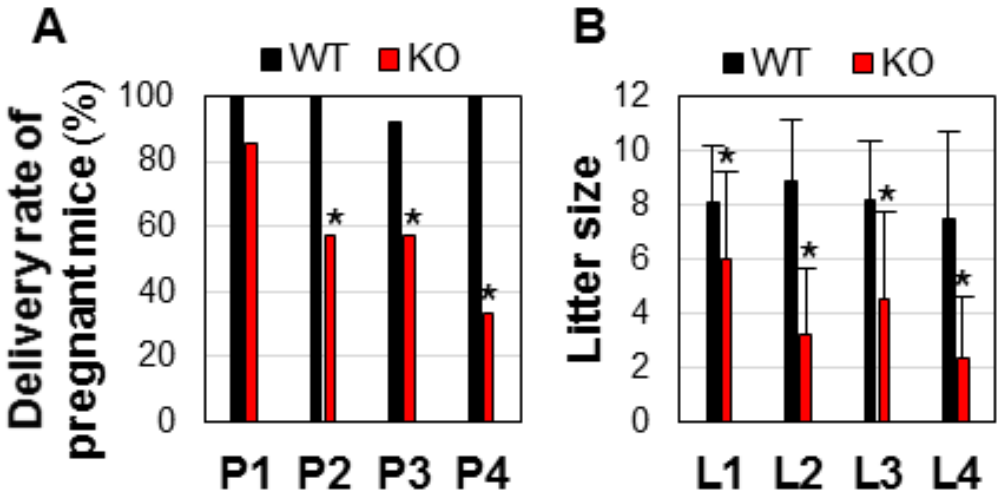

Figure 1. Fertility test from four consecutive pregnancies. A. Delivery rates of four consecutive pregnancies (P1-P4) in the same cohort of wild type (WT) and *Bscl2*$^{-/-}$ (KO) females. N=20, 18, 12, and 8 for WT P1, P2, P3, and P4, respectively; N=27, 21, 14, and 9 for KO P1, P2, P3, and P4, respectively. B. Litter sizes from four consecutive deliveries (L1-L4). N=20, 18, 11, and 8 for WT L1, L2, L3, and L4, respectively; N=23, 12, 8, and 3 for KO L1, L2, L3, and L4, respectively. A & B: * P<0.05 compared to

WT on the same pregnancy / litter order; # P<0.05 compared to 1st pregnancy (P1); error bar, standard deviation.

Characterization of parturition problems in the first term pregnancy of Bscl2$^{-/-}$ females

Data from the second cohort of mice examined for 1st pregnancy indicated that the WT and *Bscl2*$^{-/-}$ female mice had comparable plugging rate and 1st plugging latency (data not shown), indicating that the *Bscl2*$^{-/-}$ female mice had normal mating activity. However, comparing to the WT control females (N=15), there were multiple problems in the *Bscl2*$^{-/-}$ females (N=23). First, there was an overall increased gestation period in the *Bscl2*$^{-/-}$ females excluding four term pregnant *Bscl2*$^{-/-}$ females without showing pups in the cages (including one died during delivery and one euthanized on D24.5 while still pregnant) and two missed plug detection (Fig. 2A). Among the remaining 17 *Bscl2*$^{-/-}$ females with gestation periods recorded, 41.2% (7/17) females delivered by D19.5, 29.4% (5/17) by D20.5, and 29.4% (5/17) between D21.5 and D22.5 (Fig. 2A); while 80% (12/15) WT females delivered by D19.5 and the rest 20% by D20.5. Second, none of the WT females in this cohort showed parturition problems, while the *Bscl2*$^{-/-}$ females had the following issues: a few females were caught being inactive or in a stressed situation during delivery (Fig. 2B), one died on D19.5 during delivery without pups in the cage and with belly still swollen; one died after delivering two pups on D20.5 with six fetuses remained undelivered (Fig. 2C), one had prolonged delivery and delivered 5 pups on both D21.5 and D22.5, one had uterine prolapse and euthanized on D24.5, one delivered 1 pup on D22.5 and euthanized due to uterine prolapse, one had two pups delivered on D21.5 with a bloody vagina, another had a bloody vagina although no pups were found in the cage. In addition, a *Bscl2*$^{-/-}$ female that had a normal delivery on D19.5 showed undelivered dark tissues in the uterus (Fig. 2D). Another *Bscl2*$^{-/-}$ female delivered on D20.5 and was dissected one day after delivery on postpartum day 2 (PPD2). Uterine histology indicated retention of membranous structures in the

uterine lumen of this mouse (Fig. 2E). These data demonstrated parturition problems in the *Bscl2*$^{-/-}$ females.

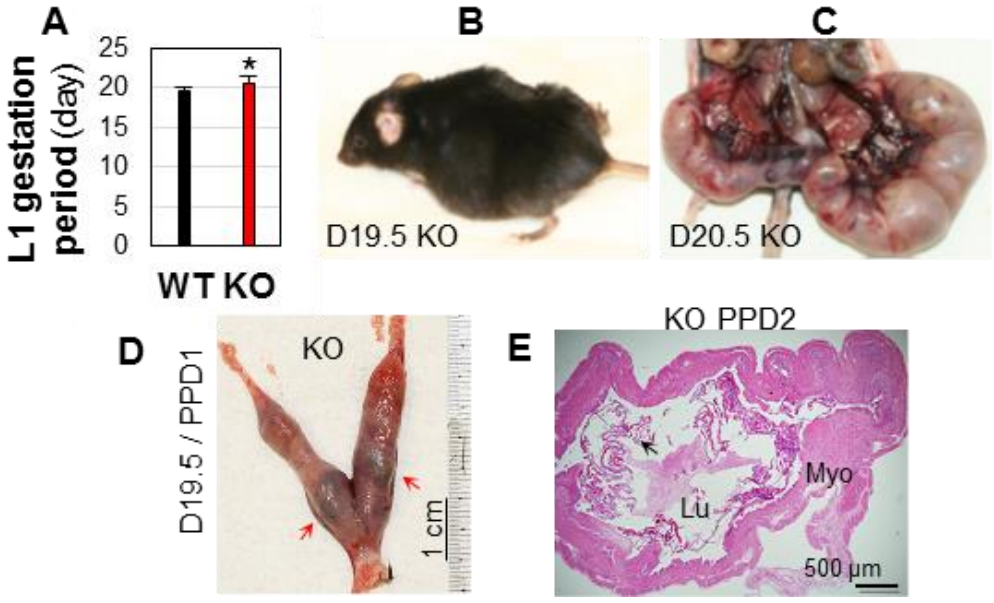

Figure 2. Parturition problems from 1st pregnancy in *Bscl2*$^{-/-}$ (KO) mice. A. Increased gestation period in *Bscl2*$^{-/-}$ (KO) females. N=11-17. * P<0.05. B. A stressed gestation day 19.5 (D19.5) *Bscl2*$^{-/-}$ female during delivery. C. A *Bscl2*$^{-/-}$ female died on D20.5 after delivering of two pups with five fetuses remained undelivered. D. A D19.5/postpartum day 1 (PPD1) *Bscl2*$^{-/-}$ uterus with undelivered tissue indicated by red arrows. E. Uterine histology of a PPD2 *Bscl2*$^{-/-}$ uterus indicating retention of membranous structures (black arrow) in the uterine lumen. Myo, myometrium; Lu, uterine lumen.

Normal embryo implantation in Bscl2*$^{-/-}$ *female mice

To determine the cause of prolonged gestation period and the reduced litter size in the *Bscl2*$^{-/-}$ females (Figs. 1, 2), pregnant WT and *Bscl2*$^{-/-}$ females mated with WT stud males were dissected on D13.5. There were comparable total numbers of implantation sites (including resorbed ones) (Fig. 3A). In the WT uteri, half (8/16=50%) had no resorbed implantation sites, the other half had 1-3 resorbed implantation sites per uterus. In the *Bscl2*$^{-/-}$ uteri, all (7/7=100%) had 1-3 resorbed implantation sites per uterus. There was an increased average number of

resorbed implantation sites in the D13.5 *Bscl2*$^{-/-}$ females (Fig. 3D). However, there were no significant differences in the average numbers and weights of healthy-looking D13.5 implantation sites between WT and *Bscl2*$^{-/-}$ females (Fig. 3C-3E), indicating normal embryo implantation timing and number of implanted embryos in the *Bscl2*$^{-/-}$ females. It also indicated that the *Bscl2*$^{-/-}$ ovaries were functional although enlarged ovaries were observed in the *Bscl2*$^{-/-}$ females (Fig. 3E). These data corroborated that the prolonged gestation period in the *Bscl2*$^{-/-}$ females was mainly contributed by parturition problems and the reduced litter size at birth in the *Bscl2*$^{-/-}$ females was also mainly contributed by parturition problems although post-implantation death could be a small contributing factor.

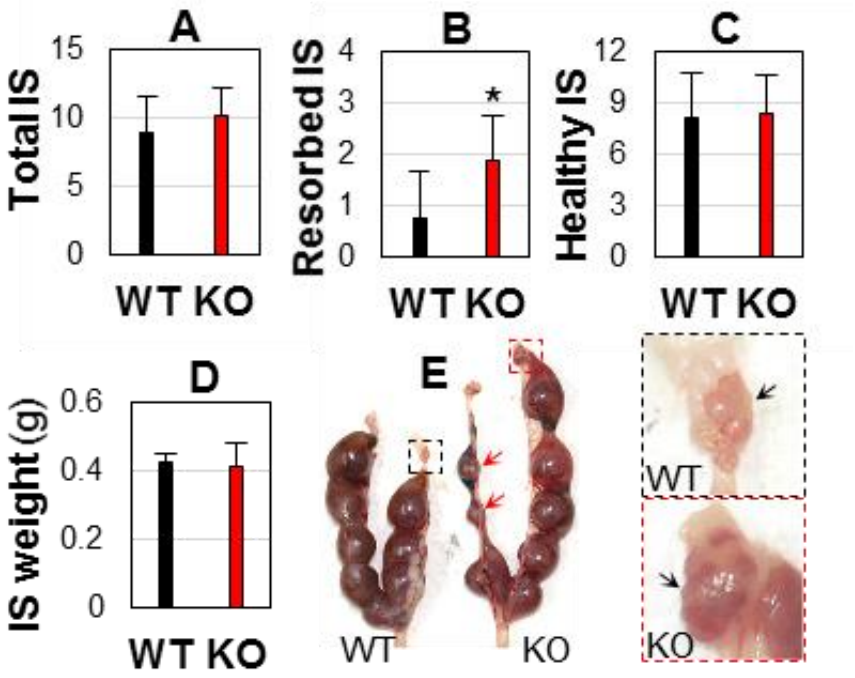

Figure 3. Gestation day 13.5 (D13.5) implantation sites (IS). WT and *Bscl2*$^{-/-}$ (KO) females (4 months old) were mated with WT stud males. A. Total number of all implantation sites. B. Number of resorbed implantation sites. C. Number of healthy implantation sites. D. Weight of healthy implantation sites. A-D: N=7-16; error bar, standard deviation; * P<0.05. E. Representative WT and KO uteri and enlarged view of right side ovaries. Red arrow, resorbed implantation sites; black arrow, ovary.

Increased uterine size in aged Bscl2$^{-/-}$ female mice

Since seipin deficiency is associated with muscle hypertrophy in both human and mouse [27, 35] and a main part of the uterus is myometrium, the smooth muscle layer, it was hypothesized that hypertrophy might occur in the *Bscl2*$^{-/-}$ myometrium. To test this hypothesis, two time points were examined: 3 weeks old and 10 months old. At 3 weeks old, there was a slight decrease but no significant difference of both body weight and uterine weight in the *Bscl2*$^{-/-}$ females compared to WT and *Bscl2*$^{+/-}$ control females (Fig. 4A, 4B). The mice at 10 months old on metestrus stage were from the cohort in Figure 1. The average body weight was significantly decreased (18.8% reduction) in the *Bscl2*$^{-/-}$ females (Fig. 4C), but the absolute uterine weight was more than tripled (Fig. 4D) and the relative uterine weight was quadrupled in the *Bscl2*$^{-/-}$ females (data not shown) relative to those in the control females. The increased uterine weight was reflected in longer uterine lengths of both uterine horns and wider cross uterine areas with thicker myometrial layer (Fig. 4E-4H). These data demonstrated myometrial hypertrophy in the adult but not the immature *Bscl2*$^{-/-}$ females.

Interestingly, it was also noticed that these10 months old *Bscl2*$^{-/-}$ females had enlarged cystic ovaries (control: 1.85 ± 0.72 mg, N=15; KO: 4.56 ± 1.17 mg, N=11, $p<0.05$; and data not shown). However, based on the comparable mating activity, implantation timing, number of D13.5 implantation sites, and weight of D13.5 implantation sites between the WT and *Bscl2*$^{-/-}$ females, it was reasonable to conclude that there was no functional defect in the *Bscl2*$^{-/-}$ ovaries.

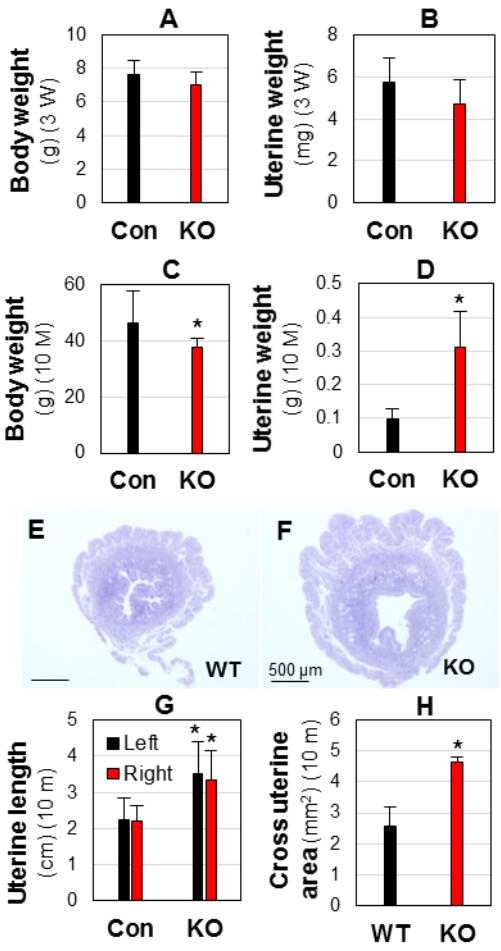

Figure 4. Body weight and uterine weight at 3 weeks old (A, B) and 10 months old at metestrus (C-H). Con, Bscl2+/+ & Bscl2+/-; WT, Bscl2+/+; KO, Bscl2-/-. A & B. Body weight (A) and uterine weight (B) at 3 weeks old. N=4-6. C & D. Body weight (C) and uterine weight (D) at 10 months old. N=7-13. E & F. Cross section of a WT uterus (E) and a KO uterus (F). G. Length of left and right uterine horns. N=7-13. H. Cross uterine area. N=3. * P<0.05; error bar, standard deviation.

Expression of Bscl2 in uterus and placenta

Since there were parturition problems (Fig. 1) and myometrial hypertrophy (Fig. 4) in the adult *Bscl2*$^{-/-}$ females, *Bscl2* mRNA expression in WT myometrium was detected using *in situ* hybridization. From pre-pubertal to adult, from early pregnancy to postpartum, the expression levels of *Bscl2* mRNA in the myometrium were not high (Fig. 5 and data not shown). However, it was noticed that *Bscl2* mRNA had increased expression levels in the uterine epithelium from pre-pubertal to adult (Fig. 5A, 5C1). The *Bscl2* mRNA was also detected in the uterine epithelium during pregnancy (Fig. 5D1, 5D2, and data not shown) and was highly expressed in the postpartum LD1 uterine epithelium (Fig. 5E1, 5E2). Interestingly, *Bscl2* mRNA was also highly detected in the labyrinth layer of placenta (Fig. 5B). The expression of *Bscl2* in the fetal membrane (Fig. 5D1, 5D2), stroma (Fig. 5A, 5C1, 5C2, 5E1, 5E2), and decidua (data not shown) was minimal.

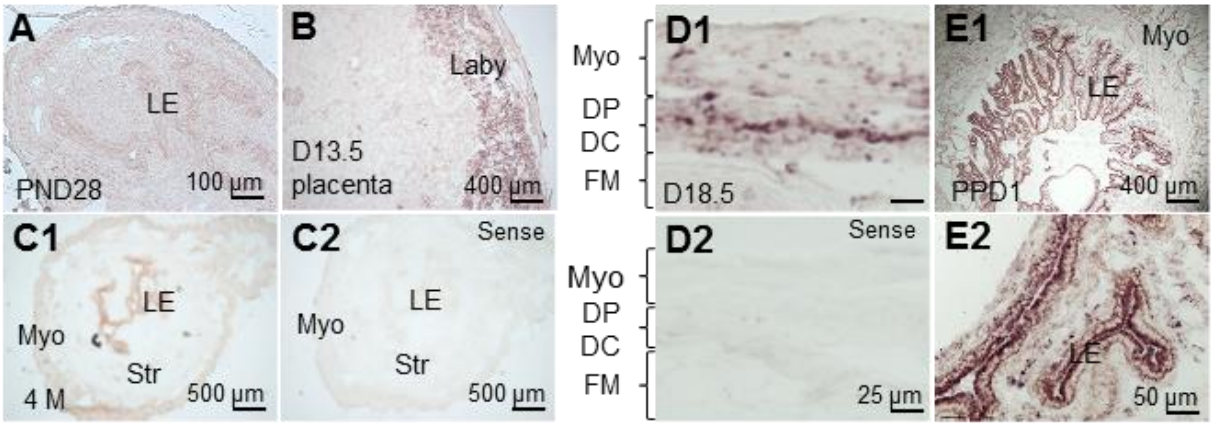

Figure 5. Expression of *Bscl2* in WT uterus and placenta. All images were from in situ hybridization using an antisense *Bscl2* cRNA probe except C2 and D2 using a sense *Bscl2* cRNA probe. A. Postnatal day 28 (PND28) uterus. B. Gestation day 13.5 (D13.5) placenta. C1-C2. Four-month old uterus at metestrus stage. D1-D2. Gestation day 18.5 (D18.5) uterus. E1. Postpartum day 1 (PPD1) uterus. E2.

Enlarged from E1. Myo, myometrium; DP, decidua parietalis; DC, decidua capsularis; FM, fetal membrane; LE, uterine luminal epithelium; Laby, labyrinth layer.

Disorganized myometrium but comparable myometrial cell proliferation and P4 and E2 levels in D18.5 Bscl2$^{-/-}$ females

Most WT females had a gestation period of 19.5 days (Fig. 2A), indicating that they delivered pups between D18.5 and D19.5. To determine the parameters prior to delivery, D18.5 females were examined. Histology of D18.5 uteri indicated disorganized smooth muscles in the *Bscl2*$^{-/-}$ uterus compared to the WT uterus (Fig. 6A, 6B). Alpha-SMA staining of the D18.5 uteri confirmed the disorganization of the uterine smooth muscles (Fig. 6C, 6D). PCNA staining indicated that PCNA positive cells were mainly detected in the uterine epithelium in both D18.5 WT and *Bscl2*$^{-/-}$ uteri, and there was minimal PCNA staining in the myometrium and no obvious difference between WT and *Bscl2*$^{-/-}$ uteri (Fig. 6E, 6F).

Since ovarian hormones, especially P4 that is critical for decidualization and decidual clock, was proposed to regulate parturition [99], serum P4 and E2 levels were measured in the term D18.5 females. No significant differences in both P4 and E2 levels were observed between the WT and *Bscl2*$^{-/-}$ females (Fig. 6G), indicating that the ovary and the placenta in the *Bscl2*$^{-/-}$ females were functional in producing these hormones.

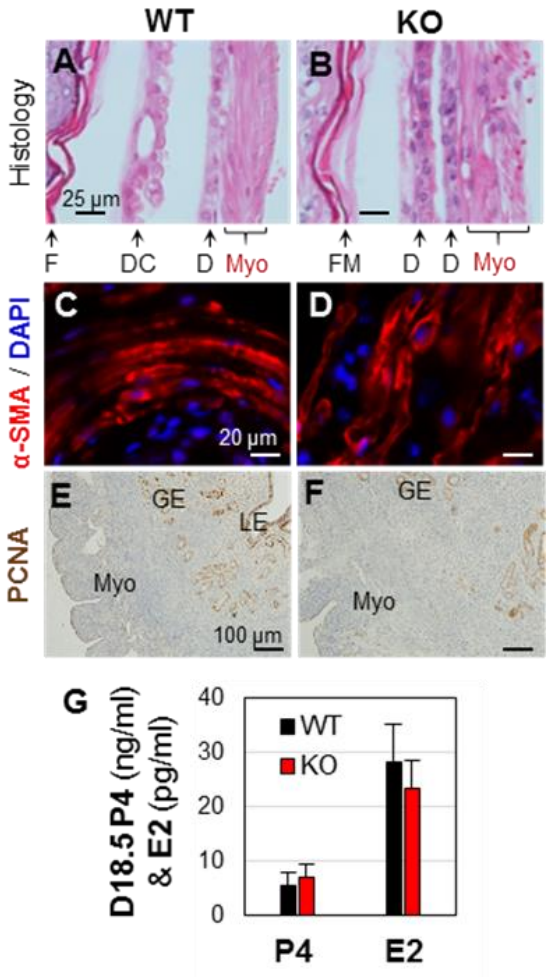

Figure 6. Parameters from near term D18.5 wild type (WT) and *Bscl2*$^{-/-}$ (KO) mice. A. WT uterine histology. B. KO uterine histology. C & D. Alpha-smooth muscle actin (α-SMA) staining of circular myometrium in WT (C) and KO (D) uteri. Red, α-SMA staining; blue, DAPI staining. E & F. PCNA staining (brown) in WT (E) and KO (F) uteri. A,B,E,F: FM, fetal membrane; DC, decidua capsularis; DP, decidua parietalis; Myo, myometrium; LE, uterine luminal epithelium; GE, glandular epithelium. G. Serum levels of progesterone (P4) and 17β-estradiol (E2). N=6-7; error bar, standard deviation.

Altered uterine autophagy in postpartum day 1 (PPD1) Bscl2$^{-/-}$ females

It has been suggested that autophagy is involved in postpartum uterine involution [100, 101]. Microtubule-associated protein light chain 3 (LC3) is widely used to monitor autophagy. LC3 immunofluorescence of four months old PPD1 uteri revealed differences between WT and

Bscl2$^{-/-}$ uteri. LC3 was highly detected in the myometrium of both WT and *Bscl2*$^{-/-}$ uteri. The inner circular and outer longitudinal smooth muscles were organized and tightly associated in the WT uterus (Fig. 7A, 7B). Those in the *Bscl2*$^{-/-}$ uteri were not as organized, for example, the thickness of circular smooth muscle surrounding the endometrium varied greatly in different areas, and the longitudinal smooth muscle bundles were loosely organized and not tightly associated with the inner circular smooth muscle layer (Fig. 7D, 7E). In addition, LC3 had higher expression in the *Bscl2*$^{-/-}$ endometrium, especially in the uterine luminal epithelium (Fig. 7D, 7F) compared to WT endometrium (Fig. 7A, 7C), and the difference in the LC3 expression levels between myometrium and endometrium was more in the WT compared to that in the *Bscl2*$^{-/-}$ (Fig. 7). These data indicated autophagy in the postpartum uterine involution but there was increased autophagy in PPD1 *Bscl2*$^{-/-}$ uterine luminal epithelium and disorganized myometrium in PPD1 *Bscl2*$^{-/-}$ uterus.

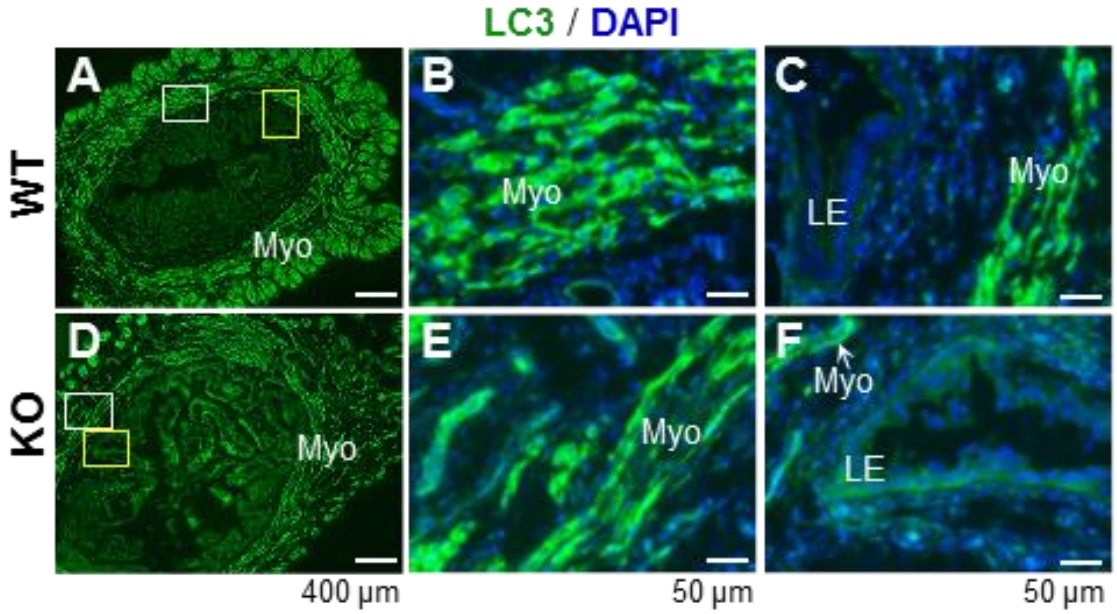

Figure 7. Immunofluorescence detection of LC3 in postpartum day 1 wild type (WT) and *Bscl2*$^{-/-}$ (KO) mice. Green, LC3; blue, DAPI. A. WT uterus. B. Enlarged from the white rectangle area in A. C. Enlarged from the yellow rectangle area in A. D. KO uterus. E. Enlarged from the white rectangle area in D. F. Enlarged from the yellow rectangle area in D. Myo, myometrium; LE, uterine luminal epithelium.

3.5 Discussion

Berardinelli-Seip congenital lipodystrophy (BSCL) is an autosomal recessive disease accompanied with lipodystrophy, diabetes and hypertriglyceridemia, and muscle hypertrophy is among the most common clinical features of BSCL [27, 35, 87, 88, 91]. This study revealed that seipin deficiency led to uterine smooth muscle hypertrophy in middle-aged mice but not in the prepubertal mice. Since *Bscl2* mRNA had relatively low expression levels in the myometrium from prepubertal to adult and throughout the pregnancy, it was possible that uterine smooth muscle hypertrophy was the result of a systemic effect similar as muscle hypertrophy in other areas of seipin-deficient mice.

A previous study demonstrated that *Bscl2*$^{-/-}$ mice had dramatically increased plasma insulin levels by 10 weeks old and they had insulin resistance [35]. Insulin has many major

effects on muscle cells, including increased rate of glucose transport across the cell membrane, increased rate of glycolysis, increased rate of glycogen synthesis and decreased rate of glycogen breakdown, increased uptake of triglyceride from the blood into muscle cells, decreased rate of fatty acid oxidation, and increased rate of protein synthesis but decreased rate of protein degradation [90]. Consequently, insulin can lead to muscle hypertrophy. Since there was no obvious increase of myometrial cell proliferation in the *Bscl2*$^{-/-}$ uterus, the increased uterine myometrium in the middle-aged *Bscl2*$^{-/-}$ uterus was likely the result of muscle hypertrophy instead of hyperplasia.

Myometrial contraction is a prerequisite for natural parturition. It is mediated by elevated $[Ca^{2+}]_i$ [80-82]. Both sarcoplasmic reticulum (SR) Ca^{2+} efflux [83, 84] and extracellular Ca^{2+} influx [85, 86] in myometrial smooth muscle cells are important for myometrial contractions during pregnancy via regulating $[Ca^{2+}]_i$. The molecular mechanisms regulating Ca^{2+} mobility in the myometrium and uterine contractility during parturition are not fully understood. It has been demonstrated that seipin physically interacts with the sarco/endoplasmic reticulum Ca^{2+}-ATPase (SERCA) and mutated seipin causes decreased ER Ca^{2+} and increased $[Ca^{2+}]_i$ in adipocytes [34]. It is unknown if seipin has a similar function in regulating $[Ca^{2+}]_i$ in myometrial smooth muscle cells as seen in adipocytes. It is known that SERCA plays a critical role for myometrial smooth muscle contraction [89]. Despite relatively low levels of expression, *Bscl2* mRNA was detected in the pregnant and nonpregnant myometrium. Muscle hypertrophy can be resulted from dysregulated Ca^{2+} [102, 103] and seipin mutation leads to increased $[Ca^{2+}]_i$ in adipocytes [34]. Although no data about $[Ca^{2+}]_i$ in the *Bscl2*$^{-/-}$ myometrium, based on the above information, it is speculated that seipin-deficiency in the myometrium might contribute to myometrial hypertrophy in *Bscl2*$^{-/-}$ female mice via dysregulated $[Ca^{2+}]_i$ in the myometrium.

Uterine myometrium has to be maintained in quiescent state during pregnancy and transformed into highly coordinated contractile state for parturition, and the P4 and E2 levels play important roles in regulating myometrium activities [79]. Since serum P4 and E2 levels were not altered in the near term *Bscl2*$^{-/-}$ females, it indicated functional ovary and placenta in the *Bscl2*$^{-/-}$ females and P4 and E2 were unlikely to contribute to the parturition problems in the *Bscl2*$^{-/-}$ females.

Parturition requires synchronized uterine smooth muscle contraction [79]. It was noticed that the myometrium was disorganized in the near term and postpartum day 1 *Bscl2*$^{-/-}$ uteri. The disorganization included highly varied thickness of circular smooth muscles, loosely associated longitudinal smooth muscle bundles, and loosely associated inner circular smooth muscle layer with longitudinal smooth muscle layer. These disorganizations could impair the synchronized uterine smooth muscle contraction required for parturition, thus couldn't mount sufficient myometrial contraction for parturition. It is currently unknown about the mechanisms of seipin in regulating uterine smooth muscle organization.

The postpartum uterus undergoes involution to return to pre-pregnant state. Since uterine smooth muscle hypertrophy is a main contributing factor for the increased uterine size during pregnancy, the reduction of uterine smooth muscle cell size is expected to be a main cellular mechanism for postpartum uterine involution, in which autophagy has been implicated [100, 101]. Autophagy is activated during stress conditions, such as starvation. The postpartum uterine myometrium is under starvation condition due to reduced blood flow after delivery of fetus and placenta. The strong LC3 staining in the WT and *Bscl2*$^{-/-}$ postpartum uterine myometrium confirmed autophagy in these cells. There was increased LC3 staining in the postpartum day 1 *Bscl2*$^{-/-}$ uterine luminal epithelium and *Bscl2* mRNA had the highest expression level in the

postpartum day 1 WT uterine luminal epithelium. The significance of increased LC3 staining in the postpartum day 1 *Bscl2*$^{-/-}$ uterine luminal epithelium and the relationship between *Bscl2* mRNA expression and LC3 staining in the postpartum day 1 uterine luminal epithelium are unknown.

This study demonstrates that seipin deficiency in mice leads to disorganized myometrium and defective parturition. It remains to be investigated about how seipin deficiency leads to myometrial disorganization to affect parturition. This study establishes and verifies the associations among lipodystrophy, myometrial function, and parturition.

Acknowledgements

The authors thank Dr. Weiqin Chen for providing *Bscl2*$^{-/-}$ mice and a suggestion on discussion, Mr. Christian Lee Anderson for assistance on mouse dissection, the Office of the Vice President for Research, Interdisciplinary Toxicology Program, and Department of Physiology and Pharmacology at the University of Georgia, and the National Institutes of Health (NIH R15HD066301 and NIH R01HD065939 (co-funded by ORWH and NICHD) to XY) for financial support.

Competing interests

The authors declare no conflict of interest.

CHAPTER 4

SEIPIN DEFICIENCY LEADS TO INCREASED ER STRESS AND APOPTOSIS IN MAMMARY GLAND ALVEOLAR EPITHELIAL CELLS DURING LACTATION

Ahmed E. El Zowalaty, Rong Li, Weiqin Chen, and Xiaoqin Ye. Manuscript submitted to *Biology of Reproduction*.

4.1 Abstract

Seipin is an integral endoplasmic reticulum (ER) membrane protein encoded by Berardinelli–Seip congenital lipodystrophy type 2 (*BSCL2*/*Bscl2*) gene. *Bscl2*$^{-/-}$ females had reduced nursing rate. Milk protein concentration from lactation day 1 (LD1) *Bscl2*$^{-/-}$ females was ~7% of the control. It was hypothesized that seipin was critical for lactation. *Bscl2* was upregulated and highly detected in the LD1 WT mammary gland alveolar epithelial cells. LD1 *Bscl2*$^{-/-}$ mammary glands lacked adipocytes and alveolar clusters and had varied alveolar morphology: from interconnected mammary gland alveoli with dilated lumen and sloughed epithelial cells to undifferentiated mammary gland alveoli with unexpanded lumen. Comparable levels of whey acidic protein (WAP, a major component in rodent milk) staining and Nile Red lipid droplet staining between WT and *Bscl2*$^{-/-}$ LD1 alveolar epithelial cells indicated normal milk protein synthesis and lipid syntheses in LD1 *Bscl2*$^{-/-}$ mammary glands. In the LD1 *Bscl2*$^{-/-}$ alveolar epithelial cells associated with unexpanded lumen, there appeared to have less lipid droplets in larger sizes compared to those associated with dilated lumen. There was no obviously impaired proliferation detected by PCNA staining but increased apoptosis detected by Cleaved Caspase-3 staining in LD1 *Bscl2*$^{-/-}$ alveolar epithelial cells. Increased protein disulfide isomerase (PDI) expression in the LD1 *Bscl2*$^{-/-}$ mammary gland alveolar epithelial cells indicated increased ER stress. This study demonstrates increased ER stress and apoptosis in LD1 *Bscl2*$^{-/-}$ mammary gland alveolar epithelial cells and reveals a novel *in vivo* function of seipin in lactation.

4.2 Introduction

The mammary gland undergoes tremendous side-branching and alveologenesis to prepare for lactation [104]. A lactating mouse can secrete ~30 g of lipids in milk during the 20 days of lactation [105] and 98% of milk lipids are triglycerides [106]. A lactating mouse mammary gland can rapidly take up injected radiolabeled fatty acids and convert them into lipid droplets [107]. Micro lipid droplets formed in the endoplasmic reticulum (ER) of a lactating mouse mammary gland consist of a triacylglycerol-rich core coated with a layer of proteins and polar lipids. This coating enhances aggregation of lipids into droplets. The lipid droplets are released from the ER in the mammary gland epithelium and fused with cytoplasmic lipid droplets, which are precursors of milk lipids [106] and are surrounded by the bilayer milk lipid globule membrane [108]. ER is also the site for synthesis of milk proteins [109]. Interestingly, seipin is identified as a protein in the milk lipid globule membrane [110]. A recent study demonstrates that seipin is required for converting nascent to mature lipid droplets, possibly through seipin at ER-lipid droplet contact sites [111].

Seipin is an integral endoplasmic reticulum membrane protein encoded by Berardinelli–Seip congenital lipodystrophy type 2 (*BSCL2*/*Bscl2*) gene [28]. It has been shown that seipin physically interacts with the sarco/endoplasmic reticulum Ca^{2+}-ATPase (SERCA) in adipocytes [34]. Seipin is required for adipocyte differentiation and lipid droplet accumulation [28, 33, 35, 112, 113]. Seipin deficiency results in lipodystrophy and muscle hypertrophy in human and mouse [27, 35, 87, 88]. Knockout of seipin in mice or in the fibroblasts of a human patient with seipin-based lipodystrophy results in small lipid droplets and an increase in the number of lipid droplets [37]. Since milk production from lactation also involves lipid droplet formation [108] and seipin is a protein in the milk lipid globule membrane [110], it suggests a potential role of seipin in lactation.

We have been investigating the roles of seipin in pubertal development and reproduction using *Bscl2*$^{-/-}$ mice [87, 88]. Previously we reported abnormalities in 5 weeks old *Bscl2*$^{-/-}$ mouse mammary glands, such as enlarged lymph nodes, longer and wider mammary gland ducts, and more terminal end buds (TEB) [88], suggesting altered pubertal mammary gland development. We observed that many neonatal pups from *Bscl2*$^{-/-}$ females died within a few days of birth, it promoted us to investigate the function of *Bscl2*$^{-/-}$ mammary glands in lactation. Here we reported a novel role of seipin in lactation.

4.3 Materials and Methods

Animals. *Bscl2*$^{-/-}$ mice in C57BL/6J background were derived from an original colony at Baylor College of Medicine with backcrosses to C57BL/6J background for five generations [35]. Genotyping was done as previously described [87, 88]. *Bscl2*$^{+/+}$ (wild type) and *Bscl2*$^{+/-}$ females were used as the genotype control for *Bscl2*$^{-/-}$ females. They were housed in polypropylene cages with free access to food and water on a 12 h light/dark cycle (0600–1800) at 23±1°C with 30–50% relative humidity at the College of Veterinary Medicine animal facility at the University of Georgia. The animals were sacrificed by CO_2 inhalation followed with cervical dislocation. All methods used in this study were approved by the University of Georgia Institutional Animal Care and Use Committee (IACUC) Committee and conform to National Institutes of Health guidelines and federal law.

Lipid droplet analysis. Frozen sections (10 um) of 4th inguinal mammary glands were stained with Nile Red (N3013, Sigma) in the dark for 20 minutes at room temperature and counterstained with DAPI.

Quantification of milk protein concentration. The right 4th inguinal mammary glands from individual mice were fixed in formalin at room temperature for overnight. Milk content leaked to the fixative. Protein concentration in the fixative was determined by Bradford assay and A595

protein absorbance was measured using a nanodrop. A standard curve was prepared using bovine serum albumin.

Histology and whole mount of mammary gland. On lactation day 1 (LD1), the day new pups were found, the LD1 females were euthanized and the mammary glands were dissected. The left side mammary glands were snap frozen. The right 4th inguinal mammary gland was fixed in formalin, dehydrated in a series of 50%, 70%, 80%, 90%, 100 % ethanol and two changes of xylene, embedded in paraffin for histology. The right 4th inguinal mammary glands from another set of LD1 mice were used for whole mount as previously described [88, 92, 114].

***In situ* hybridization.** Sense and antisense cRNA probe synthesis and *in situ* hybridization were carried out as previously described [87, 96] on sections from gestation day 13.5 (D13.5, WT) and LD1 (WT and *Bscl2*$^{-/-}$) 4th inguinal mammary glands.

Immunohistochemistry. Frozen sections (10 um) of 4th inguinal mammary glands were used for immunohistochemistry and immunofluorescence as previously described [74, 87] using the following antibodies: PDI (1:200, ab2792, Abcam), Cleaved Caspase-3 (1:300, Asp175, Cell Signaling), PCNA (1:1,000, D3H8P, Cell Signaling), E-Cadherin (1:300, 24E10, Cell Signaling), WAP (1:200, sc-14832, Santa Cruz Biotechnology).

Statistical Analysis. Data are presented as mean±SD. Two-tailed Fisher's exact test was used for nursing rate. Two-tailed unequal variance student t-test was used for milk protein concentration. Significance level is set at $P<0.05$.

4.4 Results

Bscl2$^{-/-}$ *females have impaired lactation*

Bscl2$^{-/-}$ females were poor breeders when they were mated with WT males. One problem was during postpartum. Among the 22 *Bscl2*$^{-/-}$ females (2-4 months old, mated with WT stud males) that delivered pups, 13 of them had all pups dead by PND5 due to lack of milk. The

successful nursing rate in *Bscl2*$^{-/-}$ females (9/22=40.9%, P<0.0001) was significantly decreased compared to control (53/53=100%) (Fig. 1A). When pups (*Bscl2*$^{+/-}$, N=5) from *Bscl2*$^{-/-}$ females (mated with WT stud males) were fostered by WT nursing females, all of them survived. These observations indicated a maternal problem in the *Bscl2*$^{-/-}$ females. When lactation day 1 (LD1) mammary glands were fixed in 10% formalin, milk released from the WT mammary glands made the solution opaque but it was translucent from the *Bscl2*$^{-/-}$ mammary glands (Fig. 1B). In addition, the average protein concentration in the solutions from *Bscl2*$^{-/-}$ mammary glands was only ~7% of the control (Fig. 1C). These data indicated reduced milk release from the LD1 *Bscl2*$^{-/-}$ mammary glands.

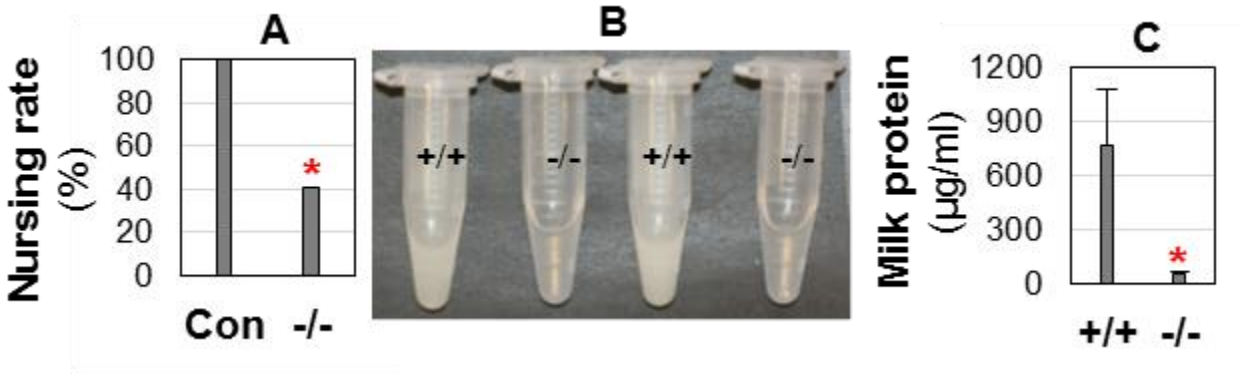

Figure 1. Reduced nursing rate and milk protein concentration in the lactation day 1 (LD1) *Bscl2*$^{-/-}$ females. A. Nursing rate. N=22-53. Con: +/+ and +/-. * P<0.05. B. Representative images of formalin solutions used to fix individual LD1 mammary glands. C. Protein concentration in the formalin solutions. N=5-7; * P<0.05; error bar, standard deviation.

Bscl2*$^{-/-}$ *mammary gland histology

Whole mount LD1 mammary glands showed alveolar clusters in the WT females but not in the *Bscl2*$^{-/-}$ females (Fig. 2A), which had mammary gland alveoli spread out more like a sheet instead of clusters (Fig. 2B). The LD1 *Bscl2*$^{-/-}$ mammary glands also had enlarged ducts (Fig. 2B). Histology confirmed the clusters of secretory mammary gland alveoli that were surrounded

by adipocytes in the LD1 WT mammary glands (Fig. 2C, 2C1). The appearances of the alveoli in the LD1 *Bscl2*$^{-/-}$ mammary glands varied greatly: some had mammary gland alveoli interconnected with dilated lumen (Fig. 2D, 2D1); some had small mammary gland lobules with heterogeneity in the expansion of alveolar lumen and sloughed epithelial cells in the lumen (Fig. 2E, 2E1); while others had small mammary gland lobules and non-secretory alveoli with unexpanded lumen (Fig. 2F, 2F1). There was interlobular connective tissue but absent of adipocytes in the LD1 *Bscl2*$^{-/-}$ mammary glands (Fig. 2D-2F, 2D1-2F1). The lack of adipocytes in the mammary gland was consistent with lipodystrophy in the *Bscl2*$^{-/-}$ females [88].

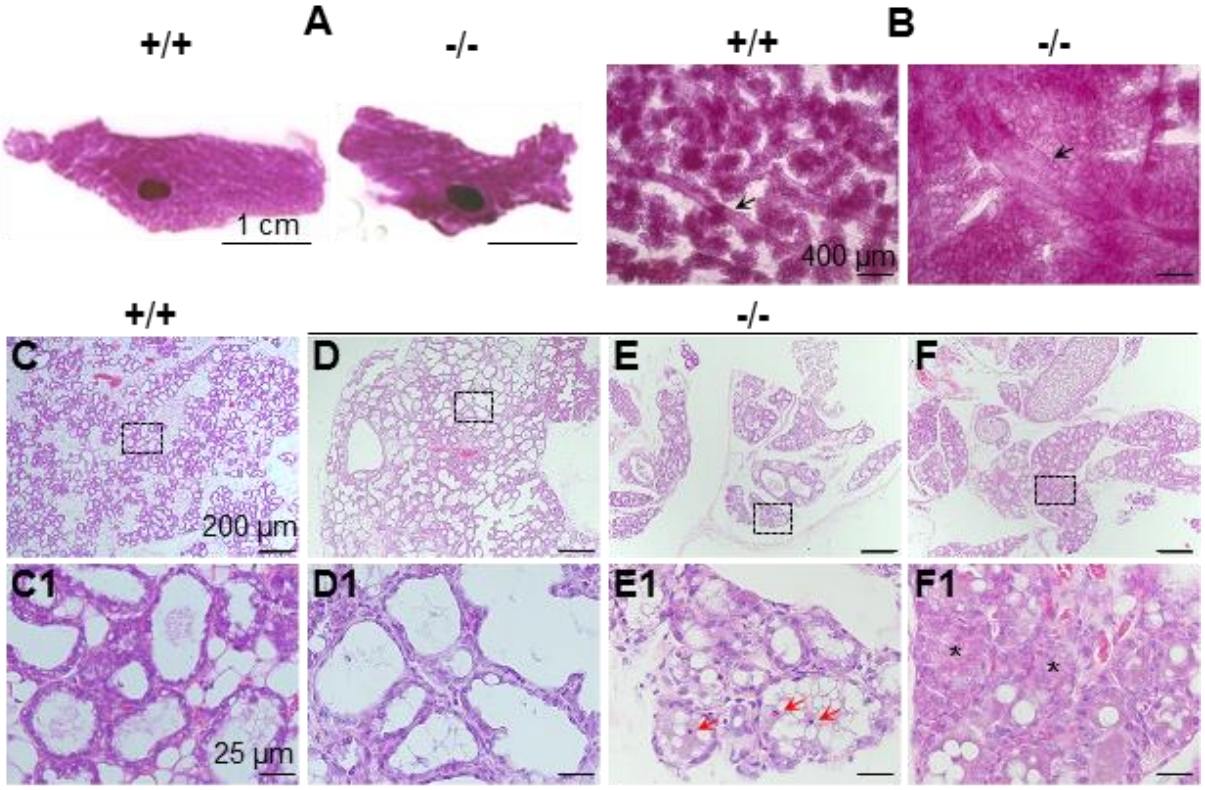

Figure 2. Whole mount and histology of lactation day 1 wild type (+/+) and *Bscl2*$^{-/-}$ (-/-) mammary glands. A & B. Whole mount. Black arrows in B, mammary gland duct. C-F1. Histology. C1-F1, enlarged from the rectangle areas in C-F, respectively. Red arrows in E1,

apoptotic cells; black stars in F1, non-expanded alveolar lumen; scale bars, 1 cm (A), 400 µm (B), 200 µm (C-F), or 25 µm (C1-F1).

Expression of Bscl2 in LD1 mammary glands

In situ hybridization indicated that *Bscl2* had a low level of expression in the D13.5 WT mammary gland (Fig. 3A). *Bscl2* was upregulated and highly detected in the LD1 WT mammary gland alveolar epithelial cells (Fig. 3B). It appeared that *Bscl2* was also detectable in the adipocytes, but at a much lower level than in the LD1 epithelial cells (Fig. 3A, 3B). The same *Bscl2* antisense probe also detected some signals in the LD1 *Bscl2*$^{-/-}$ mammary gland (Fig. 3C) but the signals were much weaker than that in the WT LD1 mammary gland (Fig. 3B). No specific signal was detected in an LD1 WT mammary gland using a sense *Bscl2* probe (data not shown). The high expression of *Bscl2* in the LD1 WT mammary gland epithelial cells suggested a local function of *Bscl2* in the mammary gland epithelium.

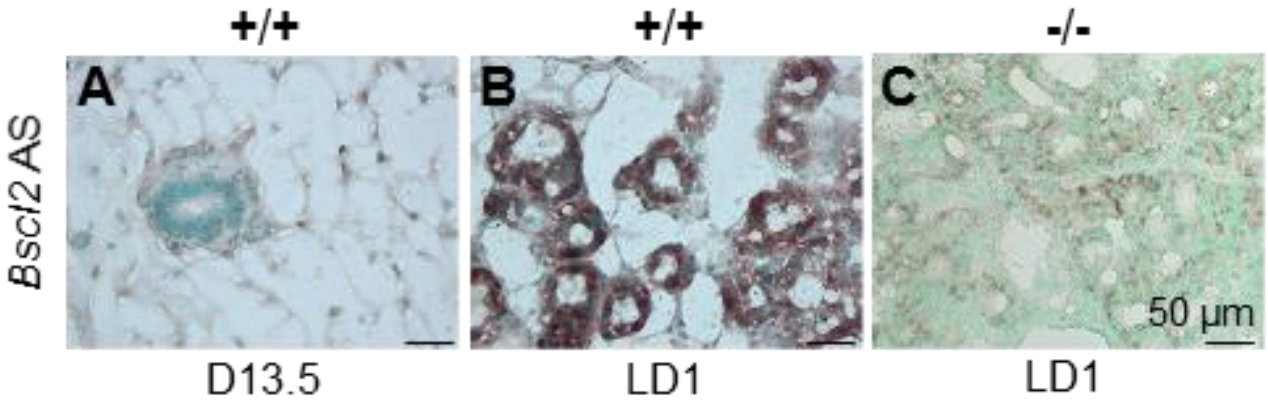

Figure 3. Detection of *Bscl2* mRNA in gestation day 13.5 (D13.5) wild type (WT) and LD1 mammary glands by *in situ* hybridization using an antisense *Bscl2* probe. A. D13.5 WT. B. LD1 WT. C. LD1 *Bscl2*$^{-/-}$. Scale bar, 50 µm.

Expression of WAP in LD1 mammary gland

Since there was reduced milk protein secretion in the *Bscl2*$^{-/-}$ LD1 mammary glands (Fig. 1B, 1C), was there reduced milk protein production in the *Bscl2*$^{-/-}$ LD1 mammary gland epithelial cells? Whey acidic protein (WAP), a major component in rodent milk [115], was examined in LD1 mammary gland frozen sections using immunofluorescence. WAP was detected in all mammary gland epithelial cells with more intense labeling on the apical side of epithelial cells in the LD1 WT mammary glands (Fig. 4A-4C). Similar WAP expression pattern was also detected in the LD1 *Bscl2*$^{-/-}$ mammary gland epithelial cells with enlarged alveolar lumen (Fig. 4D-4F). However, in the alveoli with unexpanded lumen, the WAP expression in the epithelial cells was detected throughout the cytoplasm and many epithelial cells did not show strong apical WAP staining (Fig. 4G-4I) as seen in WT and *Bscl2*$^{-/-}$ LD1 mammary glands that had enlarged alveolar lumen (Fig. 4A-4F). There appeared to have no obvious difference in the expression level of WAP in the mammary gland epithelial cells between WT and *Bscl2*$^{-/-}$ LD1 mammary glands (Fig. 4). No specific signal was detected in the negative control (data not shown). These data demonstrated no defective synthesis of WAP in the *Bscl2*$^{-/-}$ LD1 mammary gland alveolar epithelial cells.

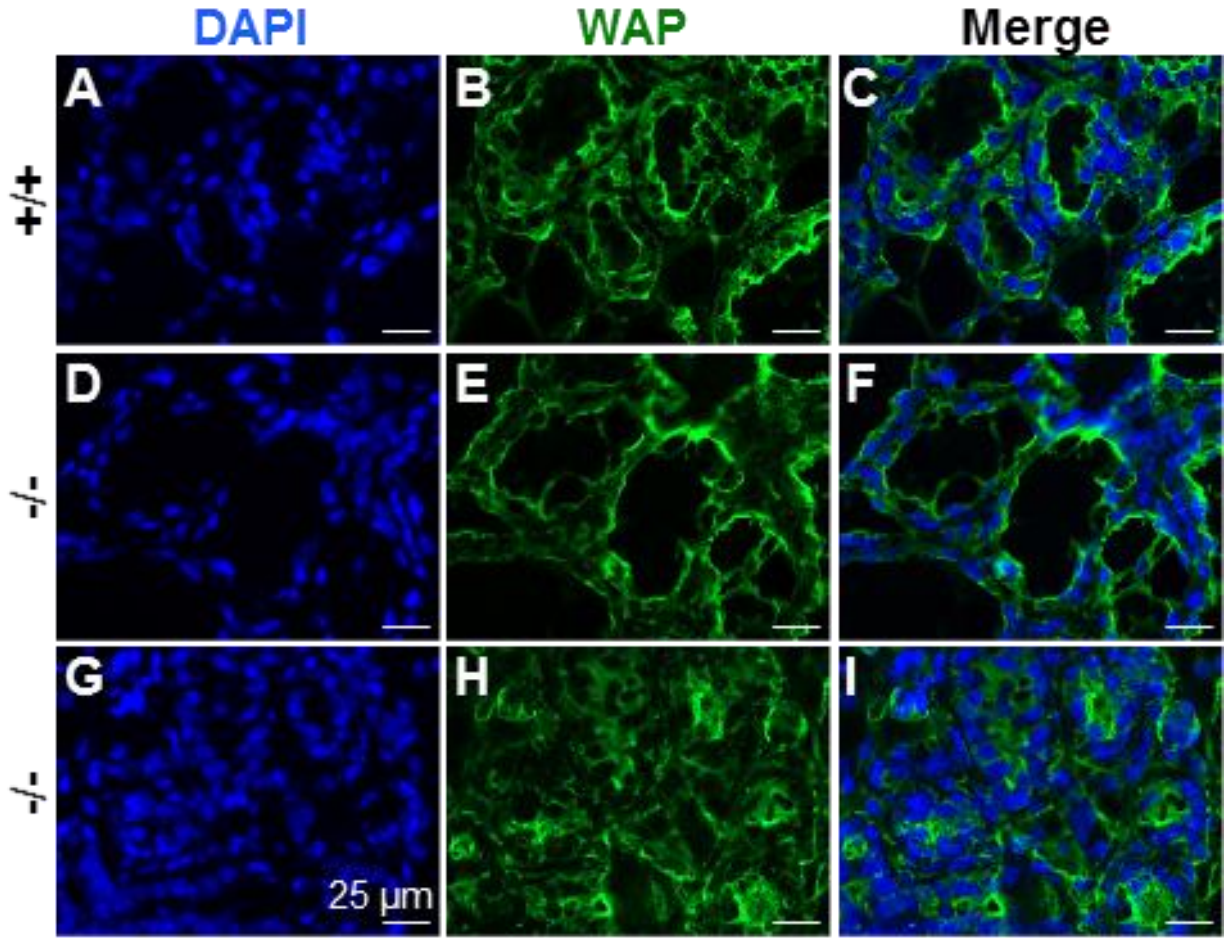

Figure 4. Detection of whey acidic protein (WAP) in LD1 mammary glands. A-C. Wild type. D-F. *Bscl2*$^{-/-}$ LD1 mammary gland with enlarged alveolar lumen. G-I. *Bscl2*$^{-/-}$ LD1 mammary gland without enlarged alveolar lumen. Scale bar, 25 µm.

Lipid droplets in LD1 Bscl2*$^{-/-}$ *mammary gland

In addition to milk protein, another important component of milk is fat. Nile Red lipid droplet staining of frozen LD1 mammary gland sections showed some very large fluorescent irregular smears in the WT that were absent from LD1 *Bscl2*$^{-/-}$ mammary gland sections (Fig. 5). These smears most likely indicated adipocytes that were absent from the LD1 *Bscl2*$^{-/-}$ mammary gland (Fig. 2). Although the LD1 mammary gland structures differed greatly (Fig. 2), the density of lipid droplets appeared comparable between LD1 WT and *Bscl2*$^{-/-}$ mammary glands in areas

with alveoli (Fig. 5). The sizes of the lipid droplets varied greatly in both WT and *Bscl2*$^{-/-}$ LD1 mammary glands (Fig. 5). It appeared in the LD1 *Bscl2*$^{-/-}$ mammary glands that larger lipid droplets were seen in the areas with expanded alveolar lumen than in the areas with less expanded/secretory alveolar lumen, indicated by denser nuclei in the DAPI staining (Fig. 5G). These data indicated that lipid synthesis was not impaired but lipid droplet aggregation might be impaired in the *Bscl2*$^{-/-}$ mammary gland with undifferentiated alveoli.

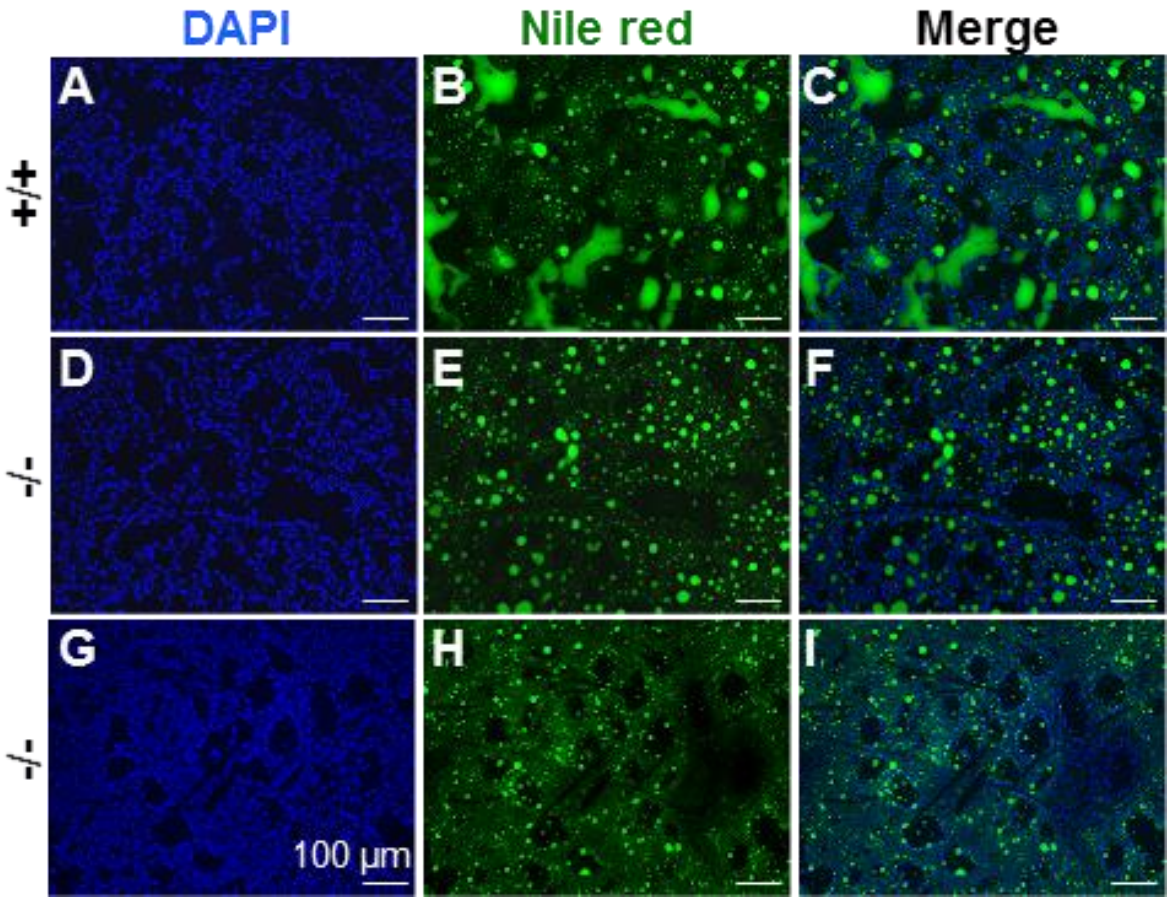

Figure 5. Detection of lipid droplets in LD1 mammary glands using Nile Red staining. A-C. Wild type. D-F. *Bscl2*$^{-/-}$ LD1 mammary gland with enlarged alveolar lumen. G-I. *Bscl2*$^{-/-}$ LD1 mammary gland without enlarged alveolar lumen. Green dots, lipid droplets; scale bar, 100 µm.

Alveolar epithelial cell proliferation and apoptosis in LD1 Bscl2*$^{-/-}$ *mammary gland

Since milk protein WAP synthesis and lipid synthesis in the *Bscl2*$^{-/-}$ mammary glands were not obviously impaired, to find out the causes for reduced milk secretion, cell proliferation and apoptosis in the LD1 mammary glands were detected by PCNA staining and Cleaved Caspase-3 staining, respectively. Immunohistochemistry detected PCNA staining in the round nuclei of most alveolar epithelial cells, some elongated nuclei of myoepithelial cells, as well as some nuclei of adipocytes in the WT LD1 mammary glands (Fig. 6A, 6A1). In the *Bscl2*$^{-/-}$ LD1 alveoli, PCNA staining was overall weaker than that in the WT (Fig. 6B); in the alveoli with epithelial cells lining up the entire lumen, which were often not expanded, most epithelial cells were PCNA positive (Fig. 6B1) as seen in the WT (Fig. 6A1); in other alveoli with dilated lumen and / or with scattered epithelial cells, most epithelial cells were also PCNA positive (Fig. 6B2); in the alveoli with depleted epithelial cells, the PCNA positive cells were myoepithelial cells with elongated nuclei (Fig. 6B2).

Cleaved Caspase-3 positive cells were rarely detected in the WT LD1 mammary gland alveoli (Fig. 6C) but more frequently detected in the *Bscl2*$^{-/-}$ LD1 mammary gland alveoli (Fig. 6D), which could be in the alveolar epithelial cells (Fig. 6D1), or detached epithelial cells in the alveolar lumen (Fig. 6D2, 6D3). Some LD1 *Bscl2*$^{-/-}$ alveoli had a few or lack of epithelial cells (Fig. 6D3), which could explain reduced number of cells with round nuclei in the PCNA staining (Fig. 6B2). E-Cad staining revealed organized alveolar epithelial cells in the LD1 WT mammary gland (Fig. 6E), but disorganized and often “flattened” or absent, especially in the alveoli with dilated lumen and sloughed epithelial cells, in the LD1 *Bscl2*$^{-/-}$ mammary gland (Fig. 6F). The *Bscl2*$^{-/-}$ alveoli with scattered epithelial cells or without epithelial cells were most likely resulted from epithelial cell apoptosis as seen in Fig. 6D3. These data indicated normal alveolar

epithelial cell proliferation but increased alveolar epithelial cell apoptosis in the *Bscl2*$^{-/-}$ LD1 mammary glands.

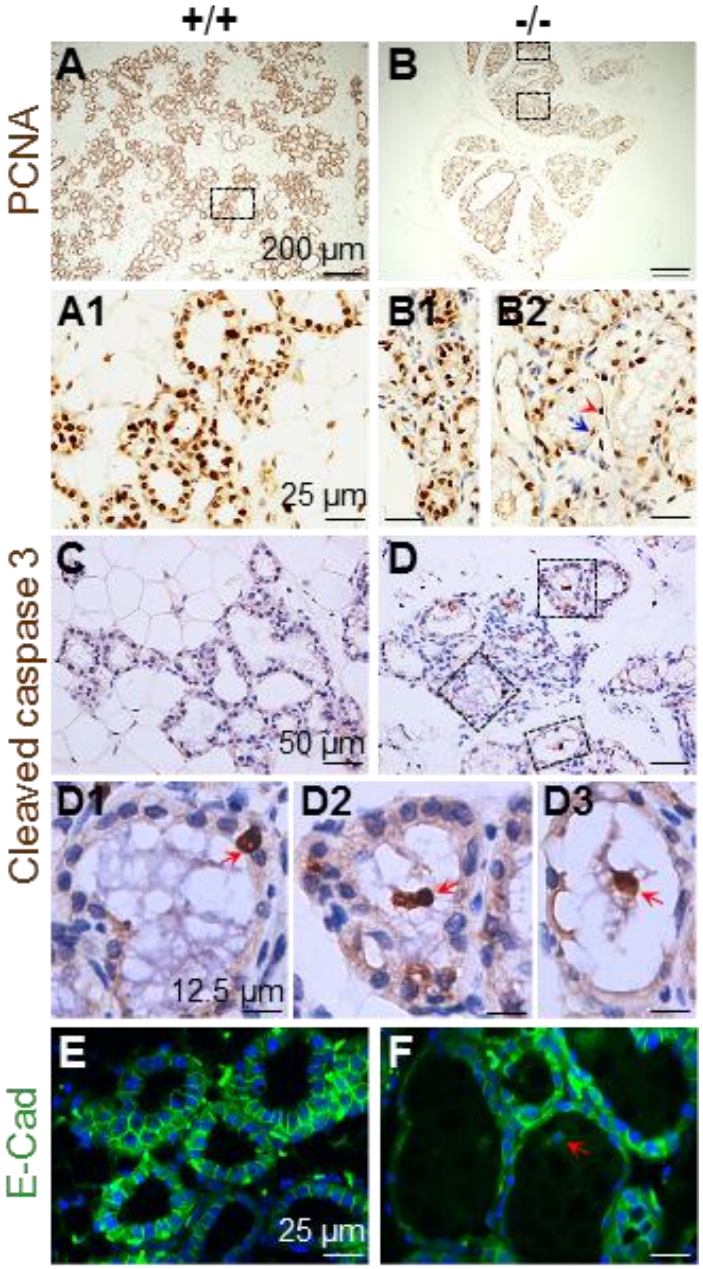

Figure 6. Detection of PCNA, cleaved caspase 3, and E-Cad in LD1 mammary glands using immunohistochemistry or immunofluorescence. A-B2. PCNA. A1-B2, enlarged from the rectangle areas in A and B, respectively. Red arrowhead in B2, an alveolar epithelial cell; blue

arrowhead in B2, a myoepithelial cell. C-D3. Cleaved caspase 3. D1-D3, enlarged from the rectangle areas in D; red arrows, cleaved caspase 3 positive cells in the alveolar epithelium and lumen. E-F. Merged images of E-Cad (green) and DAPI (blue) staining. Red arrow in F, sloughed epithelial cell in alveolar lumen.

ER stress in LD1 Bscl2$^{-/-}$ mammary gland

Since seipin is localized in the ER and mutant forms of seipin can activate the unfolded protein response (UPR) pathway and induce ER stress-mediated cell death in cultured cells [116], it was hypothesized that seipin-deficiency in the *Bscl2*$^{-/-}$ mammary gland caused ER stress leading to apoptosis in the alveolar epithelial cells. To test this hypothesis, protein disulfide isomerase (PDI), an ER chaperone induced during ER stress and an important player in UPR pathway [117], was examined in the LD1 WT and *Bscl2*$^{-/-}$ mammary glands. PDI was detected in the cytoplasm of all alveolar epithelial cells (Fig. 7). The expression of PDI in WT alveoli was relatively comparable among all epithelial cells except stronger signal in a few cells (Fig, 7A-7C). The PDI signal in many LD1 *Bscl2*$^{-/-}$ alveolar epithelial cells was much stronger than that in the WT epithelial cells regardless of their localizations in the alveoli with most retained epithelial cells (Fig. 7D-7F) or in the alveoli with a few remaining epithelial cells (Fig. 7G-7I). Detached *Bscl2*$^{-/-}$ alveolar epithelial cells in the lumen appeared to have weaker PDI staining than those attached epithelial cells (Fig. 7G-7I). These results indicated increased ER stress in the LD1 *Bscl2*$^{-/-}$ alveolar epithelial cells.

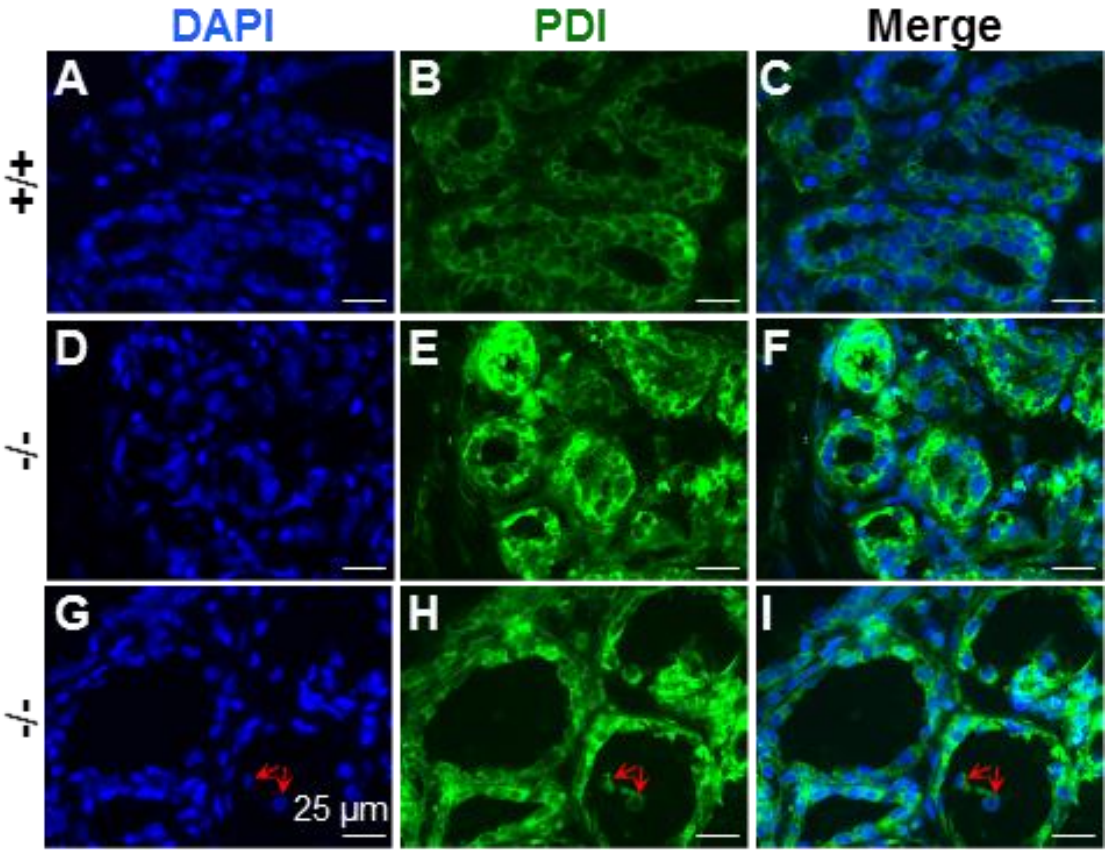

Figure 7. Increased expression of protein disulfide isomerase (PDI) in Bscl2-/- LD1 mammary glands. A-C. Wild type. D-F. Bscl2-/- LD1 mammary gland with most retained alveolar epithelial cells. G-I. Bscl2-/- LD1 mammary gland a few remaining alveolar epithelial cells. Red arrows in G-I, sloughed epithelial cells in alveolar lumen; scale bar, 25 µm.

4.5 Discussion

This study reveals a novel *in vivo* role of seipin in lactation, the process of milk secretion from the mammary glands. Two main categories of components in the milk are proteins and lipids, which are originally produced in the mammary alveolar epithelial cells. Nearly 60% of lactating *Bscl2*$^{-/-}$ female mice failed to nurse their pups, accompanied with dramatically reduced secretion of milk proteins. However, the expression level of WAP (a major component in rodent milk [115]) and the density of lipid droplets in the lactation day 1 (LD1) *Bscl2*$^{-/-}$ mammary

alveolar epithelial cells appeared comparable to control, indicating that the *Bscl2*$^{-/-}$ mammary alveolar epithelial cells were functional in protein synthesis and lipid synthesis for milk production. This study demonstrates abnormal morphology in LD1 *Bscl2*$^{-/-}$ mammary alveoli: from undifferentiated and non-secretory alveoli with unexpanded lumen to alveoli with dilated lumen and sloughed epithelial cells. These conditions compromise milk production in the *Bscl2*$^{-/-}$ mammary gland.

Seipin is an integral endoplasmic reticulum (ER) membrane protein [28] that is required for adipocyte differentiation and lipid droplet accumulation [28, 33, 35, 112, 113]. However, heterogeneities in cell differentiation and lipid droplet accumulation were observed in the LD1 *Bscl2*$^{-/-}$ mammary gland epithelial cells. It was noticed that the poorly differentiated LD1 *Bscl2*$^{-/-}$ mammary gland alveolar epithelial cells had less polarity in WAP cellular distribution, which normally accumulates in the apical side of the differentiated alveolar epithelial cells. The poorly differentiated LD1 *Bscl2*$^{-/-}$ mammary gland alveoli appeared to have less lipid droplets aggregated into larger ones. These observations indicate that seipin plays an important role in mammary gland alveolar epithelial cell differentiation. The poorly differentiated LD1 *Bscl2*$^{-/-}$ mammary gland alveolar epithelial cells impair milk secretion, which contributes to reduced milk production and nursing in the *Bscl2*$^{-/-}$ lactating mice.

On the other hand, some LD1 *Bscl2*$^{-/-}$ mammary gland alveolar epithelial cells were well differentiated and had comparable cellular distribution of WAP with control. These cells had accumulation of larger lipid droplets. A recent study in Drosophila and human cells [111] demonstrates that seipin forms discrete and dynamic foci in the ER that interact with nascent lipid droplets to enable their conversion into larger, mature lipid droplets. In the absence of seipin, most nascent lipid droplets often fail to grow, which is consistent with the smaller lipid

droplets seen in the poorly differentiated LD1 *Bscl2*$^{-/-}$ mammary gland alveoli. Interestingly, it was also reported in the above study [111] that those lipid droplets that did grow, they eventually expanded into giant lipid droplets characteristic of seipin deficiency. The two patterns of lipid droplets observed in the poorly and well-differentiated LD1 *Bscl2*$^{-/-}$ mammary gland alveolar epithelial cells in this study may reflect both differentiation status and the function of seipin in lipid droplet growth.

LD1 *Bscl2*$^{-/-}$ mammary gland alveolar epithelial cells had normal proliferation but increased apoptosis, which led to the slough of many alveolar epithelial cells into the lumen and subsequently, reduced alveolar epithelial cells for milk secretion. Accompanying with the increased apoptosis, there was increased ER stress in the LD1 *Bscl2*$^{-/-}$ mammary gland alveolar epithelial cells indicated by the increased expression of PDI, an ER chaperone induced during ER stress and an important player in UPR pathway [117]. Although it has been suggested that changes in ER stress pathway in the mammary gland during lactation are normal adaptions to the changing physiological state [118], and activation of UPR signaling pathway in responding to ER stress is initially protective [117], prolonged ER stress is pro-apoptotic [117]. One study reveals that mutant forms of seipin can activate the UPR pathway and induce ER stress-mediated cell death in cultured cells [116]. Another study indicates that PP2Ce, an ER membrane targeted protein phosphatase, is highly expressed in lactating mammary gland epithelium and involved in regulating ER stress, and PP2Ce deficiency leads to loss of milk production and induction of lactating mammary gland epithelial apoptosis [119], indicating that ER stress plays an important role during lactation. The increased LD1 *Bscl2*$^{-/-}$ mammary gland alveolar epithelial cell apoptosis was most likely resulted from increased ER stress.

ER stress was also induced in the mammary gland epithelium deficient of Xbp1, a key mediator of UPR, and associated with inhibition of epithelial differentiation during lactation leading to impaired milk production [115]. It was possible that increased ER stress also contributed to the poor differentiation of some LD1 *Bscl2*$^{-/-}$ mammary gland alveolar epithelial cells.

In summary, this study reveals a novel *in vivo* role of seipin in lactation. Although seipin deficiency did not have obvious effects on cell proliferation of mammary gland alveolar epithelial cells or protein synthesis and lipid syntheses in the mammary gland alveolar epithelial cells, seipin deficiency led to poor differentiation and/or increased apoptosis of mammary gland alveolar epithelial cells, both of which contribute to reduced milk production and both of which could be resulted from increased ER stress in the mammary gland alveolar epithelial cells. The molecular mechanisms of seipin in regulating ER stress during lactation remain to be elucidated.

Acknowledgements

The authors thank the Office of the Vice President for Research, Interdisciplinary Toxicology Program, and Department of Physiology and Pharmacology at the University of Georgia, and the National Institutes of Health (NIH R15HD066301 and NIH R01HD065939 (co-funded by ORWH and NICHD) to XY) for financial support.

CHAPTER 5

CONCLUSION

The clinical definition of infertility according to International Committee for Monitoring Assisted Reproductive Technology (ICMART) and WHO is the inability to achieve pregnancy after 12 months or more of regular unprotected sexual intercourse [120]. Infertility afflicts about 50 million people worldwide [121]. The National Survey of Family Growth (NSFG) data show that about 7.3 million American women of age 15–44 have impaired fertility and the cost of diagnosing and treating infertility exceeds 5 billion $ a year [122] indicating that it is a major health concern that needs to be studied and addressed. Infertility is caused by genetic factors, environmental factors or chemicals (that humans are regularly exposed to) that affect the reproductive system, or natural ageing. Therefore, in this dissertation, I have mainly studied the genetic factors that affect fertility by using *Bscl2*-deficeint mouse model to study the mechanisms of *Bscl2* in reproduction, it was possible to discover new mechanism that are critical for progression of spermatogenesis in the testis, mammary gland function and development and parturition. *Bscl2* gene is required for adipose tissue development, differentiation of adipocytes [123]. Mutations in *Bscl2* gene result in congenital generalized lipodystrophy, a disease characterized by absence of adipose tissue [124]. The roles and mechanisms of seipin in reproduction have not been investigated. *Bscl2* is highly expressed in round spermatids in the testis, mammary gland epithelium and the uterus in late gestation indicating that it may have critical roles in these processes. *Bscl2*$^{-/-}$ mice showed several phenotypes: male infertility, nursing defects in females, and parturition defects in females during delivery indicating that

Bscl2 gene is important for spermatogenesis, mammary gland development and parturition. *Bscl2*$^{-/-}$ males are infertile and have normal mating behavior. Sperm count and sperm motility are also severely reduced in *Bscl2*$^{-/-}$ males. Seipin protein starts to be detected in round spermatids and reaches a plateau on PND28. Loss of *Bscl2* resulted in increased spermatid apoptosis in *Bscl2*$^{-/-}$ male testis as detected by ISEL+. In addition, loss of *Bscl2* caused severe DNA damage in spermatids, fragmentation of the chromocenter, and disrupted acrosome in the *Bscl2*$^{-/-}$ spermatids. Loss of *Bscl2* also affected mitochondrial function and sperm motility. Using mitotracker, *Bscl2*$^{-/-}$ sperm were very weakly stained with mitotracker. Sperm motility was also severely decreased. These factors contributed to reduction in sperm count and sperm motility leading to male infertility. The functions of *Bscl2* in spermatogenesis are local to the testis and unknown mechanisms for the relationship between lipid droplets and spermatid differentiation may be discovered in the future. The relationship between endoplasmic reticulum, Golgi apparatus and acrosome formation has been established. Since seipin is an endoplasmic reticulum membrane protein, it was expected to affect round spermatids and acrosomes in the *Bscl2*$^{-/-}$ testis. Acrosome formation is a multistep process during spermatid differentiation and requires the cooperation of several intracellular organs and disruption of endoplasmic reticulum may lead to defects in acrosome formation and function. The function of *Bscl2* is involved in other reproductive organs and these include the uterus and the mammary glands. The mammary gland is an important organ for milk production. The remarkable upregulation in *Bscl2* mRNA expression from D13.5 pregnant mammary glands to lactation day 1 mammary gland indicates that this gene is critical for lactation as well. Indeed, *Bscl2*$^{-/-}$ females fail to nurse their pups and the pups do not reach weaning. The defect in nursing was studied extensively and nursing behavior defects have been observed in *Bscl2*$^{-/-}$ females during lactation. *Bscl2* encodes an

endoplasmic reticulum membrane protein and mutations in *Bscl2* causes endoplasmic reticulum stress. Endoplasmic reticulum stress was studied in *Bscl2*$^{-/-}$ mammary glands during lactation and upregulated expression of endoplasmic reticulum stress markers such as PDI has been observed in *Bscl2*$^{-/-}$ mammary glands. The *Bscl2*$^{-/-}$ mammary glands also showed significantly increased number of cleaved-caspase 3 positive luminal epithelium cells compared to WT mammary glands during lactation which indicates activation of cell death path ways in the *Bscl2*$^{-/-}$ mammary glands which may be a consequence of endoplasmic reticulum stress. Lipid droplets have also been disrupted in the *Bscl2*$^{-/-}$ mammary glands and potential role of lipid droplets in lactation will be investigated. In addition to lactation defects, a subgroup of *Bscl2*$^{-/-}$ females have shown difficulty delivering pups during the last days of gestation. This defect is systemic rather than a local effect of seipin deficiency in the uterus compared to local effects of seipin deficiency in mammary gland and the testis. In the future, potential roles of *Bscl2/*Seipin in cell death and endoplasmic reticulum stress in reproductive organs would be interesting to investigate. The potential roles of lipid droplets in delivery of growth factors or other intracellular messengers during spermatid differentiation will be an exciting to investigate. The potential roles of *Bscl2/*Seipin in regulation of germ cell apoptosis and mitochondrial function, mitochondrial membrane potential will be studied as well. The upregulation of seipin upon exposure to genotoxic agents as shown by previous studies [125] and the role of seipin in spermatid differentiation and spermiogenesis make *Bscl2/*Seipin a potential target for male reproductive toxins and genotoxic agents that may adversely affect the male reproductive systems and male fertility in humans.

REFERENCES

1. Wistuba J, Stukenborg J-B, Luetjens CM: Mammalian spermatogenesis. *Funct Dev Embryol* 2007, 1:99-117.
2. Hess RA, de Franca LR: Spermatogenesis and cycle of the seminiferous epithelium. In: *Molecular mechanisms in spermatogenesis.* Springer; 2009: 1-15.
3. Wistuba J, Stukenborg J-B, Luetjens CM: Mammalian spermatogenesis. *Functional development and embryology* 2007, 1(2):99-117.
4. Jan SZ, Hamer G, Repping S, de Rooij DG, van Pelt AM, Vormer TL: Molecular control of rodent spermatogenesis. *Biochim Biophys Acta* 2012, 1822(12):1838-1850.
5. ROOIJ DG, RUSSELL LD: All you wanted to know about spermatogonia but were afraid to ask. *Journal of Andrology* 2000, 21(6):776-798.
6. Aitken RJ, Findlay JK, Hutt KJ, Kerr JB: Apoptosis in the germ line. *Reproduction* 2011, 141(2):139-150.
7. Shaha C, Tripathi R, Mishra DP: Male germ cell apoptosis: regulation and biology. *Philos Trans R Soc Lond B Biol Sci* 2010, 365(1546):1501-1515.
8. Pentikäinen V: Regulation of male germ cell apoptosis. *Role of the sex steroids and the cellular death receptors Fas and TNFR1 Academic Dissertation Helsinki University Biomedical Dissertation* 2002(13):1-69.
9. Nantel F, Monaco L, Foulkes NS, Masquilier D, LeMeur M, Henriksen K, Dierich A, Parvinen M, Sassone-Corsi P: Spermiogenesis deficiency and germ-cell apoptosis in CREM-mutant mice. *Nature* 1996, 380(6570):159-162.
10. Hogan B, Costantini F, Lacy E: Manipulating the mouse embryo: a laboratory manual, vol. 34: Cold spring harbor laboratory Cold Spring Harbor, NY; 1986.
11. Wang H, Dey SK: Roadmap to embryo implantation: clues from mouse models. *Nat Rev Genet* 2006, 7(3):185-199.
12. Alberts B JA, Lewis J, et al. : Fertilization. . *Molecular Biology of the Cell 4th edition New York: Garland Science;* 2002, Available from: http://www.ncbi.nlm.nih.gov/books/NBK26843/.
13. Primakoff P, Myles DG: Penetration, adhesion, and fusion in mammalian sperm-egg interaction. *Science* 2002, 296(5576):2183-2185.
14. Bianchi E, Doe B, Goulding D, Wright GJ: Juno is the egg Izumo receptor and is essential for mammalian fertilization. *Nature* 2014.
15. Halbert SA, Becker DR, Szal S: Ovum transport in the rat oviductal ampulla in the absence of muscle contractility. *Biology of reproduction* 1989, 40(6):1131-1136.
16. Wang H, Guo Y, Wang D, Kingsley PJ, Marnett LJ, Das SK, DuBois RN, Dey SK: Aberrant cannabinoid signaling impairs oviductal transport of embryos. *Nat Med* 2004, 10(10):1074-1080.
17. Carson DD, Bagchi I, Dey SK, Enders AC, Fazleabas AT, Lessey BA, Yoshinaga K: Embryo implantation. *Dev Biol* 2000, 223(2):217-237.
18. Ramathal CY, Bagchi IC, Taylor RN, Bagchi MK: Endometrial decidualization: of mice and men. In: *Seminars in reproductive medicine: 2010*: NIH Public Access; 2010: 17.

19. Lydon JP, DeMayo FJ, Funk CR, Mani SK, Hughes AR, Montgomery C, Shyamala G, Conneely OM, O'Malley BW: Mice lacking progesterone receptor exhibit pleiotropic reproductive abnormalities. *Genes & development* 1995, 9(18):2266-2278.
20. Mitchell BF, Taggart MJ: Are animal models relevant to key aspects of human parturition? *Am J Physiol Regul Integr Comp Physiol* 2009, 297(3):R525-545.
21. Sugimoto Y, Yamasaki A, Segi E, Tsuboi K, Aze Y, Nishimura T, Oida H, Yoshida N, Tanaka T, Katsuyama M *et al*: Failure of parturition in mice lacking the prostaglandin F receptor. *Science* 1997, 277(5326):681-683.
22. Delemarre-van de Waal HA: Regulation of puberty. *Best Pract Res Clin Endocrinol Metab* 2002, 16(1):1-12.
23. Roemmich JN, Rogol AD: Hormonal changes during puberty and their relationship to fat distribution. *American Journal of Human Biology* 1999, 11(2):209-224.
24. Swerdloff RS, Odell WD: Hormonal mechanisms in the onset of puberty. *Postgrad Med J* 1975, 51(594):200-208.
25. Rockett JC, Lynch CD, Buck GM: Biomarkers for assessing reproductive development and health: Part 1--Pubertal development. *Environ Health Perspect* 2004, 112(1):105-112.
26. McCormick CM, Mathews IZ: Adolescent development, hypothalamic-pituitary-adrenal function, and programming of adult learning and memory. *Prog Neuropsychopharmacol Biol Psychiatry* 2010, 34(5):756-765.
27. Jiang M, Gao M, Wu C, He H, Guo X, Zhou Z, Yang H, Xiao X, Liu G, Sha J: Lack of testicular seipin causes teratozoospermia syndrome in men. *Proc Natl Acad Sci U S A* 2014, 111(19):7054-7059.
28. Magre J, Delepine M, Khallouf E, Gedde-Dahl T, Jr., Van Maldergem L, Sobel E, Papp J, Meier M, Megarbane A, Bachy A *et al*: Identification of the gene altered in Berardinelli-Seip congenital lipodystrophy on chromosome 11q13. *Nat Genet* 2001, 28(4):365-370.
29. Cui X, Wang Y, Tang Y, Liu Y, Zhao L, Deng J, Xu G, Peng X, Ju S, Liu G *et al*: Seipin ablation in mice results in severe generalized lipodystrophy. *Hum Mol Genet* 2011, 20(15):3022-3030.
30. Prieur X, Dollet L, Takahashi M, Nemani M, Pillot B, Le May C, Mounier C, Takigawa-Imamura H, Zelenika D, Matsuda F *et al*: Thiazolidinediones partially reverse the metabolic disturbances observed in Bscl2/seipin-deficient mice. *Diabetologia* 2013, 56(8):1813-1825.
31. Lundin C, Nordstrom R, Wagner K, Windpassinger C, Andersson H, von Heijne G, Nilsson I: Membrane topology of the human seipin protein. *FEBS Lett* 2006, 580(9):2281-2284.
32. Sim MF, Talukder MU, Dennis RJ, Edwardson JM, Rochford JJ: Analyzing the functions and structure of the human lipodystrophy protein seipin. *Methods Enzymol* 2014, 537:161-175.
33. Szymanski KM, Binns D, Bartz R, Grishin NV, Li WP, Agarwal AK, Garg A, Anderson RG, Goodman JM: The lipodystrophy protein seipin is found at endoplasmic reticulum lipid droplet junctions and is important for droplet morphology. *Proc Natl Acad Sci U S A* 2007, 104(52):20890-20895.

34. Bi J, Wang W, Liu Z, Huang X, Jiang Q, Liu G, Wang Y, Huang X: Seipin Promotes Adipose Tissue Fat Storage through the ER Ca(2+)-ATPase SERCA. *Cell metabolism* 2014, 19(5):861-871.
35. Chen W, Chang B, Saha P, Hartig SM, Li L, Reddy VT, Yang Y, Yechoor V, Mancini MA, Chan L: Berardinelli-seip congenital lipodystrophy 2/seipin is a cell-autonomous regulator of lipolysis essential for adipocyte differentiation. *Mol Cell Biol* 2012, 32(6):1099-1111.
36. Agarwal AK, Garg A: Congenital generalized lipodystrophy: significance of triglyceride biosynthetic pathways. *Trends Endocrinol Metab* 2003, 14(5):214-221.
37. Cartwright BR, Goodman JM: Seipin: from human disease to molecular mechanism. *J Lipid Res* 2012, 53(6):1042-1055.
38. Dollet L, Magre J, Cariou B, Prieur X: Function of seipin: new insights from Bscl2/seipin knockout mouse models. *Biochimie* 2014, 96:166-172.
39. Rodriguez I, Ody C, Araki K, Garcia I, Vassalli P: An early and massive wave of germinal cell apoptosis is required for the development of functional spermatogenesis. *EMBO J* 1997, 16(9):2262-2270.
40. Blanco-Rodriguez J, Martinez-Garcia C: Spontaneous germ cell death in the testis of the adult rat takes the form of apoptosis: re-evaluation of cell types that exhibit the ability to die during spermatogenesis. *Cell Prolif* 1996, 29(1):13-31.
41. Hendriks G, Atallah M, Raamsman M, Morolli B, van der Putten H, Jaadar H, Tijdens I, Esveldt-van Lange R, Mullenders L, van de Water B *et al*: Sensitive DsRed fluorescence-based reporter cell systems for genotoxicity and oxidative stress assessment. *Mutat Res* 2011, 709-710:49-59.
42. Hendriks G, Atallah M, Morolli B, Calleja F, Ras-Verloop N, Huijskens I, Raamsman M, van de Water B, Vrieling H: The ToxTracker assay: novel GFP reporter systems that provide mechanistic insight into the genotoxic properties of chemicals. *Toxicol Sci* 2012, 125(1):285-298.
43. Lightfoot RJ, Restall BJ: Effects of site of insemination, sperm motility and genital tract contractions on transport of spermatozoa in the ewe. *J Reprod Fertil* 1971, 26(1):1-13.
44. Bellve AR, Cavicchia JC, Millette CF, O'Brien DA, Bhatnagar YM, Dym M: Spermatogenic cells of the prepuberal mouse. Isolation and morphological characterization. *J Cell Biol* 1977, 74(1):68-85.
45. Blaschke AJ, Staley K, Chun J: Widespread programmed cell death in proliferative and postmitotic regions of the fetal cerebral cortex. *Development* 1996, 122(4):1165-1174.
46. Ye X, Skinner MK, Kennedy G, Chun J: Age-dependent loss of sperm production in mice via impaired lysophosphatidic acid signaling. *Biol Reprod* 2008, 79(2):328-336.
47. Burgoyne PS, Mahadevaiah SK, Turner JM: The consequences of asynapsis for mammalian meiosis. *Nat Rev Genet* 2009, 10(3):207-216.
48. Winters T, McNicoll F, Jessberger R: Meiotic cohesin STAG3 is required for chromosome axis formation and sister chromatid cohesion. *EMBO J* 2014, 33(11):1256-1270.
49. Kim Y, Fedoriw AM, Magnuson T: An essential role for a mammalian SWI/SNF chromatin-remodeling complex during male meiosis. *Development* 2012, 139(6):1133-1140.

50. Matoba S, Ogura A: Generation of functional oocytes and spermatids from fetal primordial germ cells after ectopic transplantation in adult mice. *Biol Reprod* 2011, 84(4):631-638.
51. Vernet N, Mahadevaiah SK, Ojarikre OA, Longepied G, Prosser HM, Bradley A, Mitchell MJ, Burgoyne PS: The Y-encoded gene zfy2 acts to remove cells with unpaired chromosomes at the first meiotic metaphase in male mice. *Curr Biol* 2011, 21(9):787-793.
52. Li W, Wu J, Kim SY, Zhao M, Hearn SA, Zhang MQ, Meistrich ML, Mills AA: Chd5 orchestrates chromatin remodelling during sperm development. *Nature communications* 2014, 5:3812.
53. Namekawa SH, Park PJ, Zhang LF, Shima JE, McCarrey JR, Griswold MD, Lee JT: Postmeiotic sex chromatin in the male germline of mice. *Curr Biol* 2006, 16(7):660-667.
54. Grewal SIS, Jia S: Heterochromatin revisited. *Nature Reviews Genetics* 2007, 8(1):35-46.
55. Tanaka H, Baba T: Gene expression in spermiogenesis. *Cellular and molecular life sciences : CMLS* 2005, 62(3):344-354.
56. Ravel C, Chantot-Bastaraud S, El Houate B, Berthaut I, Verstraete L, De Larouziere V, Lourenco D, Dumaine A, Antoine JM, Mandelbaum J *et al*: Mutations in the protamine 1 gene associated with male infertility. *Molecular human reproduction* 2007, 13(7):461-464.
57. Lee K, Haugen HS, Clegg CH, Braun RE: Premature translation of protamine 1 mRNA causes precocious nuclear condensation and arrests spermatid differentiation in mice. *Proceedings of the National Academy of Sciences of the United States of America* 1995, 92(26):12451-12455.
58. Kleene KC: Patterns, mechanisms, and functions of translation regulation in mammalian spermatogenic cells. *Cytogenet Genome Res* 2003, 103(3-4):217-224.
59. Russell LD, Lee IP, Ettlin R, Peterson RN: Development of the acrosome and alignment, elongation and entrenchment of spermatids in procarbazine-treated rats. *Tissue Cell* 1983, 15(4):615-626.
60. Ruiz-Pesini E, Diez C, Lapena AC, Perez-Martos A, Montoya J, Alvarez E, Arenas J, Lopez-Perez MJ: Correlation of sperm motility with mitochondrial enzymatic activities. *Clin Chem* 1998, 44(8 Pt 1):1616-1620.
61. Wang R, Sperry AO: PP1 forms an active complex with TLRR (lrrc67), a putative PP1 regulatory subunit, during the early stages of spermiogenesis in mice. *PLoS One* 2011, 6(6):e21767.
62. Berkovits BD, Wolgemuth DJ: The first bromodomain of the testis-specific double bromodomain protein Brdt is required for chromocenter organization that is modulated by genetic background. *Dev Biol* 2011, 360(2):358-368.
63. Martianov I, Brancorsini S, Gansmuller A, Parvinen M, Davidson I, Sassone-Corsi P: Distinct functions of TBP and TLF/TRF2 during spermatogenesis: requirement of TLF for heterochromatic chromocenter formation in haploid round spermatids. *Development* 2002, 129(4):945-955.
64. Martianov I, Fimia GM, Dierich A, Parvinen M, Sassone-Corsi P, Davidson I: Late arrest of spermiogenesis and germ cell apoptosis in mice lacking the TBP-like TLF/TRF2 gene. *Mol Cell* 2001, 7(3):509-515.

65. Chung SS, Wang X, Wolgemuth DJ: Male sterility in mice lacking retinoic acid receptor alpha involves specific abnormalities in spermiogenesis. *Differentiation* 2005, 73(4):188-198.
66. Boitrelle F, Albert M, Petit JM, Ferfouri F, Wainer R, Bergere M, Bailly M, Vialard F, Selva J: Small human sperm vacuoles observed under high magnification are pocket-like nuclear concavities linked to chromatin condensation failure. *Reproductive biomedicine online* 2013, 27(2):201-211.
67. Baba T, Kashiwagi Y, Arimitsu N, Kogure T, Edo A, Maruyama T, Nakao K, Nakanishi H, Kinoshita M, Frohman MA *et al*: Phosphatidic acid (PA)-preferring phospholipase A1 regulates mitochondrial dynamics. *J Biol Chem* 2014, 289(16):11497-11511.
68. Manochantr S, Chiamchanya C, Sobhon P: Relationship between chromatin condensation, DNA integrity and quality of ejaculated spermatozoa from infertile men. *Andrologia* 2012, 44(3):187-199.
69. Bailly A, Gartner A: Germ cell apoptosis and DNA damage responses. *Adv Exp Med Biol* 2013, 757:249-276.
70. Ye X, Herr DR, Diao H, Rivera R, Chun J: Unique uterine localization and regulation may differentiate LPA3 from other lysophospholipid receptors for its role in embryo implantation. *Fertil Steril* 2011, 95(6):2107-2113 e2104.
71. Diao H, Aplin JD, Xiao S, Chun J, Li Z, Chen S, Ye X: Altered spatiotemporal expression of collagen types I, III, IV, and VI in Lpar3-deficient peri-implantation mouse uterus. *Biol Reprod* 2011, 84(2):255-265.
72. Diao H, Xiao S, Li R, Zhao F, Ye X: Distinct spatiotemporal expression of serine proteases prss23 and prss35 in periimplantation mouse uterus and dispensable function of prss35 in fertility. *PLoS One* 2013, 8(2):e56757.
73. Hayashi S, Yang J, Christenson L, Yanagimachi R, Hecht NB: Mouse preimplantation embryos developed from oocytes injected with round spermatids or spermatozoa have similar but distinct patterns of early messenger RNA expression. *Biology of reproduction* 2003, 69(4):1170-1176.
74. Diao H, Xiao S, Howerth EW, Zhao F, Li R, Ard MB, Ye X: Broad gap junction blocker carbenoxolone disrupts uterine preparation for embryo implantation in mice. *Biol Reprod* 2013, 89(2):31.
75. Diao H, Paria BC, Xiao S, Ye X: Temporal expression pattern of progesterone receptor in the uterine luminal epithelium suggests its requirement during early events of implantation. *Fertil Steril* 2011, 95(6):2087-2093.
76. Li R, Zowalaty AE, Chen W, Dudley EA, Ye X: Segregated responses of mammary gland development and vaginal opening to prepubertal genistein exposure in Bscl2 female mice with lipodystrophy. *Reprod Toxicol* 2014.
77. Zheng J, Xia X, Ding H, Yan A, Hu S, Gong X, Zong S, Zhang Y, Sheng HZ: Erasure of the paternal transcription program during spermiogenesis: the first step in the reprogramming of sperm chromatin for zygotic development. *Dev Dyn* 2008, 237(5):1463-1476.
78. Baumann C, Daly CM, McDonnell SM, Viveiros MM, De La Fuente R: Chromatin configuration and epigenetic landscape at the sex chromosome bivalent during equine spermatogenesis. *Chromosoma* 2011, 120(3):227-244.

79. Renthal NE, Williams KC, Montalbano AP, Chen CC, Gao L, Mendelson CR: Molecular Regulation of Parturition: A Myometrial Perspective. *Cold Spring Harb Perspect Med* 2015, 5(11).
80. Loftus FC, Richardson MJ, Shmygol A: Single-cell mechanics and calcium signalling in organotypic slices of human myometrium. *J Biomech* 2015, 48(9):1620-1624.
81. Pehlivanoglu B, Bayrak S, Dogan M: A close look at the contraction and relaxation of the myometrium; the role of calcium. *J Turk Ger Gynecol Assoc* 2013, 14(4):230-234.
82. Jernigan NL, Resta TC: Calcium homeostasis and sensitization in pulmonary arterial smooth muscle. *Microcirculation* 2014, 21(3):259-271.
83. Kupittayanant S, Luckas MJ, Wray S: Effect of inhibiting the sarcoplasmic reticulum on spontaneous and oxytocin-induced contractions of human myometrium. *BJOG* 2002, 109(3):289-296.
84. Taggart MJ, Wray S: Contribution of sarcoplasmic reticular calcium to smooth muscle contractile activation: gestational dependence in isolated rat uterus. *J Physiol* 1998, 511 (Pt 1):133-144.
85. Tribe RM, Moriarty P, Poston L: Calcium homeostatic pathways change with gestation in human myometrium. *Biol Reprod* 2000, 63(3):748-755.
86. Wray S, Shmygol A: Role of the calcium store in uterine contractility. *Semin Cell Dev Biol* 2007, 18(3):315-320.
87. El Zowalaty AE, Baumann C, Li R, Chen W, De La Fuente R, Ye X: Seipin deficiency increases chromocenter fragmentation and disrupts acrosome formation leading to male infertility. *Cell Death Dis* 2015, 6:e1817.
88. Li R, El Zowalaty AE, Chen W, Dudley EA, Ye X: Segregated responses of mammary gland development and vaginal opening to prepubertal genistein exposure in Bscl2(-/-) female mice with lipodystrophy. *Reprod Toxicol* 2015, 54:76-83.
89. Noble K, Matthew A, Burdyga T, Wray S: A review of recent insights into the role of the sarcoplasmic reticulum and Ca entry in uterine smooth muscle. *Eur J Obstet Gynecol Reprod Biol* 2009, 144 Suppl 1:S11-19.
90. Dimitriadis G, Mitrou P, Lambadiari V, Maratou E, Raptis SA: Insulin effects in muscle and adipose tissue. *Diabetes Res Clin Pract* 2011, 93 Suppl 1:S52-59.
91. Lima JG, Nobrega LH, de Lima NN, do Nascimento Santos MG, Baracho MF, Jeronimo SM: Clinical and laboratory data of a large series of patients with congenital generalized lipodystrophy. *Diabetol Metab Syndr* 2016, 8:23.
92. Li R, Diao H, Zhao F, Xiao S, El Zowalaty AE, Dudley EA, Mattson MP, Ye X: Olfactomedin 1 Deficiency Leads to Defective Olfaction and Impaired Female Fertility. *Endocrinology* 2015, 156(9):3344-3357.
93. Diao H, Li R, El Zowalaty AE, Xiao S, Zhao F, Dudley EA, Ye X: Deletion of Lysophosphatidic Acid Receptor 3 (Lpar3) Disrupts Fine Local Balance of Progesterone and Estrogen Signaling in Mouse Uterus During Implantation. *Biol Reprod* 2015, 93(5):123.
94. Xiao S, Li R, Diao H, Zhao F, Ye X: Progesterone Receptor-Mediated Regulation of N-Acetylneuraminate Pyruvate Lyase (NPL) in Mouse Uterine Luminal Epithelium and Nonessential Role of NPL in Uterine Function. *PLoS One* 2013, 8(5):e65607.
95. Diao H, Xiao S, Zhao F, Ye X: Uterine luminal epithelium-specific proline-rich acidic protein 1 (PRAP1) as a marker for successful embryo implantation. *Fertil Steril* 2010, 94(7):2808-2811 e2801.

96. Xiao S, Diao H, Zhao F, Li R, He N, Ye X: Differential gene expression profiling of mouse uterine luminal epithelium during periimplantation. *Reprod Sci* 2014, 21(3):351-362.
97. El Zowalaty AE, Li R, Zheng Y, Lydon JP, DeMayo FJ, Ye X: Deletion of RhoA in progesterone receptor expressing cells leads to luteal insufficiency and infertility in female mice. *Endocrinology* 2017.
98. El Zowalaty A, Baumann C, Li R, Chen W, De La Fuente R, Ye X: Seipin deficiency increases chromocenter fragmentation and disrupts acrosome formation leading to male infertility. *Cell death & disease* 2015, 6(7):e1817.
99. Norwitz ER, Bonney EA, Snegovskikh VV, Williams MA, Phillippe M, Park JS, Abrahams VM: Molecular Regulation of Parturition: The Role of the Decidual Clock. *Cold Spring Harb Perspect Med* 2015, 5(11).
100. Henell F, Ericsson JL, Glaumann H: An electron microscopic study of the post-partum involution of the rat uterus. With a note on apparent crinophagy of collagen. *Virchows Arch B Cell Pathol Incl Mol Pathol* 1983, 42(3):271-287.
101. Hsu KF, Pan HA, Hsu YY, Wu CM, Chung WJ, Huang SC: Enhanced myometrial autophagy in postpartum uterine involution. *Taiwan J Obstet Gynecol* 2014, 53(3):293-302.
102. Semsarian C, Wu MJ, Ju YK, Marciniec T, Yeoh T, Allen DG, Harvey RP, Graham RM: Skeletal muscle hypertrophy is mediated by a Ca2+-dependent calcineurin signalling pathway. *Nature* 1999, 400(6744):576-581.
103. Chiu C, Tebo M, Ingles J, Yeates L, Arthur JW, Lind JM, Semsarian C: Genetic screening of calcium regulation genes in familial hypertrophic cardiomyopathy. *J Mol Cell Cardiol* 2007, 43(3):337-343.
104. Macias H, Hinck L: Mammary gland development. *Wiley interdisciplinary reviews Developmental biology* 2012, 1(4):533-557.
105. Schwertfeger KL, McManaman JL, Palmer CA, Neville MC, Anderson SM: Expression of constitutively activated Akt in the mammary gland leads to excess lipid synthesis during pregnancy and lactation. *Journal of lipid research* 2003, 44(6):1100-1112.
106. Chong BM, Reigan P, Mayle-Combs KD, Orlicky DJ, McManaman JL: Determinants of adipophilin function in milk lipid formation and secretion. *Trends Endocrinol Metab* 2011, 22(6):211-217.
107. Stein O, Stein Y: Lipid synthesis, intracellular transport, and secretion. II. Electron microscopic radioautographic study of the mouse lactating mammary gland. *The Journal of cell biology* 1967, 34(1):251-263.
108. Wu CC, Howell KE, Neville MC, Yates JR, 3rd, McManaman JL: Proteomics reveal a link between the endoplasmic reticulum and lipid secretory mechanisms in mammary epithelial cells. *Electrophoresis* 2000, 21(16):3470-3482.
109. Le Parc A, Leonil J, Chanat E: AlphaS1-casein, which is essential for efficient ER-to-Golgi casein transport, is also present in a tightly membrane-associated form. *BMC Cell Biol* 2010, 11:65.
110. Picariello G, Ferranti P, Mamone G, Klouckova I, Mechref Y, Novotny MV, Addeo F: Gel-free shotgun proteomic analysis of human milk. *Journal of chromatography A* 2012, 1227:219-233.

111. Wang H, Becuwe M, Housden BE, Chitraju C, Porras AJ, Graham MM, Liu XN, Thiam AR, Savage DB, Agarwal AK *et al*: Seipin is required for converting nascent to mature lipid droplets. *Elife* 2016, 5.
112. Nolis T: Exploring the pathophysiology behind the more common genetic and acquired lipodystrophies. *Journal of human genetics* 2014, 59(1):16-23.
113. Chen W, Yechoor VK, Chang BH, Li MV, March KL, Chan L: The human lipodystrophy gene product Berardinelli-Seip congenital lipodystrophy 2/seipin plays a key role in adipocyte differentiation. *Endocrinology* 2009, 150(10):4552-4561.
114. Li R, Zhao F, Diao H, Xiao S, Ye X: Postweaning dietary genistein exposure advances puberty without significantly affecting early pregnancy in C57BL/6J female mice. *Reprod Toxicol* 2014, 44:85-92.
115. Hasegawa D, Calvo V, Avivar-Valderas A, Lade A, Chou HI, Lee YA, Farias EF, Aguirre-Ghiso JA, Friedman SL: Epithelial Xbp1 is required for cellular proliferation and differentiation during mammary gland development. *Mol Cell Biol* 2015, 35(9):1543-1556.
116. Ito D, Suzuki N: Seipinopathy: a novel endoplasmic reticulum stress-associated disease. *Brain* 2009, 132(Pt 1):8-15.
117. Perri ER, Thomas CJ, Parakh S, Spencer DM, Atkin JD: The Unfolded Protein Response and the Role of Protein Disulfide Isomerase in Neurodegeneration. *Frontiers in cell and developmental biology* 2015, 3:80.
118. Invernizzi G, Naeem A, Loor JJ: Short communication: Endoplasmic reticulum stress gene network expression in bovine mammary tissue during the lactation cycle. *J Dairy Sci* 2012, 95(5):2562-2566.
119. Ren S, Lu G, Ota A, Zhou ZH, Vondriska TM, Lane TF, Wang Y: IRE1 phosphatase PP2Ce regulates adaptive ER stress response in the postpartum mammary gland. *PLoS One* 2014, 9(11):e111606.
120. Zegers-Hochschild F, Adamson GD, de Mouzon J, Ishihara O, Mansour R, Nygren K, Sullivan E, Vanderpoel S, International Committee for Monitoring Assisted Reproductive T, World Health O: International Committee for Monitoring Assisted Reproductive Technology (ICMART) and the World Health Organization (WHO) revised glossary of ART terminology, 2009. *Fertil Steril* 2009, 92(5):1520-1524.
121. Mascarenhas MN, Flaxman SR, Boerma T, Vanderpoel S, Stevens GA: National, regional, and global trends in infertility prevalence since 1990: a systematic analysis of 277 health surveys. *PLoS Med* 2012, 9(12):e1001356.
122. Macaluso M, Wright-Schnapp TJ, Chandra A, Johnson R, Satterwhite CL, Pulver A, Berman SM, Wang RY, Farr SL, Pollack LA: A public health focus on infertility prevention, detection, and management. *Fertil Steril* 2010, 93(1):16 e11-10.
123. Payne VA, Grimsey N, Tuthill A, Virtue S, Gray SL, Dalla Nora E, Semple RK, O'Rahilly S, Rochford JJ: The human lipodystrophy gene BSCL2/seipin may be essential for normal adipocyte differentiation. *Diabetes* 2008, 57(8):2055-2060.
124. Szymanski KM, Binns D, Bartz R, Grishin NV, Li W-P, Agarwal AK, Garg A, Anderson RG, Goodman JM: The lipodystrophy protein seipin is found at endoplasmic reticulum lipid droplet junctions and is important for droplet morphology. *Proceedings of the National Academy of Sciences* 2007, 104(52):20890-20895.
125. Hendriks G, Atallah M, Morolli B, Calléja F, Ras-Verloop N, Huijskens I, Raamsman M, van de Water B, Vrieling H: The ToxTracker assay: novel GFP reporter systems that

provide mechanistic insight into the genotoxic properties of chemicals. *Toxicological Sciences* 2012, 125(1):285-298.